WEBERT SATURNINO PINTO

SOIL ZINC AVAILABILITY FROM INORGANIC AND CHELATED ZINC SOURCES AND ITS ACCUMULATION IN MAIZE, EVALUATED BY KINETICA: A COMPUTATIONAL MODELING PLATFORM

Thesis submitted to the Soils and Plant Nutrition Graduate Program of the Universidade Federal de Viçosa in partial fulfillment of the requirements for the degree of *Doctor Scientiae*.

Adviser: Renildes Lúcio Ferreira Fontes

Co-adviser: Hermínia Emília Prieto Martinez

VIÇOSA – MINAS GERAIS
2021

Ficha catalográfica elaborada pela Biblioteca Central da Universidade Federal de Viçosa - Campus Viçosa

T
P659s
2021

Pinto, Webert Saturnino, 1988-
Soil zinc availability from inorganic and chelated zinc sources and its accumulation in maize, evaluated by Kinetica : a computational modeling platform / Webert Saturnino Pinto. – Viçosa, MG, 2021.
1 dissertação eletrônica (116 f.): il. (algumas color.).

Texto em inglês.
Inclui apêndices.
Orientador: Renildes Lúcio Ferreira Fontes.
Tese (doutorado) - Universidade Federal de Viçosa.
Referências bibliográficas: f. 91-99.
DOI: https://doi.org/10.47328/ufvbbt.2021.127
Modo de acesso: World Wide Web.

1. Solos - Teor de zinco. 2. Quelatos. 3. Micronutrientes. 4. Calagem dos solos. 5. Cinética. 6. Aplicações Web. I. Universidade Federal de Viçosa. Departamento de Solos. Programa de Pós-Graduação em Solos e Nutrição de Plantas. II. Título.

CDD 22. ed. 631.43

Bibliotecário(a) responsável: Alice Regina Pinto CRB6 2523

WEBERT SATURNINO PINTO

SOIL ZINC AVAILABILITY FROM INORGANIC AND CHELATED ZINC SOURCES AND ITS ACCUMULATION IN MAIZE, EVALUATED BY KINETICA: A COMPUTATIONAL MODELING PLATFORM

Thesis submitted to the Soils and Plant Nutrition Graduate Program of the Universidade Federal de Viçosa in partial fulfillment of the requirements for the degree of Doctor Scientiae.

APPROVED: June 16, 2021.

Assent:

Webert Saturnino Pinto
Author

Renildes Lúcio Ferreira Fontes
Adviser

ACKNOWLEDGEMENTS

To the Maize Breeding Program of the Universidade Federal de Viçosa (Programa Milho® UFV) for the kind and generous donation of germplasm materials.

This study was financed in part by the Coordenação de Aperfeiçoamento de Pessoal de Nível Superior – Brasil (CAPES) – Finance Code 001.

This study was financed in part by the the Fundação de Amparo à Pesquisa do Estado de Minas Gerais (FAPEMIG).

This study was financed in part by the Conselho Nacional de Desenvolvimento Científico e Tecnológico (CNPq).

“We can’t just conclude that science puts too much power into the hands of morally feeble technologists or corrupt, power-crazed politicians and decide to get rid of it. Advances in medicine and agriculture have saved more lives than have been lost in all the wars in history. Advances in transportation, communication, and entertainment have transformed the world. The sword of science is double-edged.”

–Carl Edward Sagan*, Why We Need To Understand Science.*

ABSTRACT

PINTO, Webert Saturnino, D.Sc., Universidade Federal de Viçosa, June, 2021. **Soil zinc availability from inorganic and chelated zinc sources and its accumulation in maize, evaluated by Kinetica: a computational modeling platform.** Adviser: Renildes Lúcio Ferreira Fontes. Co-adviser: Hermínia Emília Prieto Martinez.

Zinc deficiency is one of the most frequent among the micronutrients. In intensely weathered soils that are already poor in Zn, applications of large amounts of lime, often without adequate incorporation, and of phosphate fertilizers are common causes of Zn deficiencies, especially in crops that are more sensitive to low Zn availability. Especially in these cases, to determine the most efficient source of Zn to be applied, it is crucial to evaluate all the variables involved in the relationship between the source, the soil, and the plant. Although the supply of Zn in the form of mineral sources may in principle be more economically viable, these compounds may present low efficiency, especially in certain soil conditions, such as alkaline soils with high Ca and Mg contents. The use of chelating agents has shown promise in the composition of Zn fertilizer sources by reducing the dependence on the availability of this nutrient in these adverse soil conditions. In addition, the use of new molecules of these agents generates low environmental liabilities because they are rapidly biodegraded. Thus, the objective of this work was to study the effect of mineral sources and chelates of Zn on the availability and uptake of this nutrient by corn plants under the effect of soil textures and liming conditions. Two groups of studies were carried out, the first to investigate the effects of sources, pH and Ca and Mg activities on the kinetic parameters of Zn uptake by plants, and the second to analyze the effect of these same factors on plant development and Zn accumulation in plant tissues. For the estimation and validation of Zn uptake kinetic parameters in plants, an easy-to-use computer application was developed, accessible by the internet, where, besides the estimates of kinetic parameters K_m, v_{max} and c_{min}, additional parameters and linear transformations of the Michaelis-Menten model, results of statistical tests of significance and fits, and graphs of the fits are returned. To evaluate the effects of Zn sources, pH, and Ca and Mg concentrations and activities on Zn acquisition mechanisms by plants, an experiment was performed to obtain the

pattern of Zn removal by plants from the culture solution. The data obtained in this experiment were used to obtain the depletion curve, relating the elemental amount of Zn in solution (q) as a function of time (t). From these curves were obtained the estimates of the maximum absorption velocity values for the saturated segment ($_sV_{max}$) of the depletion curve, and of K_m, $_aV_{max}$, and c_{min} and for the asymptotic segment (1st order). The fitting of the data to the models was performed using the Kinetica computational platform. The interpolate.LSQUnivariateSpline class of the SciPy (Python) computational library was employed for segmentation of the depletion curves, obtaining for each qxt curve two segments, the first characterized as *order 0*, describing an absorption pattern under saturated conditions of the absorption mechanisms, while the second segment was characterized as unsaturated, describing an asymptotic curve in relation to the abscissa axis of the $q(t)$ function. The estimation of the parameter $_sV_{max}$ (saturated segments) was obtained by the derivative of the *order 0* model. For the asymptotic segment, the parameters K_m, $_aV_{max}$ and c_{min} were estimated by the graph-mathematical method (RUIZ, 1985) and by direct fit to the Michaelis-Menten model. Finally, greenhouse experiments were conducted with corn plants grown under five doses of Zn (0, 4, 8, 16 and 32 mg kg^{-1} of the element) and three liming levels (pH 5.5, 6.5 and 7.5), related obtained by means of neutralization curves for each soil, and then dry matter production, and Zn content and content in plant tissues were evaluated. In general, Zn uptake was less intense and also less affected by soil conditions and liming when the source employed was Zn–EDTA, while for $ZnSO_4$ this finding is inverted. Zn–EDDS showed an intermediate behavior, favoring Zn uptake in a balanced manner regardless of soil condition, and pH and Ca and Mg activities.

Keywords: Chelates. Micronutrients. Overliming. Uptake kinetics. Web application.

RESUMO

PINTO, Webert Saturnino, D.Sc., Universidade Federal de Viçosa, junho de 2021. **Disponibilidade de zinco no solo e acumulação em milho, de fontes inorgânicas e queladas, avaliados por Kinetica: uma plataforma de modelagem computacional.** Orientador: Renildes Lúcio Ferreira Fontes. Coorientadora: Hermínia Emília Prieto Martinez.

A deficiência de zinco é uma das que ocorre com maior frequência dentre aquelas dos micronutrientes. Em solos intensamente intemperizados e já pobres em Zn aplicações de elevadas quantidades de calcário e ainda, muitas vezes, sem incorporação adequada, e de fertilizantes fosfatados são causas comuns de deficiências de Zn, sobretudo em culturas com maior sensibilidade à baixa disponibilidade deste nutriente. Especialmente nestes casos, para a determinação a fonte de Zn mais eficiente a ser aplicada é crucial avaliar em conjunto as variáveis envolvidas nas relações entre a fonte, o solo e a planta. Embora o fornecimento de Zn na forma de fontes minerais possa ser a princípio economicamente mais viável, estes compostos podem apresentar baixa eficiência, sobretudo em determinadas condições de solo, como solos alcalinos e com elevados teores de Ca e Mg. O uso de agentes quelantes tem se mostrado promissor na composição de fertilizantes fontes de Zn ao reduzir a dependência da disponibilidade deste nutriente destas condições adversas de solo, além de que o uso de novas moléculas destes agentes gera baixo passivo ambiental, por serem rapidamente biodegradadas. Assim o objetivo com este trabalho foi estudar o efeito de fontes minerais e quelatas de Zn na disponibilidade e na absorção deste nutriente por plantas de milho sob efeito de texturas de solo e de condições de calagem. Foram realizados dois grupos de estudos, o primeiro para a investigação dos efeitos das fontes, do pH e das atividades de Ca e Mg nos parâmetros cinéticos de absorção de Zn pelas plantas, e o segundo para a análise do efeito deste mesmos fatores no desenvolvimento das plantas e acúmulo de Zn nos tecidos vegetais. Para estimativa e validação de parâmetros de cinética de absorção em plantas, foi desenvolvida uma aplicação de computador acessível pela internet e de fácil utilização, onde, além das estimativas dos parâmetros cinéticos K_m, v_{max} e c_{min} , são retornados parâmetros adicionais e de tranformações lineares do modelo de Michaelis-Menten, resultados de testes estatíscos de significân-

cia e ajustes, além de gráficos dos ajustes. Para avaliar os efeitos das fontes de Zn, do pH e das concentrações e atividades de Ca e Mg nos mecanismos de aquisição de Zn pelas plantas, foi realizado um experimento para a obtenção do padrão de remoção de Zn pelas plantas da solução de cultivo. Os dados obtidos neste experimento foram utilizado para obtenção da curva de depleção, relacioanando a quantidade elementar de de Zn em solução (q) em função do tempo (t). A partir destas curvas foram obtidas as estimativas dos valores da velocidade máxima de absorção para o segmento saturado ($_{s}V_{max}$) da curva de depleção, e de K_m, $_{a}V_{max}$ e c_{min} e para o segmento assintótico (1ª ordem). O ajuste dos dados aos modelos foi realizado por meio da plataforma computacional Kinetica. Foi empregando a classe interpolate.LSQUnivariateSpline, da biblioteca computacional SciPy (Python) para segmentação das curvas de depleção, obtendo-se para cada curva qxt dois segmentos, sendo o primeiro caracterizado como de *ordem 0*, descrevendo um padrão de absorção sob condições de saturação dos mecanismos de absorção, enquanto o segundo segmento caracterizou-se como não saturado, descrevendo uma curva assintótica em relação ao eixo das abcissas da função $q(t)$. A estimativa do parâmetro $_{s}V_{max}$ (segmentos saturado) foi obtida pela derivada do modelo de *ordem 0*. Para o segmento assintótico, estimaram-se os parâmetros K_m, $_{a}V_{max}$ e c_{min} pelo método gráfico-matemático (RUIZ, 1985) e por ajuste direto ao modelo de Michaelis-Menten. Por fim, foram realizados experimentos de cultivo em casa de vegetação com plantas de milho cultivadas sob cinco doses de Zn (0, 4, 8, 16 e 32 mg kg^{-1} do elemento) e três níveis de calagem (pH 5.5, 6.5 e 7.5), relacionados obtidos por meio de curvas de neutralização para cada solo, sendo então avaliados a produção de matéria seca, e teor e conteúdo de Zn nos tecidos vegetais. De maneira geral a absorção de Zn foi menos intensa e também menos afetada pelas condições de solo e calagem quando a fonte empregada foi Zn–EDTA, sendo que para $ZnSO_4$ esta constatação se inverte. Zn–EDDS apresentou comportamento intermediário, favorecendo equilibradamente a absorção de Zn independentemente da condição de solo e pH e atividades de Ca e Mg.

Palavras-chave: Quelatos. Micronutrientes. Supercalagem. Cinética de absorção. Aplicação web.

LIST OF ILLUSTRATIONS

LIST OF TABLES

LIST OF ACRONYMS AND ABBREVIATIONS

AIC	Akaike information criterion
API	Application Programming Interface
BIC	Bayesian information criterion
c_{min}	Minimum uptake concentration
cZn_{AP}	Zinc concentration of plant aerial part ($mg\,kg^{-1}$)
IDS	N–(1,2–dicarboxyethylene)–D,L–asparagine acid
DTPA	Diethylenetriamine–pentaacetic acid
dZn	Zinc supplied dose ($mg\,kg^{-1}$)
EDDHA	Ethylenediamine–N,N'–bis(2–hydroxyphenylacetic acid)
EDDS	[S,S]ethylenediamine–N,N'–disuccinic acid
FTIR	Fourier Transform Infrared Spectrometry
FTIR ATR	Fourier Transform Infrared Spectrometry with Attenuated Total Reflectance
GLDA	N,N–bis(carboxylmethyl)–L–glutamic acid
GUI	Graphical User Interface
HTTP	Hypertext Transfer Protocol
HTTP/GET	Hypertext Transfer Protocol GET request
HTTP/POST	Hypertext Transfer Protocol POST request
JSON	JavaScript Object Notation
K_m	Michaelis constant
$LVAd_{cla}$	Clay Latossolo Vermelho–Amarelo distrófico típico (Oxisol)
$LVAd_{scl}$	Sandy–Clay Loam Latossolo Vermelho–Amarelo distrófico típico (Oxisol)
MGDA	Methylglycinediacetic acid
NFT	Nutrient film technique
PAR	Photosynthetically active radiation
pH_S	Soil hydrogen potential
qZn_{APPt}	Zinc content of aerial part of plants per pot (mg/pot)
RMSE	Root mean square error
RSS	Residual sum of squares
$srcZn$	Zinc source
URL	Uniform Resource Locator

v_{max}	Maximum uptake rate
$w\mathrm{DM}_{\mathrm{APPt}}$	Dry matter weight of plants aerial part per pot
WTPS	Permuted Wald–type statistic
Zn–EDDS	Zinc ethylenediamine–N,N'–disuccinic complex
Zn–EDTA	Zinc ethylenediaminetetraacetic complex
$ZnSO_4$	Zinc sulfate
${}_a v_{max}$	Asymptotic segment v_{max} estimated value
${}_s v_{max}$	Saturate segment estimated v_{max} value
*l*Lm	Low–liming condition
*h*Lm	High–liming condition

SUMMARY

CHAPTER 1

GENERAL INTRODUCTION

Nutrient deficiencies in plants are often and most of the time are unapparent. However, they still significantly reflect on plant tissue contents and, consequently, on yields. Generally when signs or symptoms of deficiency become detectable in annual crops it is already too late to fix the fault and avoid productivity losses and crop products quality. In this scenario, micronutrients deficiencies are the most critical as the most neglected probably being the ones causing most losses. Among these deficiencies, zinc's is the one that occurs most frequently worldwide (Figure 1.1).

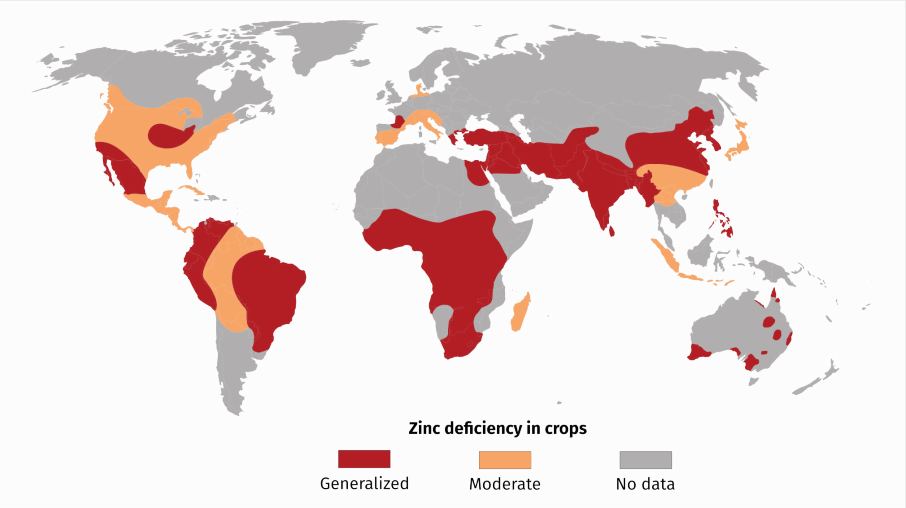

Figure 1.1: Zn's deficiencies in crops. Adapted from: (STONE; F., 2008)

Zn is essential for both plants and animals as it is the structural constituent of enzymes and regulator co-factor in enzymes involved in numerous metabolic pathways. Millions of hectares of crops and approximately one-third of the world's population (Figure 1.2) suffer from inadequate zinc intake (ALLOWAY, 2009).

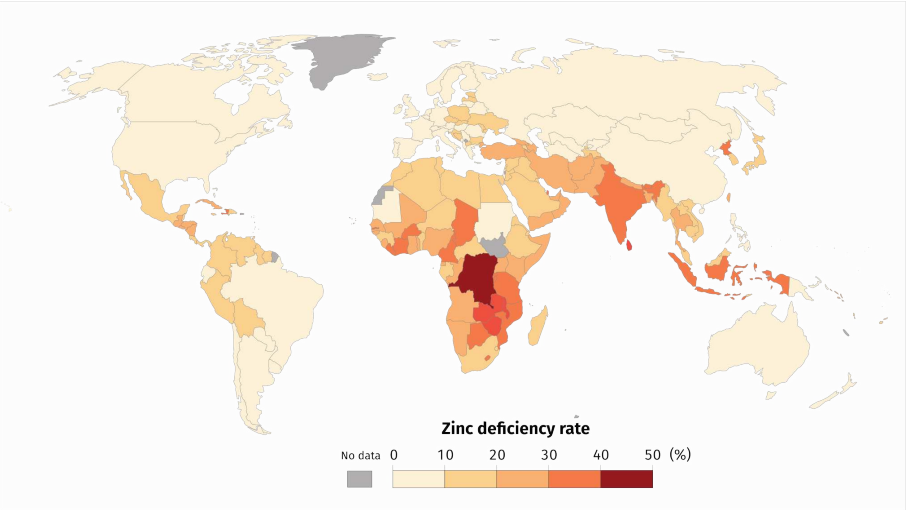

Figure 1.2: Zn's deficiencies in populations. Adapted from: (WESSELLS; BROWN, 2012)

Limiting conditions for Zn availability include calcareous soils, high pH, phosphate, and iron oxides contents. Application of massive doses of limestone and phosphate fertilizers are also factors that increase Zn deficiencies, especially in crops with a higher sensitivity to low availability of this nutrient. This situation is more prone to happen for plants growing on intensely weathered tropical soils that already count meager Zn contents, like the ones found in the Brazilian 'Cerrado' region.

The choice of the best strategy to tackle Zn low availability in soils, upon each set of conditions, depends on a more holistic comprehension of the relations in the soil-plant interface among the nutrient chemical species, soil solid phase, and the plant (Figure 1.3).

The evaluation of these interactions is possible through analyzing the equilibrium constants for the source dissolution and formation (K_1), adsorption and desorption of nutrient species by the soil (K_2) and roots surface (K_3). The uptake kinetic parameters (K_m, $v_{max}$and c_{min}) can provide information on how plants are affected by the environmental conditions on the nutrient's acquisition. Thus, obtaining information on these relations is of high importance, for example, when employing mechanistic models (BARBER, S A, 1995) for the comprehension of the soil-plant system.

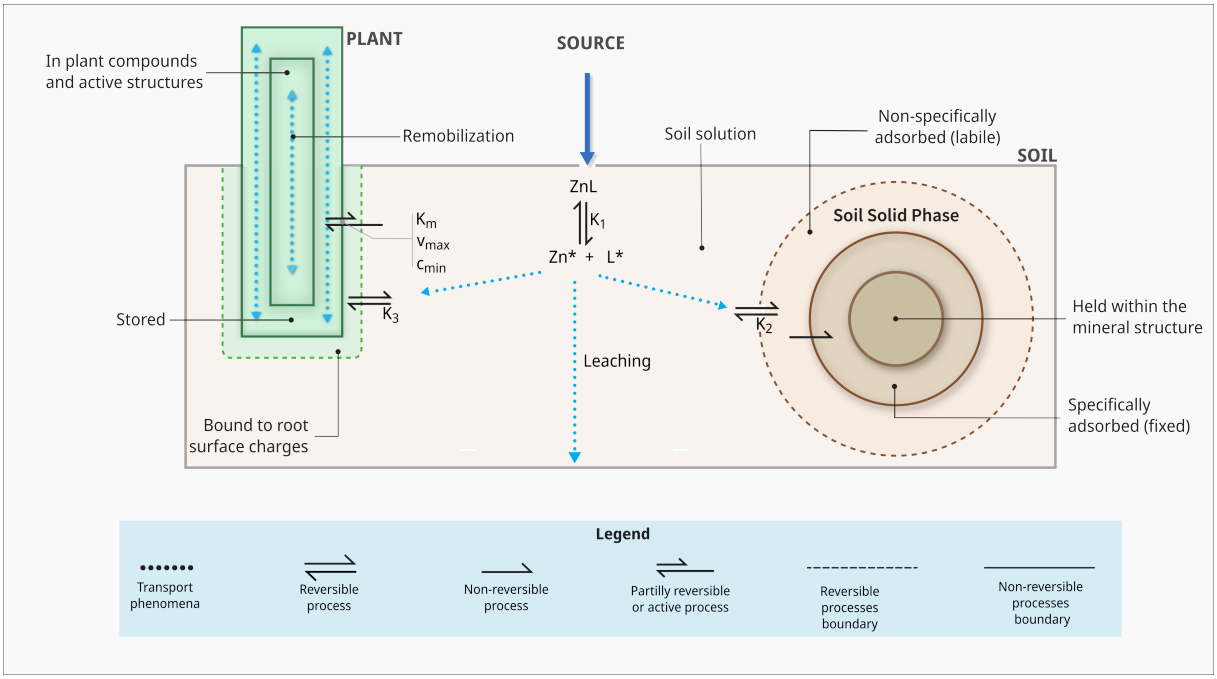

Figure 1.3: Zn in soil-plant continuum

The relations among all ionic species are also of noted relevance the so-called iono-sphere, as an emerging concept, (GRIFFITHS; ROY, et al., 2020). These variables' information can lead to significant insights and be applied in modeling the soil-plant system in a more practical sense for finding an efficient Zn or any other nutrient source.

The current work comprises four chapters. The first contains an introduction to the subject, including justification and highlights on the relevance of the research. It included as well a brief literature review, and the results of preliminary work done to fulfill theoretical gaps and inconsistencies.

In the second chapter, we portray the development of Kinetica, a web-based appli-cation, and API for estimating the ion uptake kinetic parameter values in plants, from data obtained from solution depletion experiments. We use the application in the sub-sequent chapter.

The aim of Chapter 3 is to investigate the outcome of excessive liming on the Zn kinetics uptake parameter values (K_m, v_{max}, and c_{min}) and the potential effect of different Zn sources on mitigating the negative effects of overliming. To cross-examine these factors, we set up an experiment where maize plants grow in nutrient solution and at a certain development stage were subject to a Zn depletion experiment, under the effect of liming conditions and mineral and chelated sources of Zn. Data obtained was modeled using Kinetica (Chapter 2) and other computational tools. Finally, the obtained

parameter values went under statistical analysis and interpretation.

In Chapter 4 we targeted to examine the overliming condition effect on the efficiency of two chelating agents, EDTA and EDDS, in comparison with zinc sulfate, a traditional widely employed inorganic zinc source in the formulation of fertilizers for soil application to crops. To do so, we conducted greenhouse experiments growing maize plants in soil with contrasting properties, different Zn sources and doses, and liming conditions.

Finally, in Chapter 5 we wrap up with the global insights brought by our study and also the future perspectives and questions raised with the so far results.

CHAPTER 2

KINETICA: WEB-BASED APPLICATION AND API FOR ESTIMATING ION-UPTAKE KINETIC PARAMETER VALUES IN PLANTS

ABSTRACT

The estimates of the ion uptake kinetic parameters Michaelis constant (K_m), maximum uptake rate or velocity (v_{max}), and minimum uptake concentration (c_{min}) are relevant criteria to evaluate the influx characteristics of nutrients and other ions of interest in plant studies and obtaining these constants has been a common approach in both the agricultural and environmental research fields. To make this an attainable task, some mathematical and graphical methods and techniques are available. However, an accessible and reliable tool, facilitating the estimation of the uptake kinetic parameter values joining these concepts, was still missing. Aiming at that, we developed Kinetica, a web-based application, and an API (Application Programming Interface) for estimating the ion uptake kinetic parameter values in plants, for data obtained from solution-depletion experiments, employing the graphical-mathematical method and the non-linear direct fitting to the Michaelis-Menten model. A back-end application API was built with *Python*, encapsulated into the Flask Web Framework. A user-friendly graphical front-end, named Kinetica Web-App, was also developed. The application is accessible on `http://kinetica.ufv.br` or `http://app.kinetica.cloud`, where users can insert the data obtained from the depletion experiment and rapidly have the parameter values estimated. The results then become available for visualization on the web browser and to be saved to the user's device. Alternatively, the experimental data can be sent directly to the Kinetica API (`http://api.kinetica.ufv.br` or `http://api.kinetica.cloud`) through any web client capable of managing HTTP requests. In that case, results are sent back as a JSON (JavaScript Object Notation) object, and data parsing and visualization will rely on the client features. Kinetica API results include estimated uptake kinetic parameter values (K_m, v_{max}, c_{min}), depletion equations, Michaelis-Menten model fittings, Linearized plots (Lineweaver-Burk, Eadie-Hofstee, and Hanes-Woolf), and statistical data.

Keywords: Plant mineral nutrition, nutrient uptake, Michaelis-Menten equation, K_m, v_{max}, c_{min}, software, Graphical-Mathematical Method, direct fitting, least-squares fit, *Python*

2.1 INTRODUCTION

Estimates of uptake kinetic parameter values can reveal relevant information on how plants react under the effect of specific environmental variables conditions, not only to the ion lability but, in a more holistic concept, to the ion bioavailability. For instance ion-uptake kinetic parameters can be affected by plant species, cultivars, root and plant age, plant nutrient status, light, atmosphere and growth medium temperatures, water potential, aeration, mechanical impedance, and nutrient supply (BARBER, S. A., 1979; TINKER; NYE, 2002). For this reason, uptake kinetic parameters become of interest in both environmental and agricultural related studies.

Concerning crop plants, kinetics parameters can be an asset developing agricultural systems with increased nutrient use efficiency, by aiding to set better fertilizer application strategies, crop management, and on the processes of breeding and selecting plant varieties with improved nutrient uptake capabilities under abiotic stress conditions or low nutrient availability (ABBÈS et al., 1995; ARAÚJO et al., 2015; GRESPAN; DIAS; NOVAIS, 1998; GRIFFITHS; ROY, et al., 2020; HORN et al., 2006; LI, Q. et al., 2017; LIMA et al., 2005; MACHADO; FURLANI, 2004; MARTINEZ et al., 2015; MENG et al., 2016; PAULA et al., 2018; RENGEL; GRAHAM, 1996; SANES et al., 2013; YORK; SILBERBUSH; LYNCH, 2016).

Furthermore, by providing information on the plant side of the soil-plant relationship, the uptake kinetic parameter values may become key input variables for modeling nutrient uptake from the soil, as for the mechanistic models (BARBER, S A, 1995; LIN; KELLY, 2010; MALAGOLI; LE DEUNFF, 2014; SILBERBUSH; BEN-ASHER; EPHRATH, 2005).

In the environmental research field, ion-uptake kinetics by plants and algae are useful when looking for potential bio accumulators, either for the removal of contaminants from soil and water bodies (CHUNG et al., 2002; LI, J. et al., 2015; LUBSCH; TIMMERMANS, 2018; LUO; LIU; XU, 2012; MARTÍNEZ; RICO, 2004; ROFKAR; DWYER, 2011; ROLEDA; HURD, 2019) or tracing the possible transference of toxic elements

from the soil throughout the food chain (ABEDIN; FELDMANN; MEHARG, 2002; MULLINS; SOMMERS, 1986; NOCITO et al., 2002; ZHANG et al., 2020).

Some studies also employ ion-uptake kinetics to understand the dynamics of native plant communities and to detect disturbances endangering these regional ecosystems (BRIX et al., 2010; CHRISTIANSEN; ANDERSEN; JENSEN, 2016; GRAS; KOCH; MADDEN, 2003; MOZDZER; ZIEMAN; MCGLATHERY, 2010; OLESEN et al., 2018; STAPEL et al., 1996; ZHU; ZHUANG, 2013), and to predict plants response to the global climate changes (BASSIRIRAD, 2000; BASSIRIRAD et al., 2000; COTT; CA-PLAN; MOZDZER, 2018; ZHU; IVERSEN, et al., 2016).

2.1.1 Estimating ion uptake kinetic parameters values in plants: Current approaches

Obtaining the values of uptake kinetic parameters is not a straightforward task since it requires finding values for v_{max}, K_m, and, less commonly, c_{min} coefficients for the Michaelis-Menten equation, a rectangular hyperbola. However, some approaches and tools have helped to overcome this challenge. One strategy was to employ linearized versions of the Michaelis-Menten equation.

Epstein and Hagen (1952), when proposed the similarities of enzyme kinetics and nutrient uptake kinetics by plants, already employed the Lineweaver and Burk plot (DIXON, 1953), a linear transformation of the Michaelis-Menten equation and also known as the double-reciprocal plot, where the inverse of uptake rate values ($1/v$) are plotted against the inversed values of ion concentration ($1/c$), to estimate the values of K_m and v_{max}. Later other authors also employed different linearization approaches, like the Eadie-Hofstee (HOFSTEE, 1952) and Hanes-Woolf (HANES, 1932) plots.

The work of Claassen and Barber (1974) made it possible to estimate the uptake kinetic parameter values by measuring the depletion of an ion by plant uptake from a solution during a period and fitting the ion quantities (q) as a function of time (t), $q(t)$. The derivative $-\delta q/\delta t$ will give the influx rate at any point in the adjusted depletion equation.

Nevertheless, some uncertainties arise on whether each of these methods results in reliable estimates for ion-uptake parameter values. Van Rees (1994) investigated the estimation of the parameter values by four distinct methods: direct adjust, Lineweaver-

Burk plot, third-degree polynomial, and the Bhat method (BHAT, 1983). The author concluded that all the methods resulted in similar values in the uptake kinetic parameters, and the more effortless approach was the Lineweaver-Burk plot, while direct adjusting the parameters was very time-consuming due to the guessing of the initial estimates.

Ritchie and Prvan (1996), concerned about the errors the K_m and v_{max} estimates by linearization methods, conducted a simulation study where they compared the validity of these parameter estimates both obtained by direct adjust to the Michaelis-Menten equation and by the Lineweaver-Burk plot approaches. They verified that the direct fitting to Michaelis-Menten results in more reliable estimates in comparison to an unweighted Lineweaver-Burk plot, which is subject to return biased estimates.

Claassen and Barber (1974) mention the visual or graphical estimation of the tangent slope to the depletion curve of a series of points over the length of the curve as a workaround to estimate v_{max}. The visual estimation is a straightforward and practical technique, but rattling susceptible to errors obtaining the estimates due to subjective inference over the data. To avoid the inconsistency of obtaining the uptake kinetic parameter values by a graphical estimation, Ruiz (1985) formulated the Graphical-Mathematical method, which segments the depletion curve into two intervals, obtaining the parameters estimated values from the fitted equations to each segment.

Later Ruiz and Fernandes Filho (1992) developed *Cinética*, a Windows® application for estimating v_{max} and K_m values by employing this method. *Cinética* is a functional and straightforward application, and many researchers have employed it to estimate nutrient uptake kinetics parameters K_m and v_{max}. However, it lacks further statistical analysis on the estimates, and alternative estimation and interpretation methods. Moreover, Cinética is outdated, and users may meet operating system compatibility issues when running the application on the newer versions of Windows®.

Wrought by that, we developed Kinetica, an open and cross-platform application, and API for estimating ion uptake parameter values by plants.

2.2 MATERIALS AND METHODS

2.2.1 Theoretical background and data modelling methods

Epstein and Hagen (1952) observed that the plant ion uptake rates plotted against concentration would design a rectangular hyperbola, quite similar to that of the classical Michaelis-Menten enzyme kinetics (Figure 2.1). They then proposed that two kinetic constants, K_m (Michaelis constant or the concentration at half-saturation) and v_{max} (maximum absorption rate or maximum velocity), could describe characteristics of individual membrane carriers.

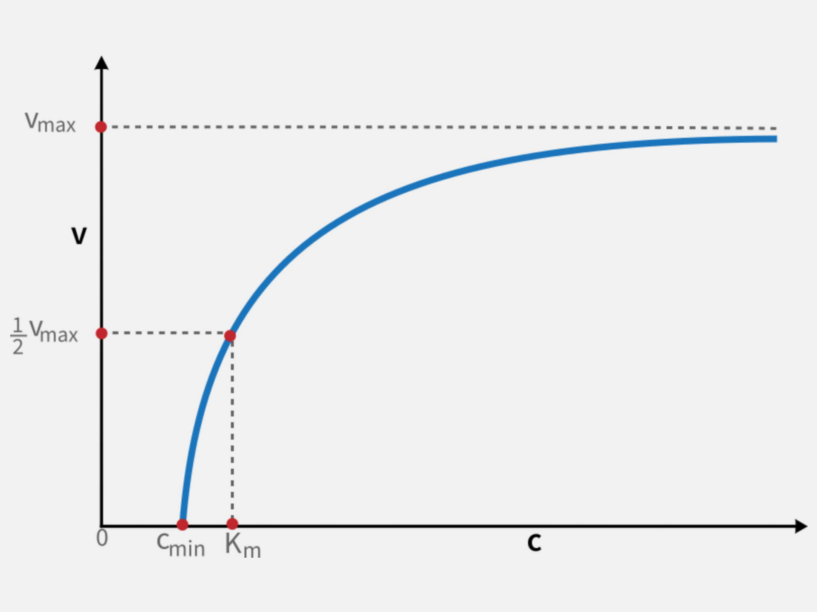

Figure 2.1: Plot for the Michaelis-Menten model adapted for plant nutrient uptake kinetics. The uptake rate or velocity (v) theoretically reaches its maximum (v_{max}) when $c \rightarrow \infty$; K_m is the value of c when $v = \frac{1}{2} v_{max}$; c_{min}, the value of c when $v = 0$)

However, by directly employing this approach, the estimates of ion uptake rates could only be obtained using short term absorption by excised roots of isotopically labeled ions or long-term absorption by intact roots from solutions maintained approximately at a constant concentration. In the first case, it is only possible the study of ions with convenient isotope for labeling, and for both cases, separate measurements of uptake are necessary for each of a graded series of ion concentrations in order to establish the relationship between the rate of absorption and concentration Claassen and Barber (1974).

Another criticism of this technique is that holding the ion concentration in the root media may not reflect the soil conditions for the ion uptake Reid and Hayes (2003). In order to circumvent these limitations, Claassen and Barber (1974) developed a method that characterizes the ion uptake as the decrease of its quantity (q) from the solution, which is dependent of ion concentration (c) and the solution volume (v), as shown in Equation 2.1:

$$q = c\,V \tag{2.1}$$

A plot of q as a function of time, t, gives a curve showing the depletion of the ion from solution resulting from plant absorption and is called depletion curve (Figure 2.2). The net influx at any point is given by $-\delta q/\delta t$. The slope of the curve can be calculated by expressing q as a function of t and calculating the derivative or, in a less accurate manner, by visual (graphical) estimation of the slope of the tangent of the depletion curve.

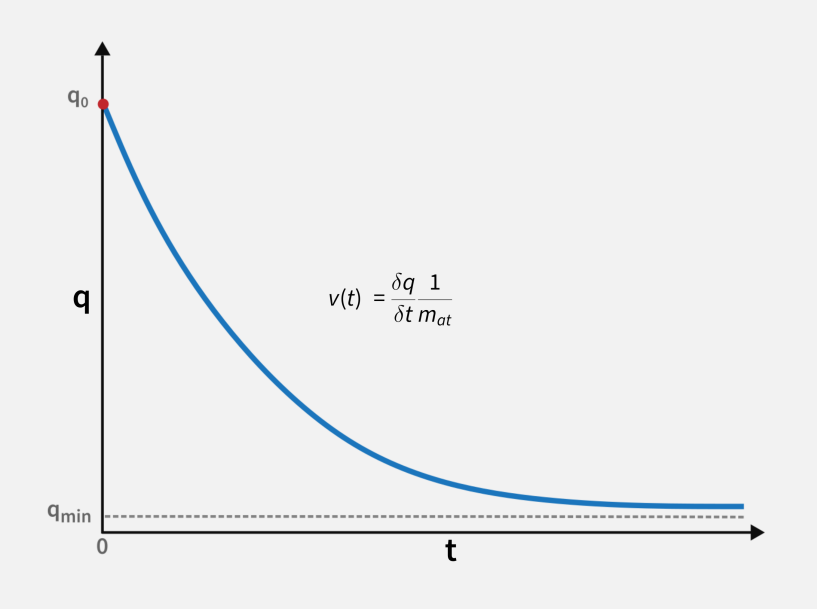

Figure 2.2: General ion depletion curve in plants. Ion quantity in the bulk solution (q) diminishes, from the initial ion quantity (q_0), as the time of contact (t) of the plant absorbing tissue increases, in an asymptotic trend until it reaches a minimum quantity (q_{min}) where ion net influx equals zero.

The term c_{min} was later introduced, in order to compensate for an unreachable theoretical ion amount for plant uptake. Considering that, if plants reduce the ion quantity from the solution until the net influx reaches zero, a minimum concentration, different

from zero, will remain. The first to establish the basis for this concept was Nielsen (1972). He considered a system where ion influx into roots is intrinsically related to the ion flux by diffusion through a radial distance from the root surface. The ion concentration on the root environment (c_r) is constant and equals to c_{min}. Driven by the concentration gradient, the ion influx into the root is different from zero until the ion concentration in the bulk solution (c) equals c_{min}. Mathematically, c_{min} then can be defined by Equations 2.2 and 2.3:

$$c = c_r = c_{min} \tag{2.2}$$

$$c_{min} : c(v \rightarrow 0) \tag{2.3}$$

The Michaelis-Menten model adapted for ion uptake can then be described by Equation 2.4 (BARBER, S. A., 1979).

$$v = \frac{v_{max}\left(c - c_{min}\right)}{K_m + \left(c - c_{min}\right)} \tag{2.4}$$

Where v is the uptake rate or velocity; c_{min} the minimum concentration for positive influx; v_{max} the maximum uptake rate or velocity and c the ion instant concentration in the bulk solution and K_m the Michaelis constant or the concentration at half-saturation.

2.2.2 Graphical-Mathematical Method

As an alternative to facilitate the calculation of the K_m and v_{max} values and avoid impreciseness of an exclusive visual or graphical estimation, Ruiz (1985) came up with the Graphical-Mathematical Method. The method involves adjusting the $q(t)$ data by splitting it into two continuous segments, fitting the first to a linear function and the second to a non-linear function, as, for example, a power function (Figure 2.3).

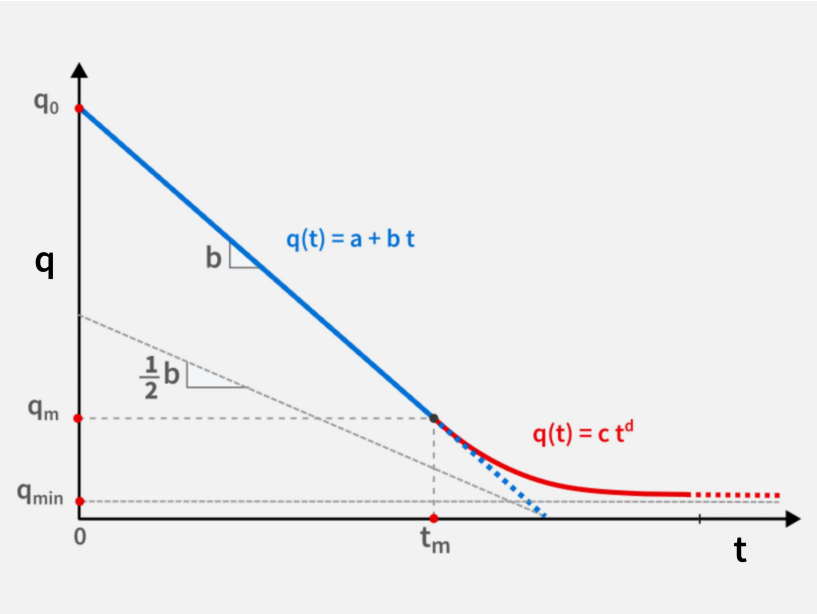

Figure 2.3: Schematic plot for the Graphical-Mathematical Method fitting a Linear-Power model. The elemental or ion quantity (q) in the bulk solution plotted against the sampling time (t) yields a depletion curve. The first segment fits a linear function ($q(t) = a + b\,t$) and, a non-linear equation better describes the second ($q(t) = c\,t^d$).

The value of v_{max} hence is given by Equation 2.5:

$$v_{max} = -\frac{b}{r_m} \tag{2.5}$$

Where b is the slope of the linear segment fitted to the depletion data, and r_m stands for the absorbing tissue measure (e.g., root mass, volume or surface area, leaf surface area).

The relation expressed by Equation 2.6 gives the estimated value of K_m:

$$K_m = \frac{q_m}{V_m} \tag{2.6}$$

Where q_m is the ion quantity for which the uptake rate equals half of v_{max}, and V_m is the corresponding volume.

The q_m value is attained by finding the value for $q(t)$ for which the derivative of q with respect to t for the non-linear segment equals half of the derivative of q with respect to t for the linear segment (Equation 2.7).

$$\frac{\delta q}{\delta t}\left(c\,t^d\right) = \frac{1}{2}\frac{\delta q}{\delta t}\left(a + b\,t\right) \tag{2.7}$$

The derivative of q with respect to t for the power function and half derivative for the linear function is given by Equation 2.8 and Equation 2.8, respectively:

$$\frac{\delta q}{\delta t}\left(c\, t^{d}\right) = c\, d\, t^{d-1} \tag{2.8}$$

$$\frac{1}{2}\frac{\delta q}{\delta t}\left(a + b\, t\right) = \frac{1}{2}\, b \tag{2.9}$$

Replacing Equations 2.8 and 2.9 in Equation 2.7, one obtains Equation 2.10:

$$\frac{1}{2}\, b = c\, d\, t^{(d-1)} \tag{2.10}$$

Given that t_m is the value of t when $q(t) = q_m$, defining $t = t_m$ in Equation 2.10 and rearranging, we will end up with Equation 2.11:

$$t_m = \left(\frac{b}{2\, c\, d}\right)^{\frac{1}{(d-1)}} \tag{2.11}$$

In this paper, we detail the mathematical procedure only for the power function. However, virtually any model could be fitted if it matches an adequate statistical adjustment and still biologically meaningful in the sense of ion uptake. In addition to the outcome of calculations by fitting the power function, Kinetica also returns the results based on the exponential model (Equation 2.12) and the reciprocal-exponential model (Equation 2.13), as initially proposed by Ruiz and Fernandes Filho (1992).

$$q(t) = c\, e^{d\, t} \tag{2.12}$$

$$q(t) = c\, e^{d\, t^{-1}} \tag{2.13}$$

The values for the instantaneous volumes, $V(t)$, can be estimated by employing Equations 2.14, 2.15, and 2.16:

$$V_l = V_0 - V_{t_n} - \sum_{t=0}^{n(t)} V_s \tag{2.14}$$

$$\dot{V}_l = \frac{V_l}{\Delta t} \tag{2.15}$$

$$V(t) = V_0 - \left(t\,\dot{V}_l + \sum_{t=0}^{n(t)} V_s \right) \tag{2.16}$$

Where V_0 is the solution volume at the beginning of the depletion experiment, V_s the sampling volume at t, $\dot{V}_l$ the volume loss rate and $n(t)$ is the sample number count at the instant t.

Equation 18 gives $v(t)$, the ion uptake rate as a function of the depletion time:

$$v(t) = \frac{\Delta q}{\Delta t \;\; r_m} \tag{2.17}$$

Where Δq is the estimated ion quantity change, Δt is the time change, and r_m is the absorbing tissue measure.

2.2.3 Parameter Direct Adjust Method

In addition to the Graphical-Mathematical method, we also implemented the estimation of the kinetics parameter values by directly fitting the instantaneous concentrations, $c(t)$, to the modified Michaelis-Menten model (Equation 2.4). This approach is also a way to estimate the c_{min} values, as the Graphical-Mathematical method is not suitable for this purpose. After estimating the instant concentrations, the data is fitted to the Michaelis-Menten Model using a direct least squares method, by employing the Levenberg-Marquardt gradient method (greedy algorithm) to minimize the objective function, packed in Scipy (VIRTANEN et al., 2020) Python library.

Ritchie and Prvan (1996) compared the estimates of v_{max} and K_m values both by direct fitting to the Michaelis-Menten model and by Lineweaver-Burk plot (linearization). They found that the least-squares method applied to the Michaelis-Menten equation would be valid and the most satisfactory means of estimating these parameters, in comparison to the Lineweaver-Burk linearization. More recently, Cho and Lim (2018), in a simulation study, compared the estimation of these parameter values by the Lineweaver-Burk plot and Eadie-Hofstee plot, and non-linear regression, by fitting directly to de Michalis-Menten model. They similarly concluded that non-linear methods could provide more reliable and accurate parameter estimates of the Michaelis-Menten equation parameters than the traditional linearization methods.

2.2.4 Linearized plots

The challenges to accurately determine the values of the kinetic parameters by directly fitting the uptake rates, as a function of ion instantaneous concentrations for the Michaelis-Menten equation, a rectangular hyperbola, are mostly in reason of computational limitations. Due to these difficulties, the linearized forms were the first way to estimate the ion uptake kinetic parameter values Epstein and Hagen (1952) and have been extensively employed ever since.

Nevertheless, this approach is subject to give estimates that are both biased and imprecise Ritchie and Prvan (1996). As an example, the Lineweaver-Burk plot (2.4-a) can be fitted based on a disproportionate high weighting of the ion concentrations for the lower *c* values, where commonly, the experimental errors are relatively more significant. Additionally, zero values of *v* are valid for the Michaelis-Menten and modified Michaelis-Menten equation 2.4), but not for the Lineweaver-Burk plot.

The Lineweaver-Burk transformation presupposes inverting the values of *v*, and the values of *c* or $c - c_{min}$. Therefore when v, c, or $c - c_{min}$ are equal to zero, the values of the reciprocal expressions ($1/v$, $1/c$, and $1/(c - c_{min})$) become arithmetically undefined. In the circumstance of fitting ion uptake kinetics data to the modified Michaelis-Menten equation, where the concentration term (*c*) is replaced by adjusted concentration ($c - c_{min}$), this issue possibly will be even more relevant, considering that the expression $c - c_{min}$ may more frequently yield zero or negative values. Even so, these plots are still relevant as a *post hoc* tool for obtaining information in studies on uptake kinetics, such as indicating the effects of competition between ions.

Kinetica delivers the plots and axis values for the three most common linearized Michaelis-Menten transformations, which are the Lineweaver-Burk (DIXON, 1953), Eadie-Hofstee (HOFSTEE, 1952), and Hanes-Woolf (HANES, 1932). The Lineweaver-Burk transformation is a double reciprocal plot, obtained inverting both sides of the Michaelis-Menten equation (Figure 2.4-a). Based on the Lineaweaver-Burk equation, it is possible to obtain the Eadie-Hofstee plot (Figure 2.4-b) by multiplying the Lineweaver-Burk equation by v and v_{max}. The Hanes-Wolf plot (Figure 2.4-c) is given by merely multiplying the Lineweaver-Burk plot by the adjusted concentration ($c - c_{min}$).

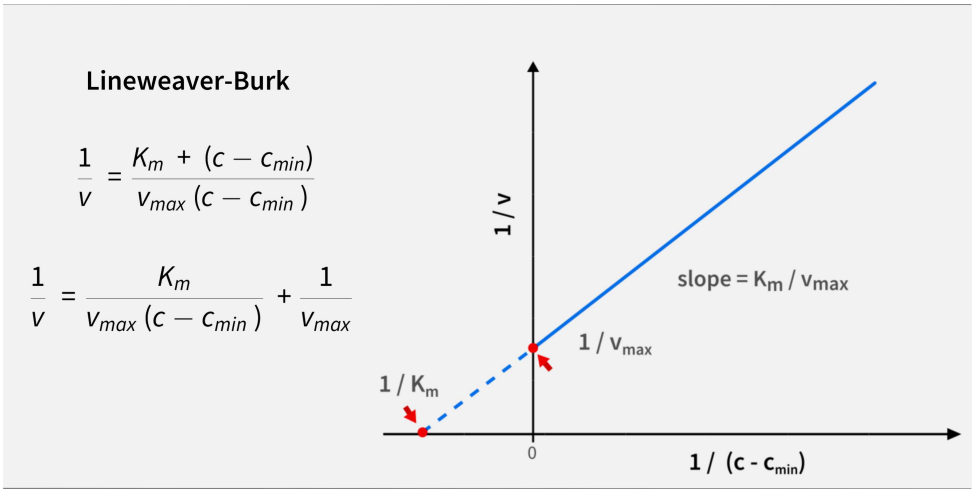

(a) Lineaweaver-Burk or double-reciprocal plot

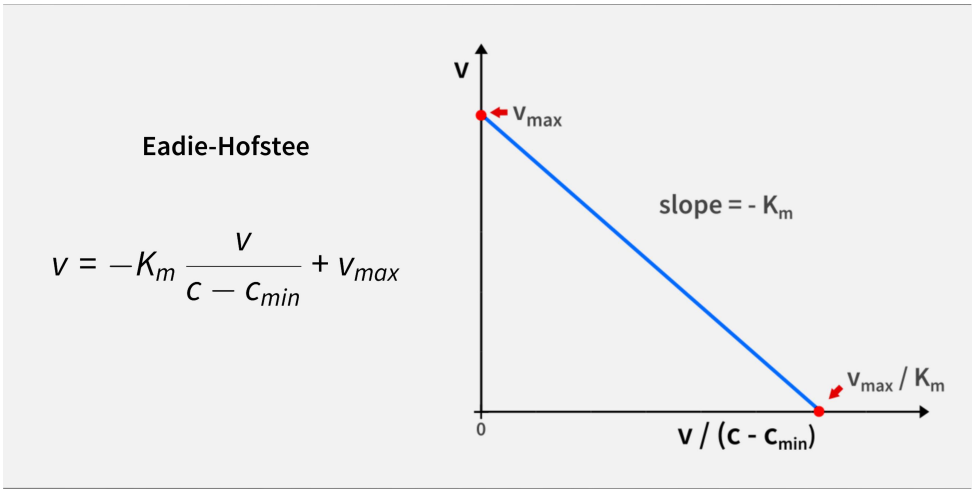

(b) Eadie-Hofstee plot

Figure 2.4: Linearization approaches for the Michaelis-Menten equation implemented on Kinetica.

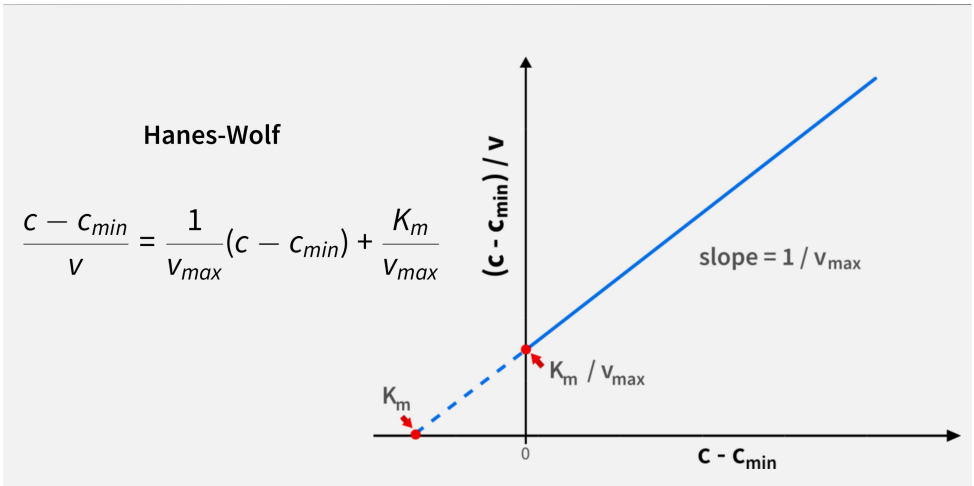

(c) Hanes-Wolf plot

Figure 2.4: Linearization approaches for the Michaelis-Menten equation implemented on Kinetica. (cont.).

2.3 RESULTS

2.3.1 Design and deployment Kinetica API and Kinetica Web-App

We developed both a front-end (Kinetica Web-App) and an independent back-end API (Kinetica API). Kinetica API is an Application Programming Interface implemented in *Python* encapsulated within the Flask Web Framework. Kinetica API is independent of Kinetica Web-App and is reachable from any web-client capable of making and managing a Hypertext Transfer Protocol POST request (HTTP/POST) Figure 2.5. Kinetica Web-App is a GUI (Graphical User Interface) front-end for Kinetica API written in HTML/CSS/JavaScript.

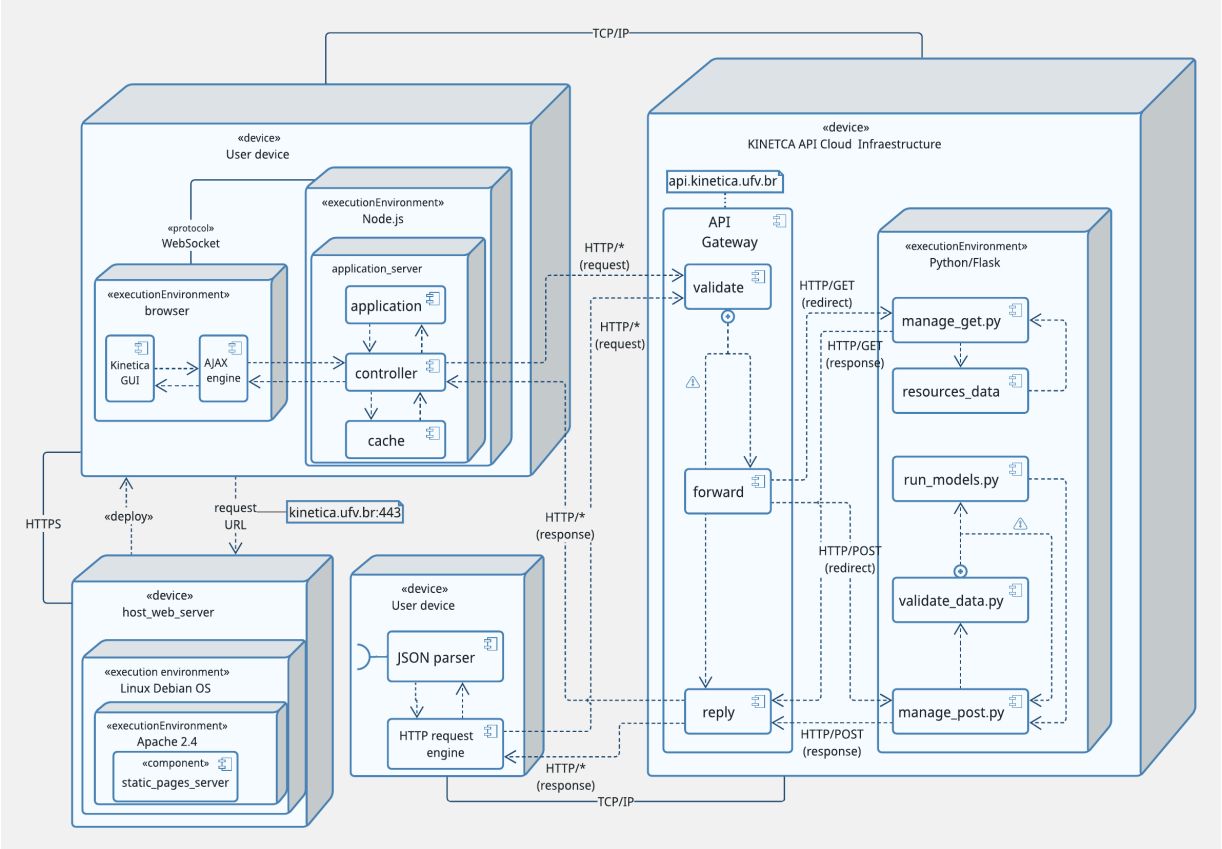

Figure 2.5: Deployment diagram for Kinetica Web-App and Kinetica API

Following, we demonstrate Kinetica API usage in both ways, by using the Kinetica WebApp and by making an HTTP request through a generic web client framework. For this second case, we employed R Statistical Language R Development Core Team (2019), more explicitly making use of the httr package Wickham (2019).

2.3.2 Kinetica Web-App

Kinetica Web-App is a user-friendly front-end application for Kinetica API built with JavaScript and formatted with HTML/CSS. One can reach the application by browsing to `http://kinetica.ufv.br` or `http://app.kinetica.cloud`, making use of any device provided with access to the internet and Hypertext Transfer Protocol (HTTP) capabilities. On the Login page (Figure 2.6), the user may enter the name, organization, a valid email address and pass the captcha challenge in order to validate the session.

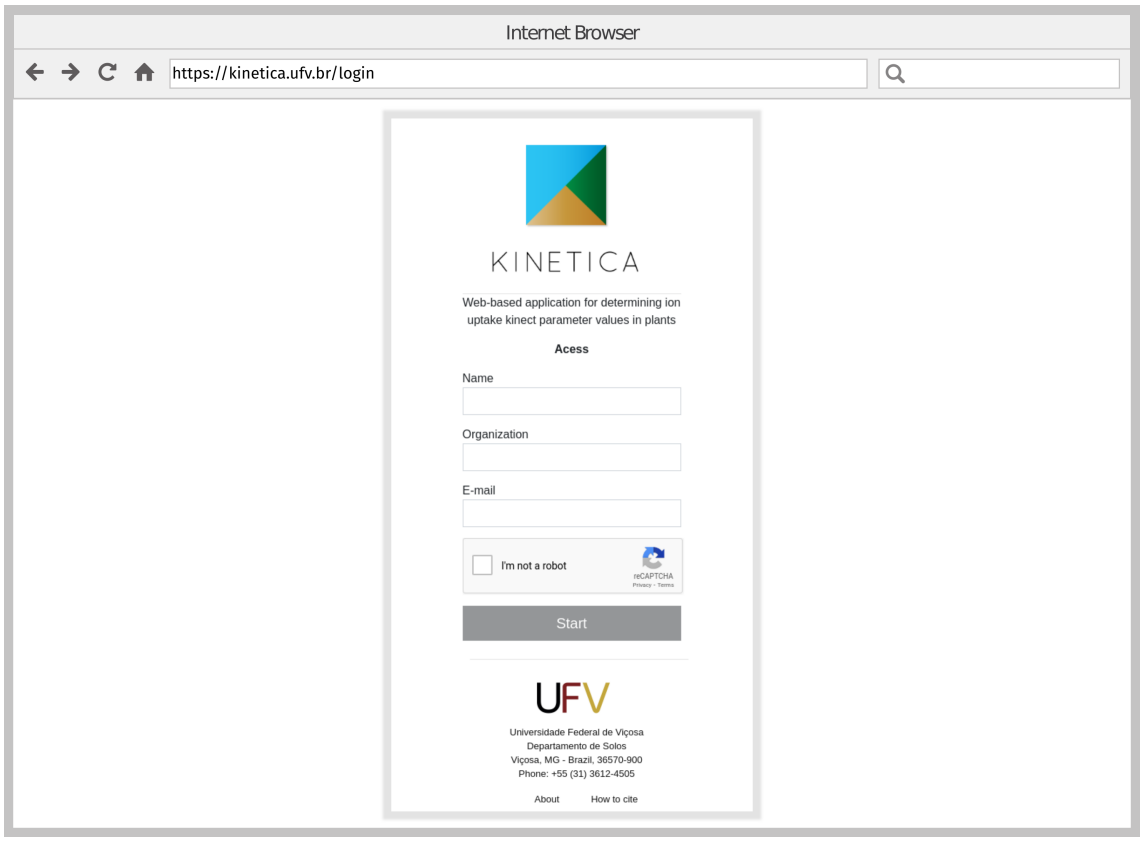

Figure 2.6: Kinetica Web-App login page

Data input page

After logging in, the application exhibits to the user the Data input page (Figure 2.7), where the data can be entered by typing or copying and pasting from any spreadsheet editor. The table on this page also has auto-fill capabilities in order to facilitate working with repetitive data patterns.

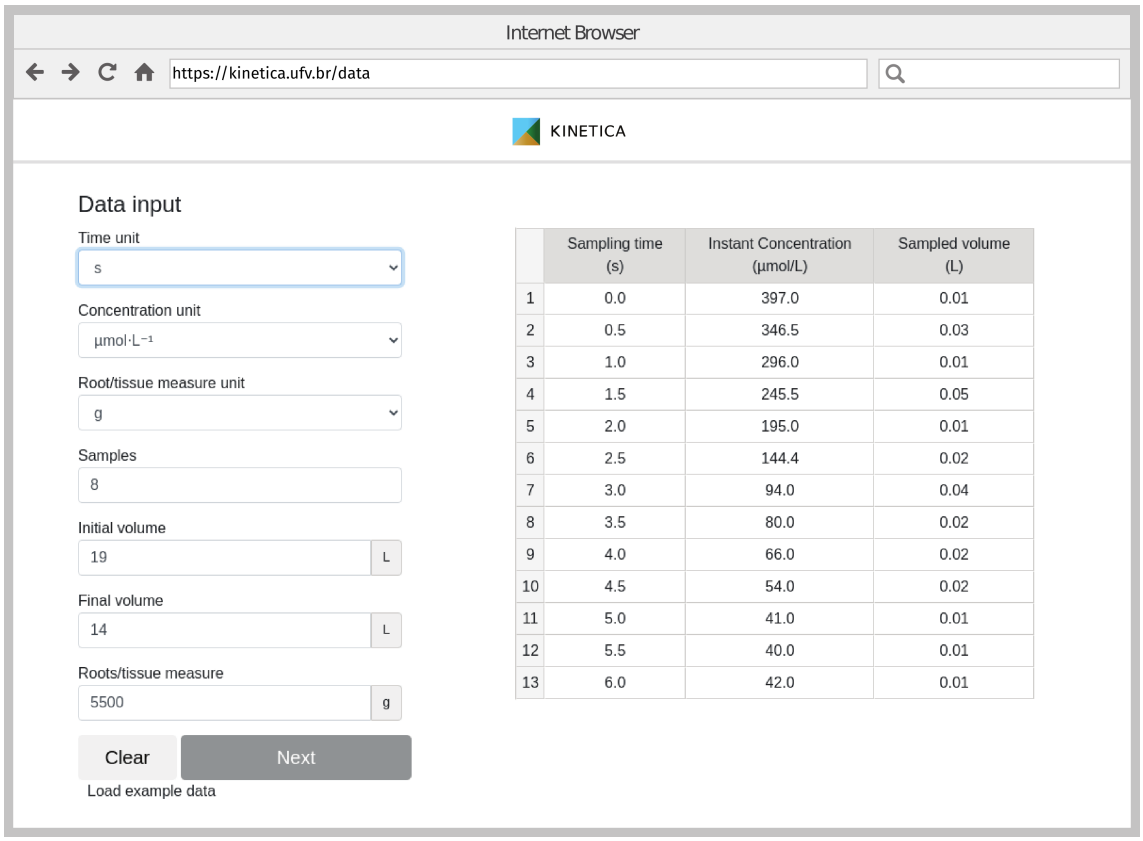

Figure 2.7: Kinetica Web-App input page. By hitting the button *Load example data* will automatically fill all the fields.

The *Time unit* and *Concentration unit* fields are drop-down menus from where the user may pick an option. Choosing an entry makes the application automatically modify the headers for the table, including the respective measure unit for each variable. It is imperative to note that, in this version, the application automatically sets the *Sampled volume* unit by extracting it from the denominator of the *Concentration unit.*

The user must input the sample volumes considering the unit shown in the table header. The column *Sampled volume* fields can be either left blank or filled with zeros, if in the sample volume was not considered as relevant or if it was replenished. When finished entering the data, the user may click on *Next*, which will send the data to the back-end processing. Once the response received from the API, the application loads the Results page (Figures 2.8, 2.9, 2.10).

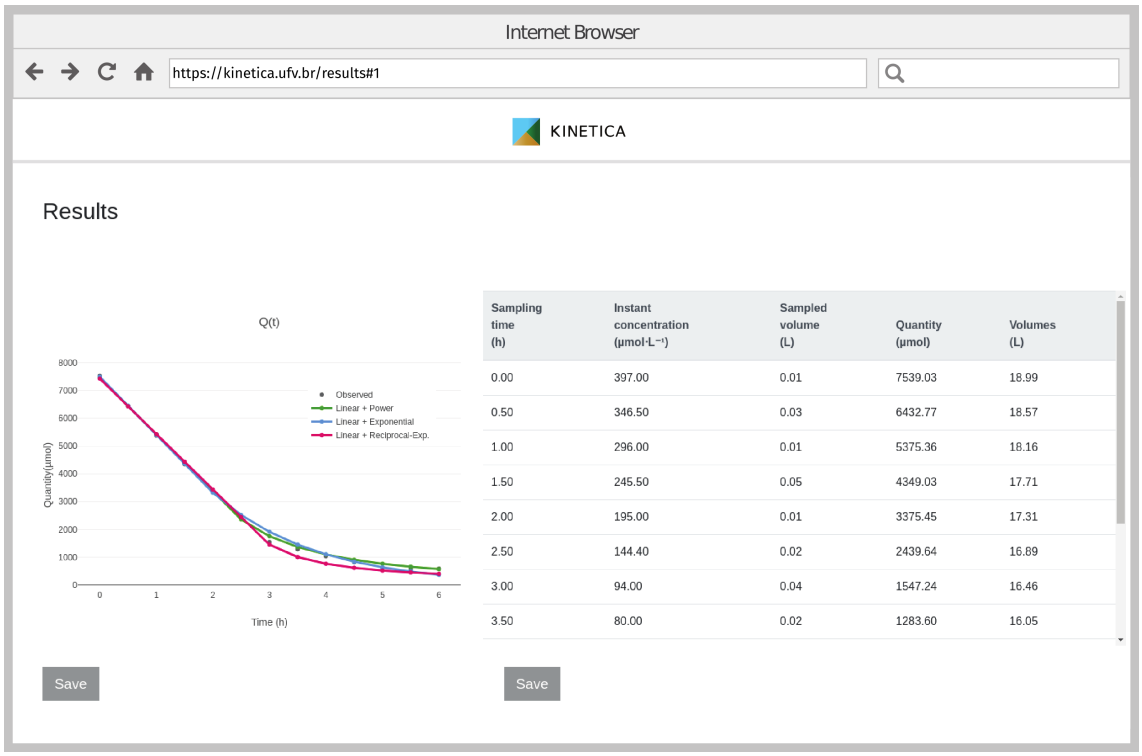

Figure 2.8: Kinetica Web-App *Results* page (section 1/3). The plots for the fitted models for the Graphical-mathematical models and a table containing primary input and estimated instant ion quantities and volumes.

The second section of *Results* (Figure 2.9 page displays the estimated ion uptake kinetic parameter values, statistical analysis results related to the models' fittings, and the significance of the estimated values for the kinetic parameters, the adjusted equations, the r squared values (simple and combined), *RSS*, *RMSE*, *AIC*, *BIC*, *t-test*, *F-test*, among others. Data from the Michaelis-Menten model fittings and the linearized plots (Lineweaver-Burk, Eadie-Hofstee, and Hanes-Woolf) are also available. All tables can be saved in ".txt", ".csv" or ".xlsx" format.

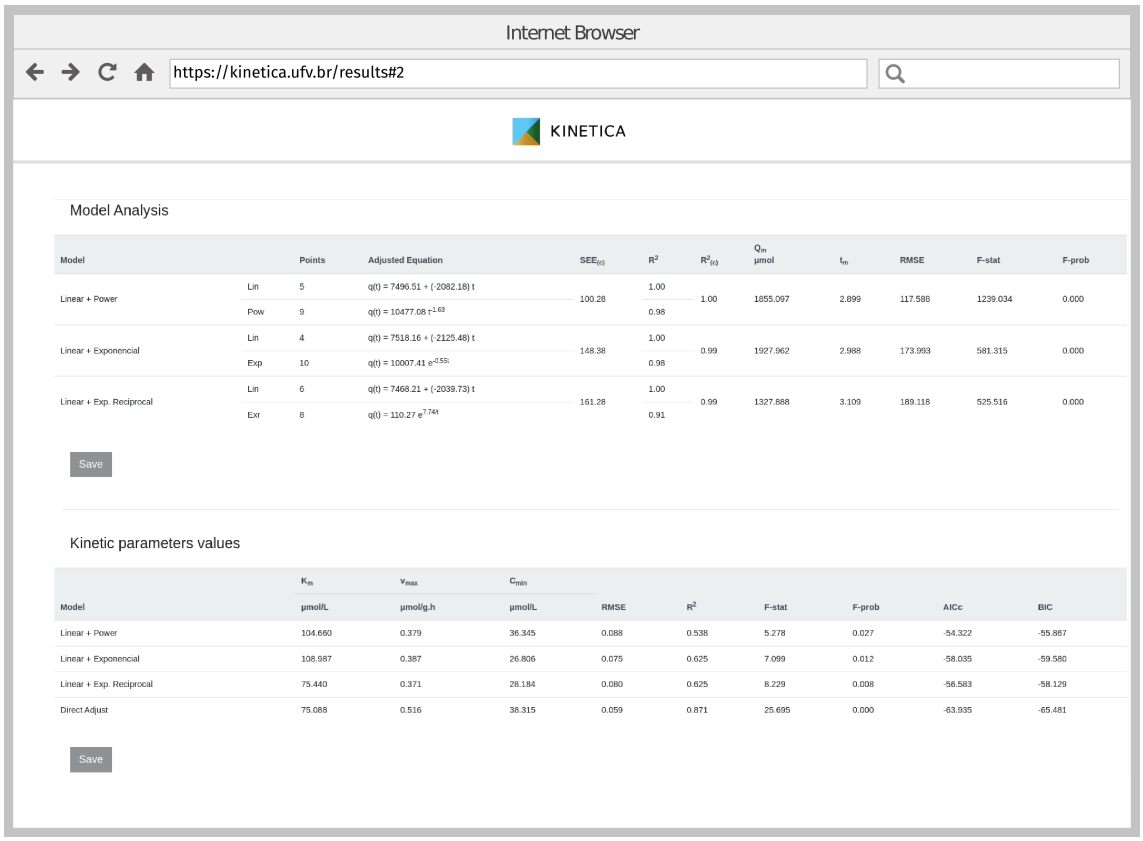

Figure 2.9: Kinetica Web-App ”Results” page (section 2/3). Model analysis results for each of the GMM fits and estimates for the uptake kinetic parameter values obtained by the Graphical-Mathematical Method and by the direct fitting to the Michaelis-Menten model.

Finally, the third section on the Results page (Figure 2.10) exhibits the charts for the Michaelis-Menten and the linearized plots for the linear-exponential model, as in the example case. The application also returns the plots for the linear-power, linear-exponential-reciprocal, and direct fit methods. All plots exhibit on this page can be saved to the users’ device or edited via the *Plotly API* service.

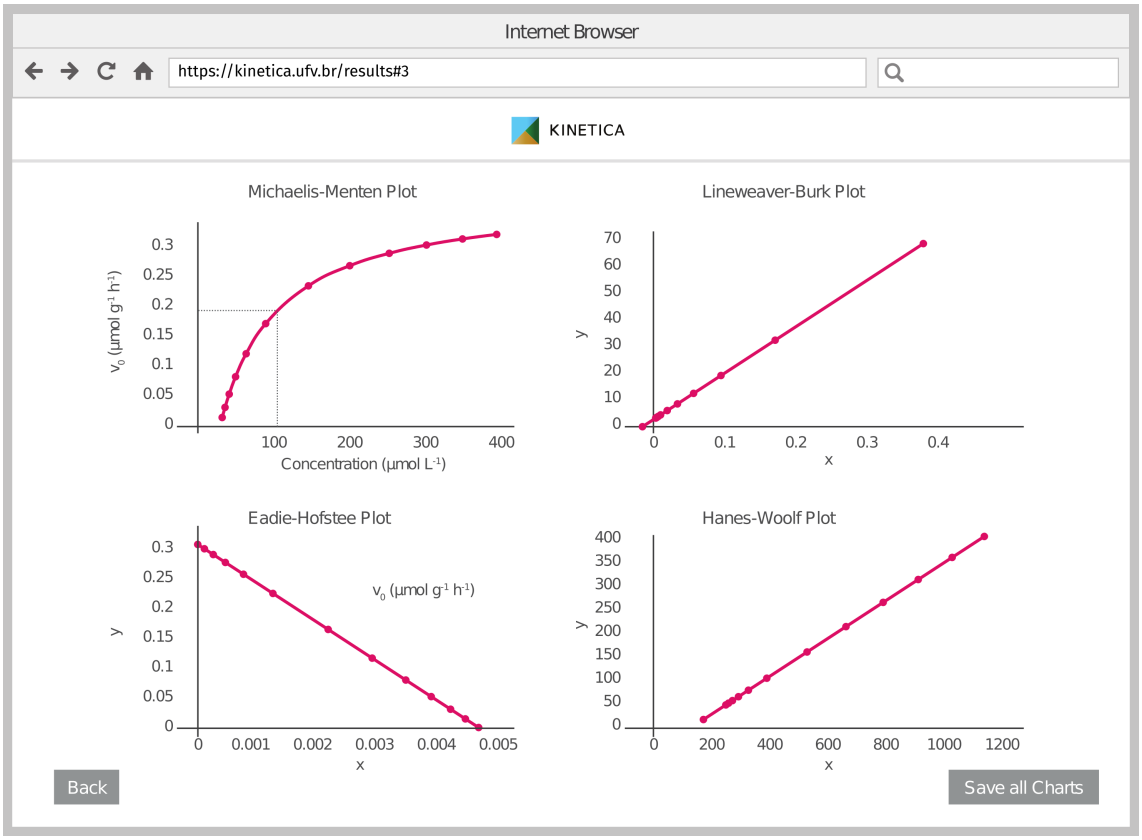

Figure 2.10: Kinetica Web-App ”Results” page (section 3/3). Michaelis-Menten and linearized plots for the linear-exponential model as an example. The application also returns the plots for the linear-power, linear-exponential-reciprocal, and direct fit methods.

For convenience, the application temporarily stores in the browser's cache the entered data, making it possible to perform any desired modification in the input dataset by clicking on ”BACK” and editing the entries in the ”Data input” page, even after getting into the Results page.

2.3.3 Kinetica API

Kinetica API accepts HTTP/POST method requests formatted in the JSON (JavaScript Object Notation) type. To get a valid example dataset over the API, users may submit an HTTP/GET request to the URI `http://api.kinetica.ufv.br` or `http://api.kinetica.cloud/?example`. In both request types, the application sends back a response to the client in a JSON/application data format.

Requests to Kinetica API are conceivable from several available services and applications, like *Postman*, *Excel VBA*, *Libre Office* Macro, and *R*, among others. One may

also choose to develop an application to communicate with the API, using any preferred programing language or framework, such as *JavaScript*, *Java*, *C-sharp*, and *Python*, for instance. Upon an HTTP/POST request, the application performs the processing on the remote server and returns the results to the client in a JSON/application format. The data package returned includes the estimated uptake kinetic parameter values (q_m, t_m, K_m, v_{max}, c_{min}), depletion equations, Michaelis-Menten model fittings, linearizations, and fit statistics (For further information, please see ***Suplemmentary Materials***).

2.3.4 Application availability

Web-Application

`http://kinetica.ufv.br` (main)

`http://app.kinetica.cloud` (alternative)

API URI

`http://api.kinetica.ufv.br` (main)

`http://api.kinetica.cloud` (alternative)

2.3.5 R Integration Script

`http://doi.org/10.5281/zenodo.3926847`

2.4 FINAL REMARKS

- Kinetica Web-App is user-friendly, presenting a straightforward and easy to work with interface, with features that facilitate data input and the visualization of results;
- Kinetica generates a relevant number of results for analysis and interpretation of uptake kinetic parameters in plants, which would require several tools separately to achieve. Some differential Kinetica features are the parameter estimation by the direct adjust method, c_{min} estimation, linearization plots for results interpretation, and support to varying volumes through samplings;
- In compliance with current software development trends, Kinetica Web-App and the API are reachable from any device connected to the internet, independently

of the operating system. Likewise, updates, fixes, and new features become promptly available from the instant its implementation on the server. Using Kinetica API, users can choose to deal with the input and the results data in any web-client of their choice;

- Kinetica does not permanently store any experimental data from the user's inputs. The application processes and manages all the client requests only by caching.

CHAPTER 3

UPTAKE KINETICS OF Zn APPLIED AS CHELATED SOURCES TO MAIZE PLANTS AFFECTED BY pH, AND Ca AND Mg

ABSTRACT

Kinetics parameters have a known potential as assets for developing agricultural systems with increased nutrient use efficiency, in selecting and breeding of plant varieties with improved nutrient uptake capabilities in face of abiotic stress conditions and low nutrient availability. Aiming to add to the comprehension of Zn kinetic uptake parameters of (K_m, v_{max}, and c_{min}) for different Zn sources, we ran an ion depletion essay on maize plants to evaluate the effects of two Zn sources, Zn–EDTA and Zn–EDDS , and a mineral source $ZnSO_4$, two solution conditions, simulating a low liming (*l*Lm) and an overliming condition(*h*Lm). The fitting of the data to the models was performed using the Kinetica computational platform. The interpolate.LSQUnivariateSpline class of the SciPy (Python) computational library was employed for segmentation of the depletion curves, obtaining for each *qxt* curve two segments, the first characterized as *order 0*, describing an absorption pattern under saturated conditions of the absorption mechanisms, while the second segment was characterized as unsaturated, describing an asymptotic curve in relation to the abscissa axis of the $q(t)$ function. The estimation of the parameter ${}_s v_{max}$ (saturated segments) was obtained by the derivative of the *order 0* model. For the asymptotic segment, the parameters K_m, ${}_a v_{max}$ and c_{min} were estimated by the graph-mathematical method (RUIZ, 1985) and by direct fit to the Michaelis-Menten model. The Zn depletion curves showed a double nonlinear pattern, with the first segment characterized by a saturation condition of Zn activity, while the second segment by an asymptotic pattern. Higher pH, and Ca and Mg activities reduced the value of c_{min} and raised the Km values on Zn uptake. Compared to Zn–EDTA, Zn–EDDS promoted faster Zn uptake, which may be due to its higher K_d^{app} and its property as a zincophore.

3.1 LITERATURE REVIEW

3.1.1 Mineral and chelated Zn sources

Zinc sources fall into four major classes: inorganic, synthetic chelates, natural organic complexes, and inorganic complexes. Inorganic sources include ZnO, $ZnCO_3$, $ZnSO_4$, $Zn(NO_3)_2$), and ZnCl. $ZnSO_4$ is possibly the most common source, being sold both in the crystalline form and in the granular form (MORTVEDT; GILKES, 1993).

Applying a zinc's mineral source, such as $ZnSO_4$ during the sowing operation is a practical solution. However, factors related to the source, soil, and the plant might hamper the fertilization efficiency. The plant uptake efficiency, the mobility of chemical species derived from the source dissolution, and interactions between the Zn species, phosphates, carbonates, and iron oxides in the soil medium are some of the most relevant of these factors .

Synthetic chelates are formed by combining a chelating agent with metal in its ionic form through a coordination bond (3.1). Applications of Zn chelates is a well-known strategy to mitigate these limitations, increasing the input Zn's availability to the plant uptake process.

$$M^{+a} + L^{-b} \rightleftarrows ML^{a-b} \tag{3.1}$$

Where: M^{+a} is the metal cation, and L^{-b} is the chelating agent (binder).

The chelate complex's stability directly affects the availability of the metallic ion to the plants and is evidenced by the chelate complex's stability constant. The equilibrium constant (*K*) will be given by 3.2

$$K = \frac{ML^{a-b}}{(M^{+a}) + (L^{-b})} \tag{3.2}$$

The most commonly used source of chelated Zn as fertilizer is Zn–EDTA (Na_2Zn-ethylenediamine-tetraacetate). The stability constant of this chelate is 17.5, much higher than that of Zn–EDTA (11.6). Thus, Zn–EDTA tends to be more stable than Ca–EDTA in soils with neutral to high pH, which may increase Zn availability to plants when this source is employed. (MORTVEDT; GILKES, 1993; NORVELL, 1991)

Besides, Zn–EDTA has high mobility in soils (BOAWN, 1973; GANGLOFF et al.,

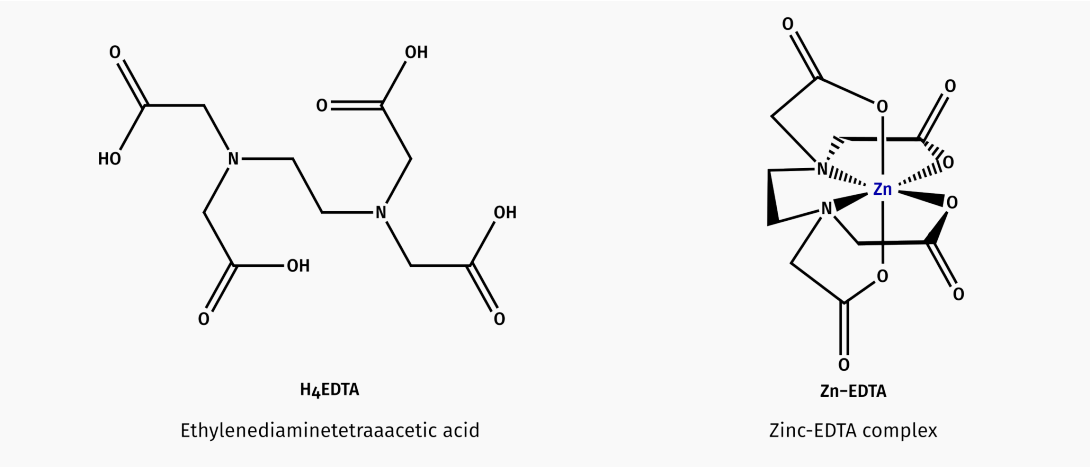

Figure 3.1: Molecular structure representation of EDTA and Zn–EDTA complex

2006). Zn–EDTA showed higher mobility than $ZnSO_4$ and was able to provide enough Zn even at the initial stage of the development of bean plants, in which the sulfate source appeared to be immobilized. Boawn (1973) also points out the water solubility among the main factors for the mobility of zinc sources in the soil.

According to Mortvedt and Gilkes (1993), the chelate Zn source Zn–EDTA can be two to five times more efficient than $ZnSO_4$ in the zinc supply for cultures.

However, the use of traditional chelating agents, such as EDTA and DTPA, also has downsides related to environmental behavior. These substances may present elevated toxicity to living organisms and show resistance to biological and even physical-chemical degradation and removal processes. As an alternative, new generation chelating agents such as EDDHA, IDS, DS, EDDS, GLDA, and MGDA emerged. These new products may be more efficient and present fewer environmental liabilities.

The development of new chelating agents has emerged as an alternative to bypass undesirable characteristics of these agents (KOLODYNSKA, 2012). New chelating agents such as o-EDHHA and EDDS have been considered for the composition of Zn and other micronutrient fertilizer sources, however few studies have targeted this subject so far.

The S,S–ethylenediamine disuccinic acid (EDDS), a structural isomer of EDTA, is one of the most promissing molecules for replacing the traditional chelating agents on fertilizers formulations. The S,S isomer of EDDS derives from L-aspartic acid, a naturally occurring amino acid, making it readily biodegradable. Its half-life lasts only for about 20 d, according to Kolodynska (2012). The industrially produced EDDS is a

mixture of four S, S(25%), R, R (25%), R, S (50%), S, R(50%) isomers.

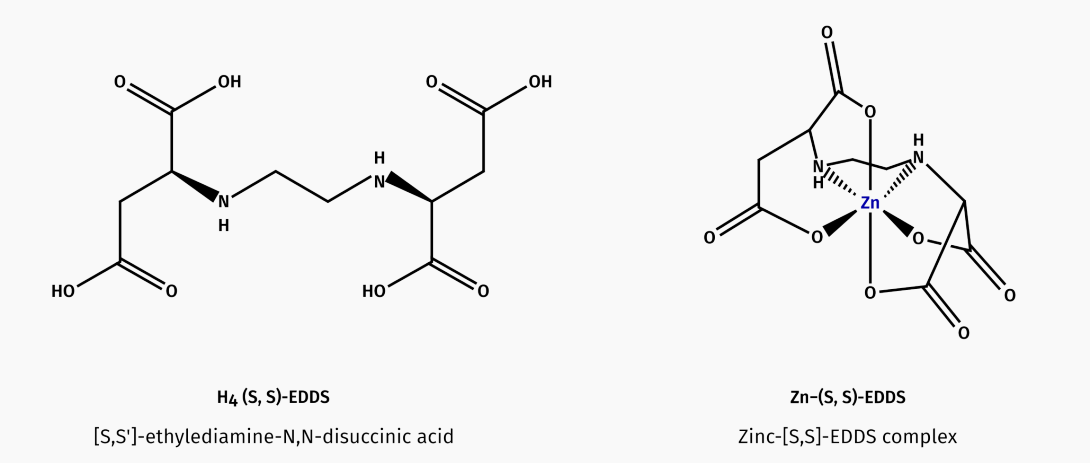

Figure 3.2: Molecular structure representation of S,S–EDDS and Zn–EDDS complex

Moreover when applied to a high Ca activity soil...

The Ca–EDDS exhibits an equilibrium constant of 13.4, while the Zn–EDDS, 4.6 (KOLODYNSKA, 2012). López-Rayo, Nadal, and Lucena (2016) studying the supply of Mn, Zn, and Cu in the nutrient solution to soybean and fava plants under high pH conditions (8.5) and $CaCO_3$ presence, verified that Zn–EDDS-fed plants exhibited higher leaf contents of this nutrient.

Such difference between the formation constants of the two complexes denotes an even higher specificity of this chelating agent by Zn, avoiding the substitution of this by Ca or other competing cations, especially in calcareous soils or under over-liming.

Although these studies consider high pH and calcium carbonate, other experiments are required in calcareous soil to extend these results to soil conditions (LÓPEZ-RAYO; NADAL; LUCENA, 2016).

3.1.2 Zinc in plants

Zn is preferably absorbed as a divalent cation (Zn^{+2}) and possibly as $ZnOH^{+}$. In the xylem's long-distance transport, the element is bound to organic acids or transported as the free divalent cation (BROADLEY et al., 2011). There are very high concentrations in the phloem, with Zn probably being complexed with organic low molecular weight solutes (KOCHIAN, 1993). The metabolic functions of Zn are based on their strong tendency to form tetrahedral complexes with N, O, and S, exerting these complexes, functional (catalytic), and structural role in enzymatic reactions.

Zn deficiency is common in plants growing on acidic soils or limestone soils. The most characteristic symptoms of dicotyledon deficiency are stunted growth due to the shortening of inter-nodes (rosette) and a drastic decrease in leaf area. Chlorosis and necrosis symptoms in older leaves are often caused by toxicity of P or B because, in Zn deficiency, the permeability of the plasma membrane of the root cells to P and also to B increases, causing these elements to be absorbed in excess. (BROADLEY et al., 2011).

In an abundant supply of Zn, toxicity can occur in non-tolerant plants, causing inhibition of root elongation (RUANO; POSCHENRIEDER; BARCELB, 1988). Frequently, Zn toxicity leads to chlorosis in young leaves, which may be a symptom of induced deficiency, such as Mg or Fe, due to the similar ionic Zn rays with these two elements. Zn concentrations varying from 15 to 20 mg kg^{-1} in leaves dry weight are considered deficient, and concentrations, ranging from 10 to 100 mg kg^{-1} in plants, would be within the optimum range of most crops. Critical toxic levels in leaves of plants are between 100 and 300 mg kg^{-1} of Zn in dry matter (MARSCHNER, 2012).

3.1.3 Zn kinetics uptake parameters

The estimate of the uptake kinetic parameter values can unveil key information on how plants react under the effect of specific environmental variables and conditions, not only to the ion lability but, in a general concept, to the ion bio-availability. In this sense, regarding crop plants, kinetics parameters can be an asset developing agricultural systems with increased nutrient use efficiency, by aiding to set better fertilizer application strategies, crop management, and in the processes of breeding and selecting plant varieties with improved nutrient uptake capabilities under abiotic stress conditions or low nutrient availability (ABBÈS et al., 1995; ARAÚJO et al., 2015; GRESPAN; DIAS; NOVAIS, 1998; GRIFFITHS; YORK, 2020; HORN et al., 2006; LI, Q. et al., 2017; LIMA et al., 2005; MACHADO; FURLANI, 2004; MARTINEZ et al., 2015; MENG et al., 2016; PAULA et al., 2018; RENGEL; GRAHAM, 1996; SANES et al., 2013; YORK; SILBERBUSH; LYNCH, 2016).

Notably, ion uptake kinetic parameters is influenced by plant species, cultivars, root and plant age, plant nutrient status, light, atmosphere and growth medium temperatures,water potential, aeration, mechanical impedance, and nutrient supply (BARBER,

S. A., 1979; TINKER; NYE, 2002).

By providing information on the plant side of the soil-plant relationship, the uptake kinetic parameter values may also be key input variables for modeling nutrient uptake from the soil, as for the mechanistic models (BARBER, S A, 1995; LIN; KELLY, 2010; MALAGOLI; LE DEUNFF, 2014; SILBERBUSH; BEN-ASHER; EPHRATH, 2005).

3.2 MATERIAL AND METHODS

We tested the kinetic uptake parameters of Zn absorption (K_m, v_{max}, and c_{min}) by maize plants under the effect of mineral and chelated sources of this micronutrient, solution pH values, and Ca and Mg activities. To this purpose, we conducted the depletion experiments employing $ZnSO_4 \cdot 7\,H_2O$ p.a. (Sigma-Aldrich, USA) and the chelated sources Zn–EDTA (Na_3EDTA, Merck, Germany, and $ZnNO_3 \cdot 6\,H_2O$, Sigma-Aldrich, USA) and Zn–EDDS ($ZnNO_3 \cdot 6\,H_2O$ and Na_3EDDS, Sigma-Aldrich, USA). Simulating a soil solution where the soil was under an over-liming condition meant a high pH value, Ca and Mg activities, and a contrast situation where pH and Ca and Mg activities are moderate.

3.2.1 Zn sources preparation and characterization

Reagents

Were employed as reagents $Na_2EDTA \cdot 2\,H_2O$ (ACS reagent ≥ 99 % w/w), Na3EDDS (35 % v/v), zinc nitrate hexahydrate – $Zn(NO_3)_2 \cdot 6\,H_2O$ (purum p.a, ≥ 99.0%) and sodium hydroxide (ACS reagent ≥ 99 % w/w) obtained from Sigma-Aldrich (USA). $ZnSO_4 \cdot 7\,H_2O$(purum p.a, ≥ 99.0%) and NaOH (puriss. 98-100.5%), from Merck(Germany).

Deionized water was obtained from a reverse osmosis system device OS10LXE (Gehaka Ltda., Brazil) and had the measured EC of ≤ 0.01 $\mu S\,cm^{-1}$ at 25 °C.

Zinc sulfate

(A) Zn 10.00 $mmol\,L^{-1}$: a mass 1.4378 g of $ZnSO_4 \cdot 7\,H_2O$ in 500 mL of deionized water.

Zinc chelates synthesis

(B) Zn 10.00mmol L^{-1}: $Zn(NO_3)_2 \cdot 6\,H_2O$

(C) $Na_2EDTA \cdot 2\,H_2O$ 10.50 mmol L^{-1}:

(D) Na_3EDDS 10.50 mmol L^{-1}

(E) NaOH 1.0 mol L^{-1}

Base chelates solutions (C and D) were prepared in a molar ratio of 1.05 in relation to the Zn from $Zn(NO_3)_2 \cdot 6\,H_2O$ solution (B), for the occurrence of excess of chelating agents in relation to Zn^{+2} ions. Zn chelated sources Zn–EDTA and Zn–EDDS were prepared by mixing and heating equal volumes of solutions of $Na_2EDTA \cdot 2\,H_2O$ and $Zn(NO_3)_2 \cdot 6\,H_2O$ and Na_3EDDS and $Zn(NO_3)_2 \cdot 6\,H_2O$, respectively, as the following: an aliquot of 100.0 mL Solution A was transferred to a glass beaker and heated using a hot plate magnetic stirrer until boiling point. Then solution C or D gradually poured. The resulting solution was maintained at 105 °C and stirred at 500 rpm for 2 h. After cooling at room temperature, the solution pH was adjusted to 6.5 by adding drops of solution D, transferred to a 500 mL volumetric flask, and the volume completed with deionized water, obtaining a 10 mmol L^{-1} Zn solution as a chelated source. The synthesized chelates were stored in amber flasks wrapped in foil at refrigerator temperature ($T \leq 5.0$ °C).

Chelates characterization

For the FTIR analysis, 25 mL aliquots of each Zn and Na chelates 10 mmol L^{-1} Zn were transferred to Petri dishes, added of 10 mL of ethanol p.a. 99% and oven-dried without forced circulation at the temperature 70°C, until partial elimination of the solvents and formation of crystals. The crystals were recovered and put to dry on filtration paper at the temperature of 80 °C. After 4.0 h, the crystals were removed from the oven and placed in a desiccator. Before the FTIR readings, a small sample of each chelates' crystals was ground in a ceramic mortar.

The FTIR spectra were obtained in a GladiATR (PIKE Technologies, USA) with attenuated total reflectance (ATR) accessory, equipped with a concave diamond prism,

coupled to a Varian 660-IR (Agilent, Technologies, USA) spectrometer. With scanning range from 4000 to 400 cm^{-1} with a total of 64 scans.

The complexation of the ions Zn^{+2} to EDTA and EDDS was evaluated through changes in the vibrational bands *v*asCO_2–, *v*sCO_2–, *v*C–N and *δ*N–H^+, since the complexation of metal ions occurs through the bonding of the two nitrogen atoms of the imine and an oxygen atom of each of the four carboxylate groups, changing the vibration intensities of the bonds.

The spectrum obtained for HNa_3EDTA before the addition of Zn^{+2} (3.3) presents a band close to 1622 cm^{-1}. Once the Zn^{+2} ions are added, the band changes to a region of 1590 cm^{-1}. In addition, there is the disappearance of the band close to 1358 cm^{-1} and the appearance of two bands close to 1113 cm^{-1}. The change of the band from 1622 cm^{-1} to 1590 cm^{-1} is attributed to the *v*asCO_2– band, while the bands at 1358 cm^{-1} and 1113 cm^{-1} are associated with the *v*C–N and *δ*N–H^+ bands. These results are in accordance with Lanigan and Pidsosny (2007) and provide evidence of Zn complexation with EDTA.

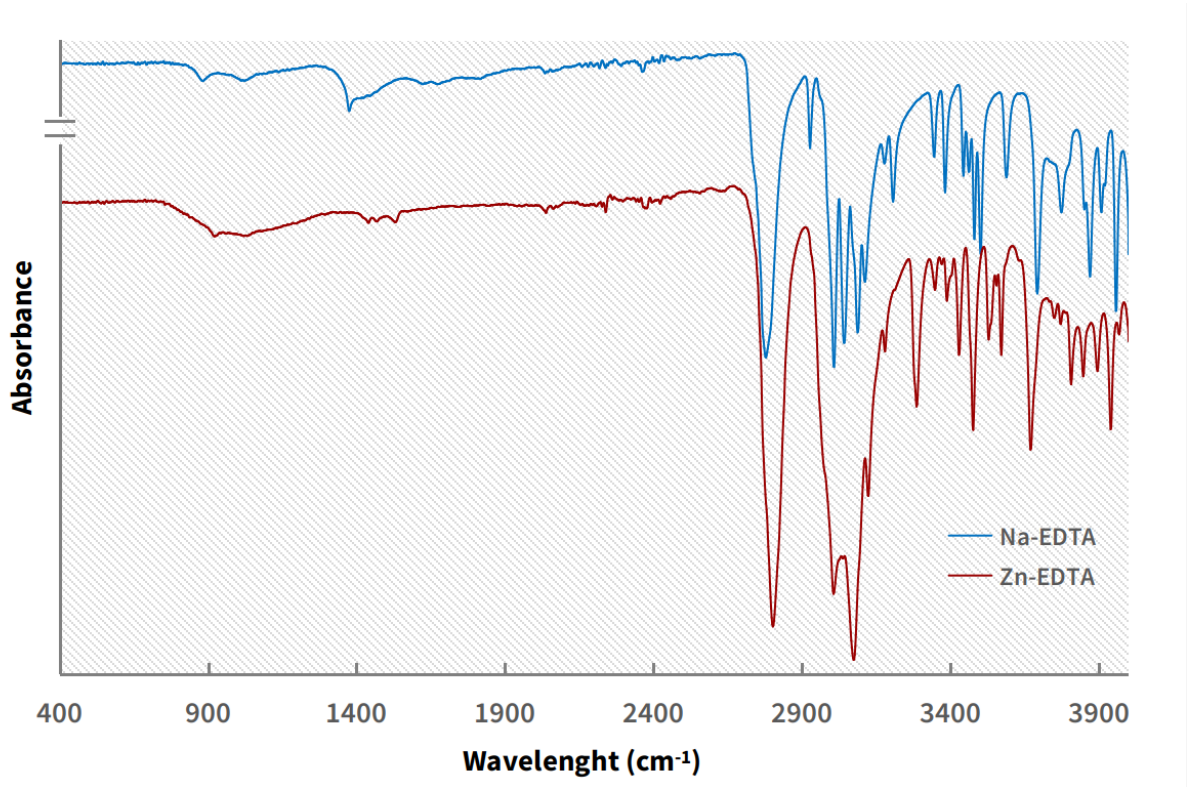

Figure 3.3: FTIR: Zn–EDTA x Na–EDTA

For EDDS (3.4), at higher pH (≥ 8.30), the ATR-FTIR spectrum has two characteristic bands of completely free ionized carboxyl groups, one at 1569 cm^{-1}, corresponding

to the asymmetric stretching vibration ($\nu as CO_2$–) and the other at 1392 cm^{-1}, attributed to symmetrical stretching vibration ($\nu s CO_2$–). Comparing the spectra obtained for the EDDS before and after the complexion with zinc ions , it is possible to observe a displacement of the characteristic peaks of the carboxylate group and a widening of the band 1392 cm^{-1} after the complexation. This change in the spectra can be justified by the presence of the complexed zinc ion by EDDS.

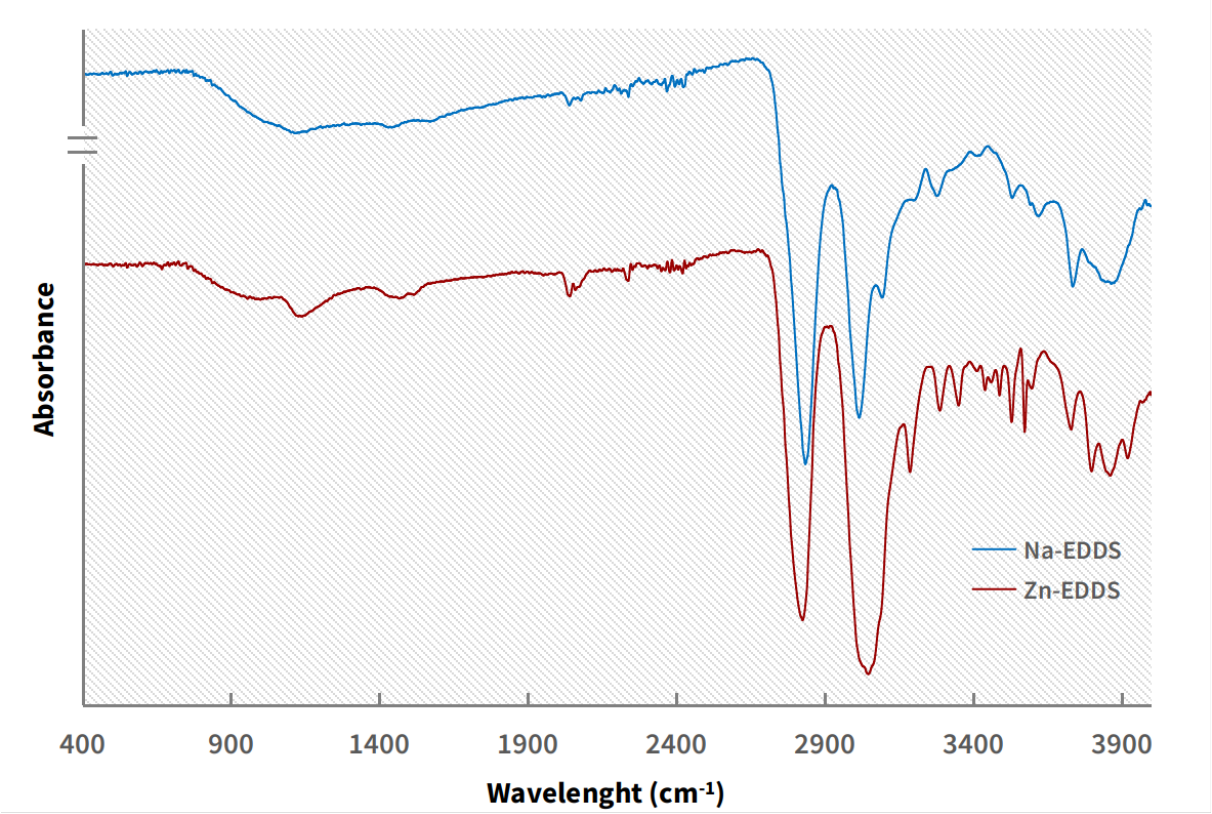

Figure 3.4: FTIR: Zn–EDDS x Na-EDDS

3.2.2 Plant cultivation

Seeds of the maize single cross hybrid BM-812 (Biomatrix, Brazil) were sown on acid-washed sand, and moisture was kept around 80% of field capacity with deionized water. Six days after emergence, seedlings were transferred to grow in an NFT system (3.5), where each row contained eight plants, spaced by 30 cm.

We employed an adapted nutrient solution from Hoagland, Arnon, et al. (1950), with the following formulation (mg L^{-1}): 223 Cl, 220 N, 180 Ca, 180 K, 62 S, 50 Mg, 25 P, 5 Fe, 0.67 Mn, 0.5 B, 0.32 Cu, 0.091 Zn, 0.024 Mo and 0.011 Na. The solution's pH was constantly checked and, when necessary, fixed to 6.00 ± 0.5 by adding a 1.00 mol L^{-1}

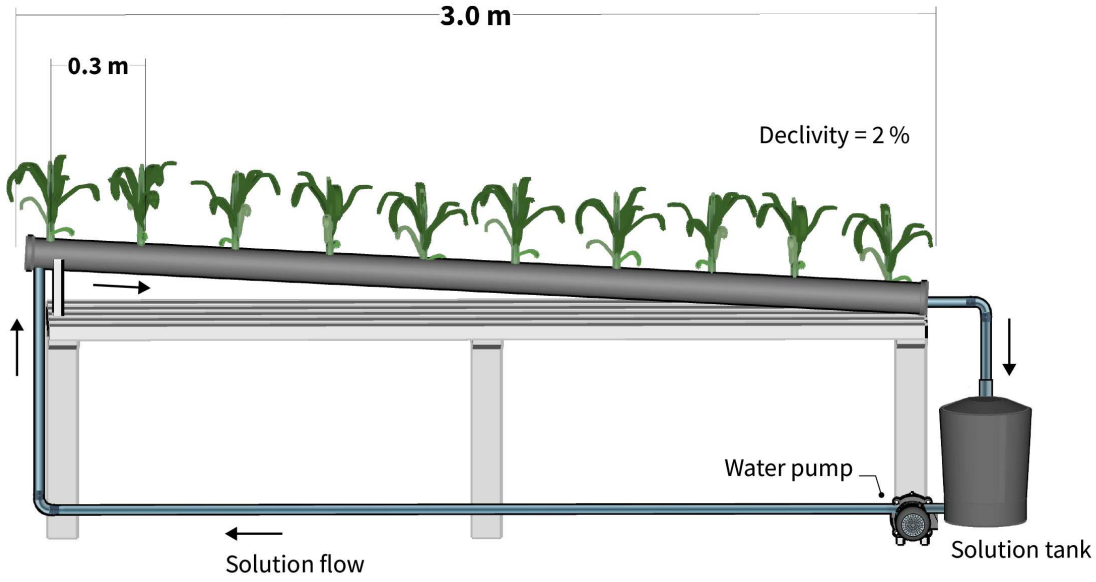

Figure 3.5: NFT system schema set for the Zn depletion experiment

HCl or NaOH solution. When the plant presented seven completely developed leaves, reaching the V_7 stage, we performed the exhaustion tests as described next.

3.2.3 Ion depletion experiments

In stage V7, all the cultivation apparatus was cleaned and decontaminated by rinsing with tap water, then with a 0.25 mol L^{-1} HCl solution, and finally, with deionized water. After that, plants were supplied with the nutrient solution's half-strength, containing all the essential elements, but Zn. After seven days, the plants were subject to the exhaustion test. The treatments comprised three Zn sources ($ZnSO_4$, Zn–EDTA, and Zn–EDDS) and two liming conditions, *l*Lm (low Ca + Mg concentration and low pH, *h*Lm , with high Ca + Mg concentration and pH), with two replicates (n = 2) in a completely randomized design, summing up 12 experimental units. Each NFT row was taken as a single experimental unit.

For homogenizing radiance conditions, supplementary PAR was provided by full-spectrum LED panels, whenever natural PAR readings felt below a PFFD of 2000 µmol m^{-1} s^{-1} photons, employing an automated micro-controlled system built with the Arduino platform and an RGB light sensor calibrated with a LI190R Quantum Sensor (Campbell Scientific, USA).

The exhaustion test solution for the conditions low Ca + Mg and low pH comprised 10 µmol L^{-1} of Zn, supplied as $ZnSO_4$, Zn–EDTA or Zn–EDDS. For the *h*Lm condition, Ca concentration was 1.00 m mol L^{-1} and Mg 0.25 m mol L^{-1}. Ca and Mg were supplied as $Ca(NO_3)_2$ and $Mg(NO_3)_2$ p.a. salts and the solution pH was buffered by the addition of MES to meet 2.5 µmol L^{-1} and hold the pH around 7.0. The sampled volume was replaced with a 10.0 mmol L^{-1} KNO_3 solution. For *l*Lm the initial concentrations of Ca and Mg were 250 µmol L^{-1} of Ca and 50 µmol L^{-1} of Mg. The pH was fixed every sampling time fit around 5.5 with 0.05 mol L HCl or KOH.

3.2.4 Data modelling and analysis

The Zn concentration of the samples was determined by atomic absorption spectrophotometry. The kinetic parameters, ${}_s v_{max}$, K_m, ${}_a v_{max}$, and c_{min}, relative to the absorption of Zn were estimated from the instant concentrations, estimated solution volumes, samplings times and roots fresh weight following the the workflow illustrated in 3.6.

Outlier data entries were removed using Dixon's Q-test (3.3), at 95% confidence level:

$$Q_{exp} = \frac{x_n - x_{n-1}}{x_n - x_1}; Q_{\alpha,n} = 0.05 \tag{3.3}$$

Q_{exp} is the Q statistic value, x_1 is the smallest (suspect) value, x_2 is the second-smallest value, and x_n is the largest value.

After outlier removal, the general depletion curves were segmented into two sequential subsets. For this task, we employed the package *pwlf* (JEKEL; VENTER, 2019), for finding four optimal break points inside the depletion curve. The package performs the piecewise linear curve fitting employing the differential evolution algorithm (STORN; PRICE, 1997), allowing data regularization and segmentation based on data patterns along a data pair sequence.

The four internal break points obtained as output from *pwlf* were used as arguments values into the method scipy.interpolate.LSQUnivariateSpline (VIRTANEN et al., 2020) to obtain the spline describing the experimental data closely, by fitting a piecewise function by least-squares accounting for the breakpoints.

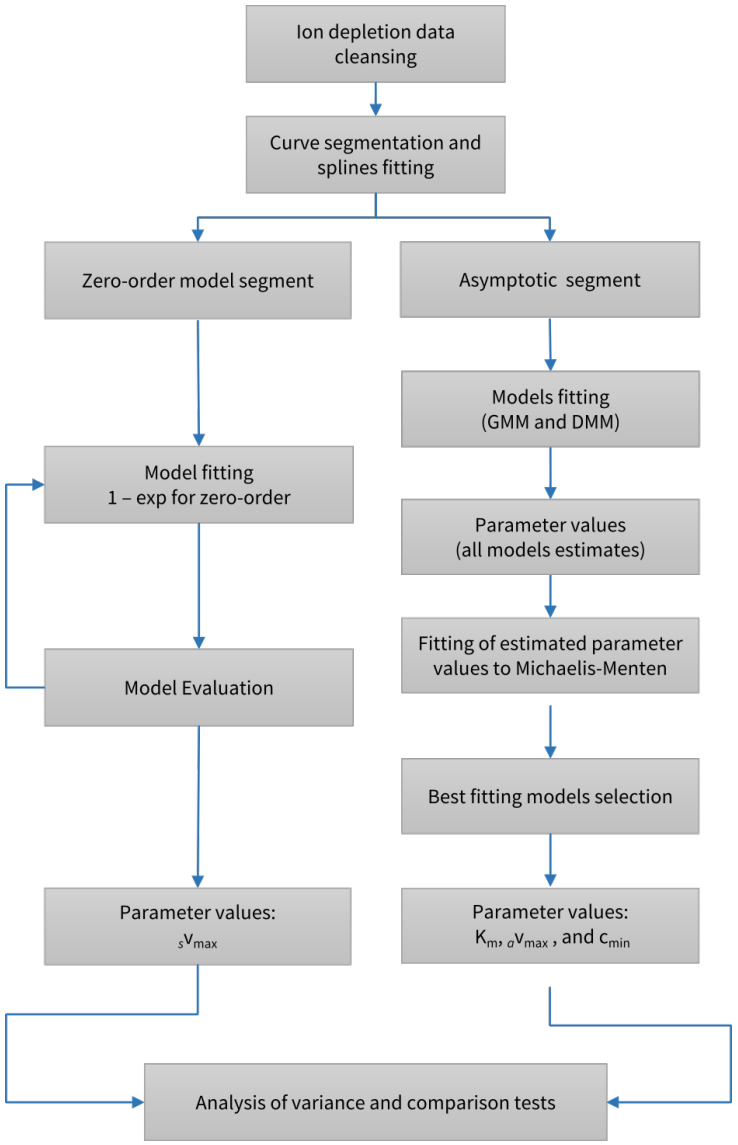

Figure 3.6: Zn's depletion data analysis workflow

The data obtained were submitted to correlation analysis by using Kendall's Tau Rank Correlation Coefficient, analysis of variance (ANOVA), normality by the Shapiro–Wilk test.

3.2.5 Estimation of uptake kinetics parameters

The data obtained for the first segment of each depletion curve was processed as a zero-order mechanism. For zero-order kinetics, the change in substrate concentration remains constant over time3.4: The transformation with product depends on v_{max}

(const.) and v (KELLER; ZELLNER, 1996)(3.5):

$$\frac{\delta c}{\delta t} = const. \tag{3.4}$$

$$v = \frac{\delta P}{\delta t} = -\frac{\delta c}{\delta t} \tag{3.5}$$

Ion depletion in solution can simply be then explained by 3.6:

$$c = c_0 - v_{max}\, t \tag{3.6}$$

For the asymptotic segments, the kinetic parameters v_{max}, and K_m, and c_{min} were estimated by the technique proposed by Claassen and Barber (1974) was used, where the concentration of each sample is multiplied by the volume of solution at the time of sample withdrawal, obtaining quantity (q) as a function of sampling time t. The kinetic parameters v_{max} and K_m are then calculated from this function, δq / δt. The c_{min} is given by estimating the concentration at the last point of the curve $q(t)$, as shown in Equation 3.7:

$$Q = c\, V \tag{3.7}$$

A plot of Q as a function of time, t, gives a curve showing the depletion of the ion from solution resulting from plant absorption and is called the depletion curve. The net influx at any point is given by $-\delta q/\delta t$. The slope of the curve can be calculated by expressing q as a function of t and calculating the derivative.

To estimate the kinetic parameters, we employed the Graphical-Mathematical Method, proposed by Ruiz (1985), which divides the function $q(t)$ into a linear segment and an asymptotic segment.

In addition to the Graphical-Mathematical method, we estimated of the kinetics parameter values by directly fitting the instantaneous concentrations, $c(t)$, to the modified Michaelis-Menten model (Equation 3.8). After estimating the instant concentrations, the data is fitted to the Michaelis-Menten Model using a direct least squares method, by employing the Levenberg-Marquardt gradient method (greedy algorithm) to minimize

the objective function, packed in *Scipy* (VIRTANEN et al., 2020) Python library.

$$v = \frac{v_{max}\left(c - c_{min}\right)}{K_m + \left(c - c_{min}\right)} \quad (3.8)$$

v is the uptake rate or velocity; c_{min} the minimum concentration for positive influx; v_{max} the maximum uptake rate or velocity and c the ion instant concentration in the bulk solution and K_m the Michaelis constant or the concentration at half-saturation.

The calculations were made from a web application developed in the Python language (Chapter II). The input data in the software were the collection times (h), the instantaneous concentration of solution zinc (μmol L^{-1}), the exhaust solution volume (L), the duration of the sampling period (h), and the mass of fine roots (g).

3.2.6 Variance analysis and comparison tests

Statistical analyzes were performed using core R (R DEVELOPMENT CORE TEAM, 2019) libraries and the packages *GFD* (FRIEDRICH; KONIETSCHKE; PAULY, 2017) and *ExpDes* (FERREIRA; CAVALCANTI; NOGUEIRA, 2014). Significant sources of variation and interactions obtained from the WTPS statistics were compared by the Student-Newman-Keuls test at the 5% probability level.

3.3 RESULTS

3.3.1 Environmental conditions

Environmental variables Environmental condition during the period of experimental data was collected sufficiently homogeneous. The atmospheric temperature (3.7) varied from 19.5 to 29.3°C, with an average value of 24.4°C. Air relative humidity (3.7) varied from 62% to 93% with a mean value of 79%. The nutrient solution temperature (3.7) had a very narrow oscillation, ranging between 21.5 to 24.9°C, and an average value of 23.4°C. The root medium temperature in determinant of nutrient uptake kinetics, impacting on root metabolic activity as in ionic activity.

Even with fluctuations of the natural PAR (3.8) during the experimental curse, the artificial PAR supplemented was effective keeping total PAR (natural + complementary) near to 2000 μmol m^{-1} s^{-1}.

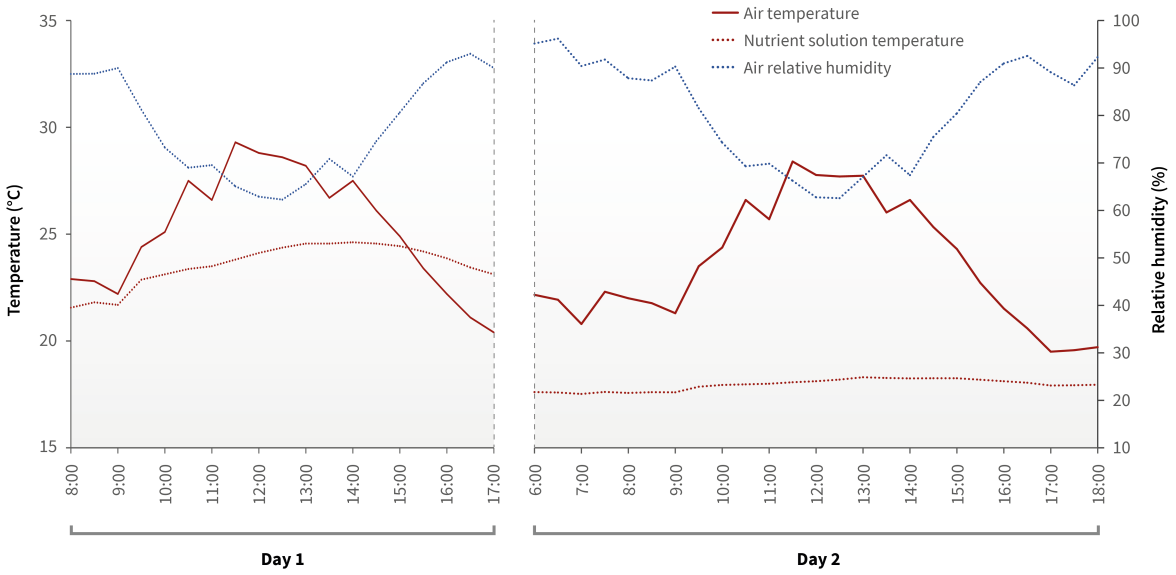

Figure 3.7: Air relative humidity, atmospheric temperature, and temperature measure in the depletion solution during the exhaustion experiment

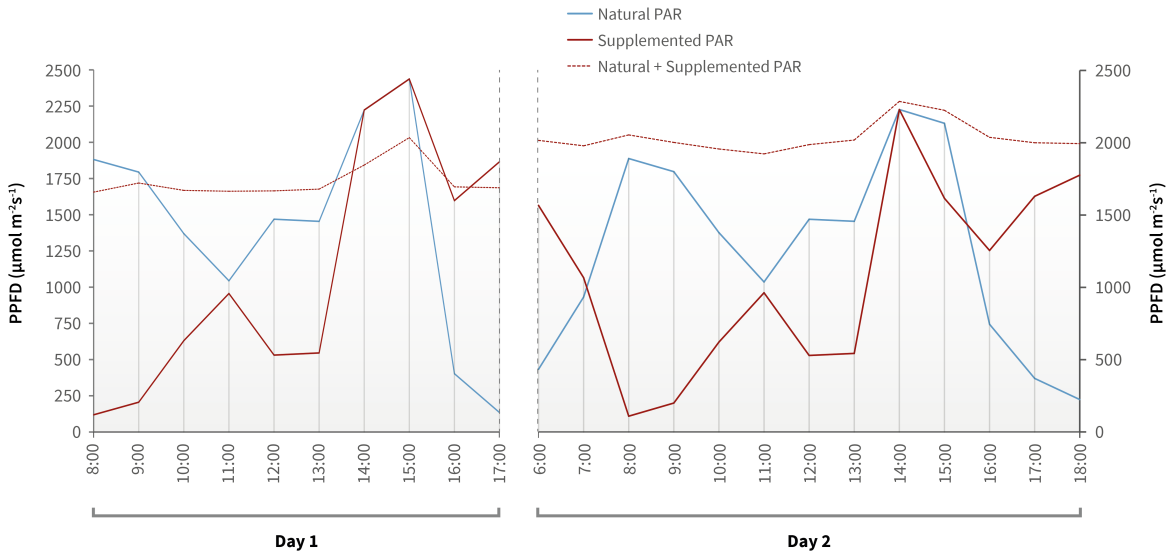

Figure 3.8: Natural and compensated PAR

3.3.2 Zn depletion in the nutrient solution

Zinc depletion curves, in both *l*Lm and *h*Lm conditions, exhibited a double non-linear pattern 3.9. The first segment characterizes the main effect of a non-mechanism, while the second draws an asymptotic trajectory towards the x-axis, characterizing a saturation uptake kinetics.

The segmentation by the differential evolution algorithm for two segments had an elevated goodness of fit and was highly significant (3.1); t br and q br are the Cartesian coordinates (x, y) for the estimated breakpoint value that indicates the beginning of predominance of an asymptotic uptake mechanism. The path described responding to Zn supply as Zn–EDTA diverges strongly from the other Zn sources, even from the other chelate and EDTA isomer, EDDS. For instance, the t br and q br values for Zn–EDTA under *h*Lm are respectively, 7.99 h and 149.471 μmol L^{-1}, while for Zn–EDDS the values 4.84 h and 81.120 μmol L^{-1}.

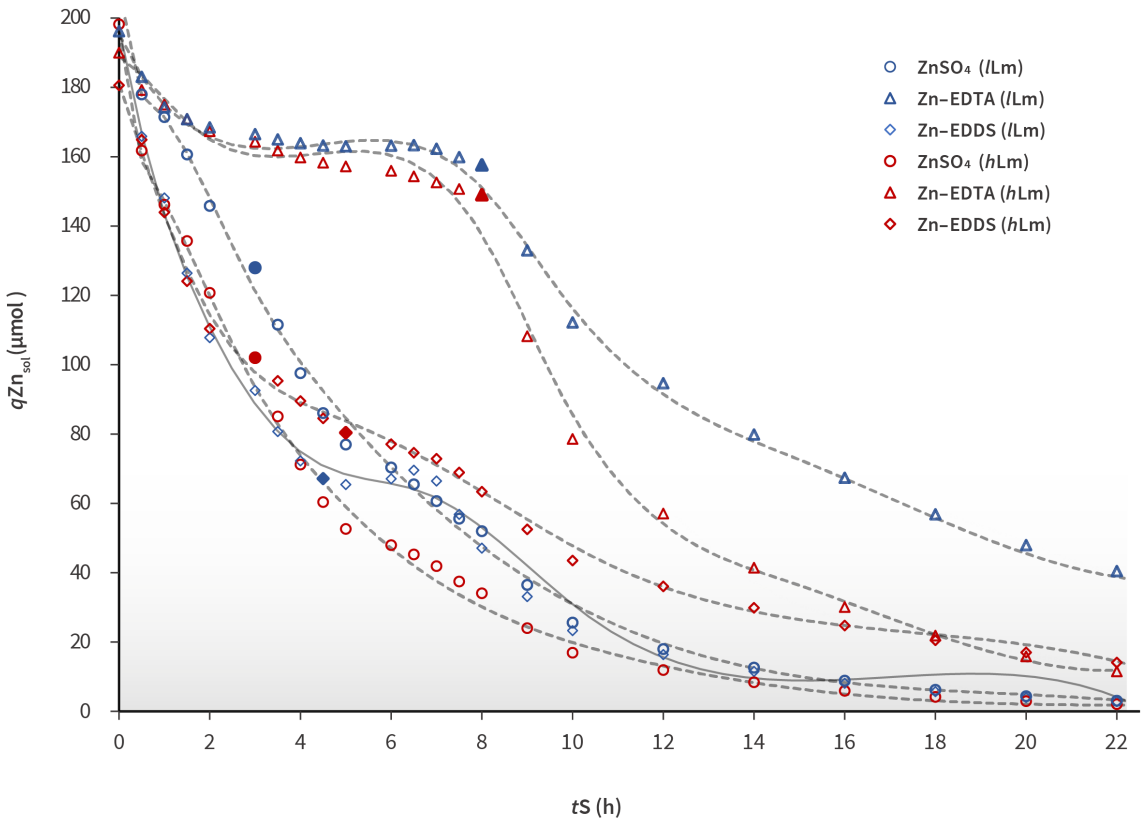

Figure 3.9: General depletion curves

3.3.3 Data analysis

To estimate the uptake kinetic parameters, a zero-order function fitted to the first. To the asymptotic the Graphical-Mathematical method and the direct fit to the Michaelis-Menten model were employed.

Table 3.1: Depletion data piecewise segmentation

Liming level	Source	t_{br}	q_{br}	RMSE	τ_b	p-value (τ_b)
	$ZnSO_4$	3.00	127.303	3.243	0.997	<0.001
***l*Lm**	**Zn–EDTA**	7.91	159.880	2.172	0.999	<0.001
	Zn–EDDS	4.37	65.848	3.648	0.921	<0.001
	$ZnSO_4$	3.00	100.719	3.238	0.960	<0.001
***h*Lm**	**Zn–EDTA**	7.99	149.471	3.852	0.834	<0.001
	Zn–EDDS	4.84	81.120	2.262	0.998	<0.001

The initial depletion curve segments, accounted for by the zero-order uptake mechanism, exhibited a strong correlation with low RMSE and high τ_b (3.2). The confidence intervals for ${}_s v_{max}$ are quite narrow, indicating a low uncertainty about this parameter estimated values. Here again the estimated values for Zn–EDTA strayed from the ${}_s v_{max}$ values for the other Zn sources, being about three-fold Zn–EDDS and four-fold smaller of the $ZnSO_4$ ${}_s v_{max}$ mean values.

Table 3.2: Zero-order uptake segment models

Liming	Source	RMSE	R^2adj.	τ_b	p-value (τ_b)	${}_s v_{max}$ 95% CI
	$ZnSO_4$	0.263	0.969	0.947	<0.001	[1.108–1.109]
***l*Lm**	**Zn–EDTA**	0.198	0.719	0.751	<0.001	[0.251–0.254]
	Zn–EDDS	0.262	0.942	0.891	<0.001	[0.734–0.735]
	$ZnSO_4$	0.289	0.958	0.925	<0.001	[1.051–1.051]
***h*Lm**	**Zn–EDTA**	0.200	0.514	0.572	<0.001	[0.191–0.193]
	Zn–EDDS	0.324	0.878	0.835	<0.001	[0.601–0.602]

To estimate the values of K_m, ${}_a v_{max}$ and c_{min} the zero-order, or the asymptotic segments where fitted both by the directly by fitting the depletion data to the Michaelis-Menten model (DMM), and indirectly by employing the Graphical Mathematical Method (GMM) (RUIZ, 1985). From the last method, three sets of parameter values were obtained, one for each association of a linear and a nonlinear function (power, exponential, exponential-reciprocal).

For choosing among the four model results (Direct adjust, Linear–Power, Linear–Exponential, and Linear–Exponential-reciprocal), the estimated values for the parameters obtained by the GMM were fitted to the Michaelis-Menten model. Then, we proceeded to compared among these models each other based on the results obtained

from the DMM. As criteria, we utilized the penalized-likelihood (AIC_c and BIC) and rank correlation (τ_b). The fittings with higher correlation and smaller values for the penalized likelihood were selected for the variation analysis and comparisons.

Table 3.3: Asymptotic segments selected models

Source	Model	RMSE	R^2 adj.	p-value (F)	τ_b	p-value (τ_b)	AIC_c	BIC
$ZnSO_4$	**LPW**	0.0028	0.509	<0.01	0.728	<0.01	-152.517	-152.315
Zn–EDTA	**LER**	0.0066	0.138	<0.05	0.944	<0.01	-87.695	-91.904
Zn–EDDS	**LPW**	0.0052	0.503	<0.01	0.998	<0.01	-115.612	-115.658
$ZnSO_4$	**LEX**	0.0021	0.562	<0.01	0.897	<0.01	-159.605	-159.404
Zn–EDTA	**LPW**	0.0085	0.514	<0.05	0.996	<0.01	-85.529	-85.903
Zn–EDDS	**LEX**	0.0026	0.309	<0.05	0.927	<0.01	-130.721	-130.767

3.3.4 Parameter analysis of variance and comparison

The results of the WTPS variance analysis at for all the estimated uptake kinetic parameters are exhibited on 3.4. The effect of liming on the parameters ${}_s v_{max}$ ($p < 0.01$), K_m ($p < 0.001$), c_{min} ($p < 0.05$, and c_{min} ($p < 0.05$). The effect of the Zn sources was consistently significant for all parameters ($p < 0.001$).

Table 3.4: Liming and source significance to parameter variation

SV	df	Parameter			
		${}_s v_{max}$	**K_m**	**${}_a v_{max}$**	**c_{min}**
Liming (L)	1	**	***	*	*
Source (S)	2	***	***	***	***
L × S	2	*	**	***	ns

Significance probability level codes: * ($p < 0.05$), ** ($p < 0.01$), *** ($p < 0.001$), and ns ($p \geq 0.05$)

Liming levels interaction with sources was found significant for ${}_s v_{max}$ ($p < 0.05$), K_m ($p < 0.01$) and v_{min}($p < 0.001$), however had no significance on c_{min} ($p \geq 0.05$).

On figure 3.10 are plotted the results of SNK comparison test for the ${}_s v_{max}$ at confidence level of 5% ($\alpha = 0.05$). The effect of liming significantly decreased the values of ${}_s v_{max}$ for all sources (3.10.a). For both levels of liming (*l*Lm and *h*Lm), the values of ${}_s v_{max}$ are greater for $ZnSO_4$, followed by Zn–EDDS , and Zn–EDTA is the zinc source that appears with smaller values (3.10.b).

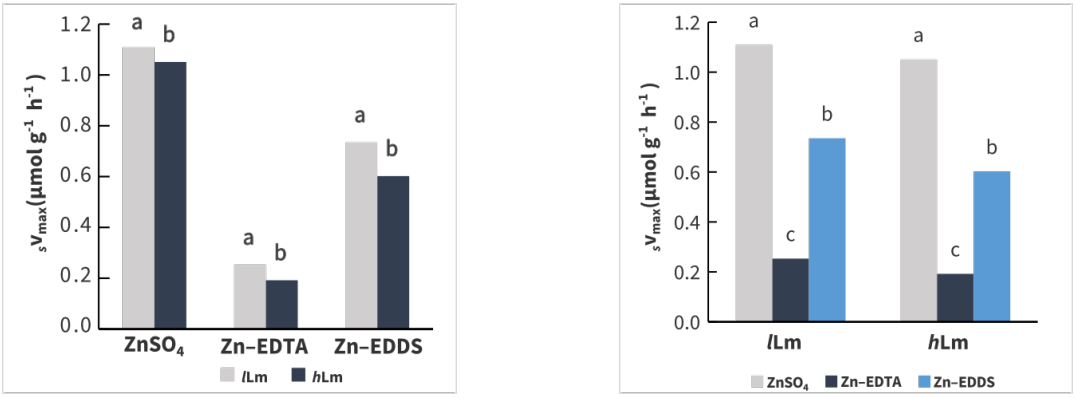

(a) Effects of Zn sources on ${}_{s}v_{max}$ inside liming (b) Effects of liming levels on ${}_{s}v_{max}$ levels

Figure 3.10: Effects of liming levels and Zn sources on ${}_{s}v_{max}$ values

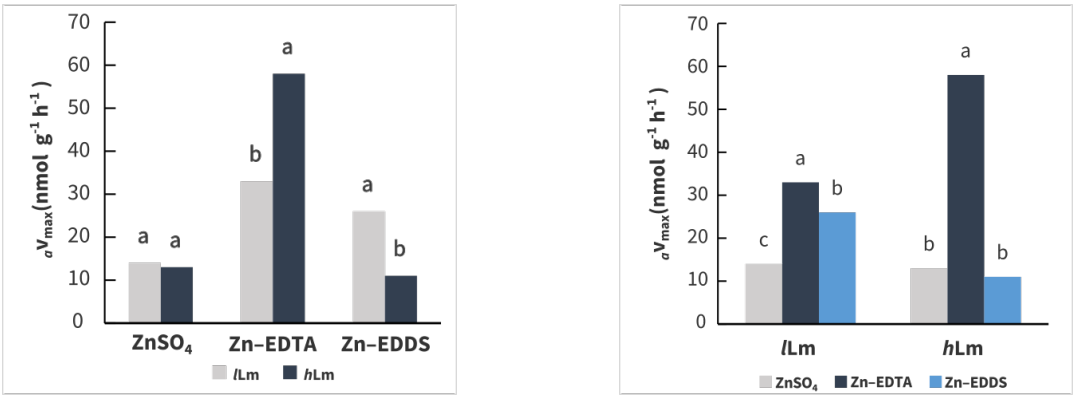

(a) Effects of Zn sources on ${}_{a}v_{max}$ inside liming (b) Effects of liming levels on ${}_{a}v_{max}$ levels

Figure 3.11: Effects of liming levels and Zn sources on ${}_{a}v_{max}$ values

On figure 3.11 bar plots show the results of SNK comparison test for the ${}_{a}v_{max}$ The effect of liming had no significant effect on ${}_{a}v_{max}$ when the Zn source was $ZnSO_4$ at confidence level of 5% ($\alpha = 0.05$). For Zn–EDTA , we found lower values for this parameter for *l*Lm in comparison to *h*Lm . When Zn–EDDS was the source the pattern inverts, and the values of ${}_{a}v_{max}$ were greater for the *l*Lm condition (3.11.a).

When evaluating the results inside *l*Lm , the values of ${}_{a}v_{max}$ are smaller for $ZnSO_4$ and broader for Zn–EDTA , followed by Zn–EDDS . In the *h*Lm condition, $ZnSO_4$ and Zn–EDDS values had no significant difference when compared with the SNK statistics at 5% confidence level, and Zn–EDTA appears with a much higher value compared to the other two sources(3.11.b). The liming levels had no significant effect on the values of K_m when the source was $ZnSO_4$ of Zn–EDDS . Conversely, when Zn–EDTA was the Zn source, the values for K_m were greater for the *l*Lm condition. Inside the liming

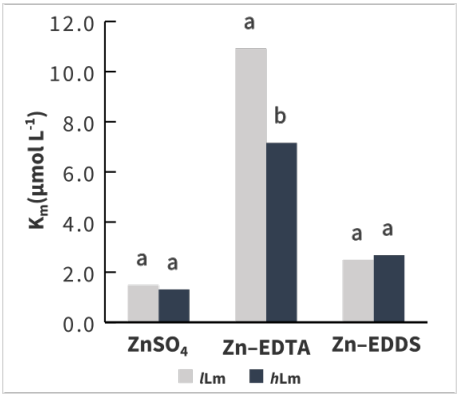

(a) Effects of Zn sources on K_m inside liming levels

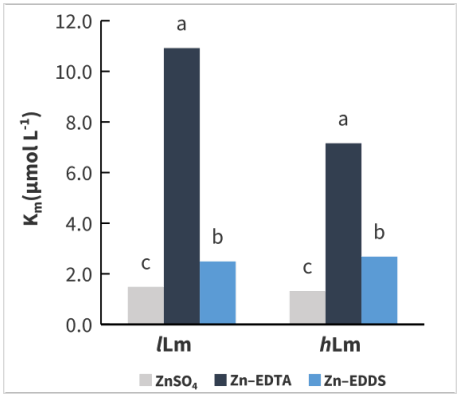

(b) Effects of liming levels on K_m

Figure 3.12: Effects of liming levels and Zn sources on K_m values

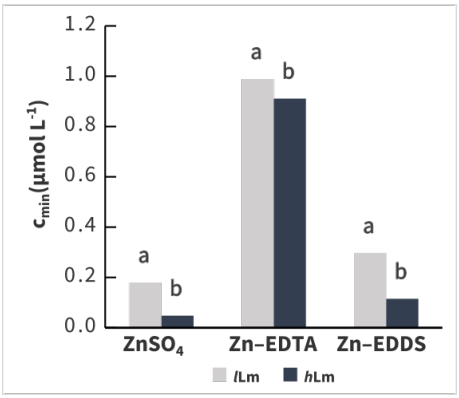

(a) Effects of Zn sources on c_{min} inside liming levels

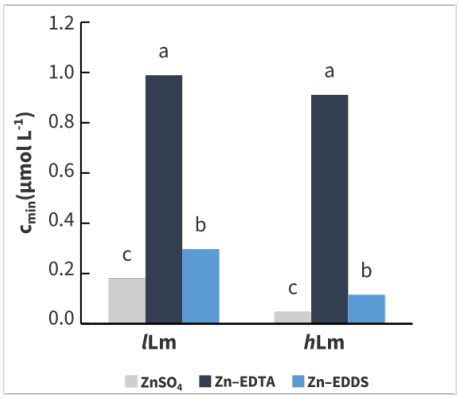

(b) Effects of liming levels on c_{min}

Figure 3.13: Effects of liming levels and Zn sources on c_{min} values

levels, $ZnSO_4$ was the source with lower values for K_m , while Zn–EDTA the highest.

For all sources, the values of c_{min} were smaller for the level *h*Lm (3.13-a). When comparing the Zn sources inside the same liming level (3.13-b), Zn–EDTA scored the highest mean values, differing statistically from Zn–EDDS and $ZnSO_4$. $ZnSO_4$ was the source that appeared with the lowest values for c_{min}.

3.4 DISCUSSION

Unarguably the fitted depletion curve patterns drawn, at least to distinct segments, pointing to the predominance of two main Zn uptake strategies by the plants in the study. The most accepted and discussed theory about the subject accounts for a dual-affinity mechanism. The first is as of 'low affinity', responsible for the Zn uptake at higher concentrations, even allowing Zn influx at toxic levels. Reid, Brookes, et al.

(1996). The other one would respond for the acquisition on lower concentrations, and then characterized as a 'high-affinity' system.

The obtained K_m values for $ZnSO_4$ and Zn–EDDS are close to those obtained by Mullins and Sommers (1986) studying Zn uptake kinetics on maize seedlings, when this constant value was 2.2 μmol L^{-1} and 1.5 μmol L^{-1} , for 16 and 22 days-old plants, respectively. The current results for K_m for Zn–EDTA are close to the value 16.0 μmol L^{-1} obtained by Bowen (1981), studying Zn kinetics on excised barley roots, where also a similar double-phase uptake mechanism was identified.

In comparison to chelate sources, more elevated initial Zn^{+2} activity when the provided source was $ZnSO_4$ and as consequence an eventually higher availability to uptake, was an expected result, since the salt $ZnSO_4$ holds a solubility product (pK_s) is 0.538 g g^{-1} at 25°C.

However, for the specific case of Zn–EDTA , both values of K_m and c_{min} tend to be much higher in comparison to $ZnSO_4$ and Zn–EDDS . Also, the ${}_sv_{max}$ values were much lower for Zn–EDTA , while ${}_av_{max}$ much lower in the same comparison.

The ${}_sv_{max}$ values were obtained from the first segment extracted from the depletion curve, where the zero-order kinetics was fitted and, in this case, ${}_sv_{max}$ depends only on the uptake rate. Foregrounded that plants were under the same initial condition, except for the Zn source, this result can only be owed to an intrinsic source characteristic. We infer that the chemical equilibrium in the solution media, distinctively altered by each source, plays the main effect. Similar results when Zn–EDTA and Zn–EDDS were compared in soil or soil-less experiments are reported (RACE et al., 2016; ORAMA et al., 2002; LÓPEZ-RAYO; CORREAS; LUCENA, 2012; LÓPEZ-RAYO; NADAL; LUCENA, 2016; CHAUHAN et al., 2015).

This diverging behavior, specially considering Zn–EDTA and Zn–EDDS , that are isomers and have similar formation constants (K_a), 13.6 for Zn–EDTA and 13.4 for Zn–EDDS , finds its explanation not in K, but in the apparent stability constants of these complexes (K_a^{app}) (3.9).

$$K_a^{app} = \frac{[ZnL^{x+2}]}{[L^x][Zn^{2+}]} \tag{3.9}$$

Where: L is ligand chelating agent;

According to Race et al. (2016), converting K to K_a^{app} is a way to convert the binding

constants to the proper conditions of the experiment (pH, ionic strength and temperature). Then, comparisons on the dissociation and availability among sources and conditions turn to be more meaningful. As in the current case, the *h*Lm condition, where pH was buffered to 7.0, the values of pK_a^{app} for Zn–EDTA and Zn–EDDS are 13.6 for Zn–EDTA and 10.6 for Zn–EDDS .

Discarding, the formation of other forms in different proportions for each Zn–EDTA and Zn–EDDS , Zn–EDDS would be able to hold a Zn^{+2} 30 times higher than Zn–EDTA , possibly clarifying why the Zn^{+2} depletion proceeded initially at much higher rates, in comparison to its isomer Zn–EDTA .

As it seems, when uptake parameter kinetics for ion uptake in plants are mentioned, the reference is to a plant to parameters sensitive to the medium, source and plant, even though these estimates may be close to the actual physiological parameter values This fact, however, does not invalidate the estimation and usage of these parameters as references for many practical applications in plant research.

Another pronounced aspect is that the kinetic parameter had distinct patterns of response in face of the imposed experimental conditions. K_m and c_{min} appear to be attached to Zn source, more than to the pH and Ca and Mg activities.

3.5 CHAPTER REMARKS

- The Zn depletion curves showed a non-linear double pattern;
- Zn depletion provided in the form of Zn–EDTA presents patterns markedly different from the patterns of $ZnSO_4$ and Zn–EDDS;
- The ${}_sv_{max}$ values for Zn–EDTA are smaller than those of other sources, regardless of the liming condition;
- $ZnSO_4$ promoted higher ${}_sv_{max}$ values; in sequence Zn–EDDS;
- The cmin parameter is mainly affected by the source, being higher for Zn–EDTA;
- A higher pH reduced the c_{min} value and elevate the K_m values;
- Compared to Zn–EDTA, Zn–EDDS promoted a faster uptake of Zn, which may be due to its higher K_d^{app} and its property as a zincophore.

CHAPTER 4

UTILIZATION EFFICIENCY OF Zn CHELATES APPLIED TO MAIZE PLANTS UNDER OVER-LIMING CONDITIONS

ABSTRACT

Chelated cationic nutrient sources is a well-known strategy to mitigate nutrient limitations, like increasing Zn availability to the plant uptake process. Using traditional chelating agents, such as EDTA, has downsides related to environmental behavior, such as toxicity to living organisms and resistance to biological and physical-chemical degradation and removal processes. Aiming more efficient and fewer environmental liabilities, new generation chelating agents such as EDDHA, IDS, DS, EDDS, GLDA, and MGDA are available. However, few studies targeted these compounds as potential substances for the composition zinc composition of micronutrient fertilizers. The aim, with this study, is to verify the efficiency of two chelating agents, and the conventional Zn source $ZnSO_4$ when applied to soil with distinct characteristics and under liming levels. We carried out greenhouse a greenhouse experiment organized in a completely randomized design, comprising two soils ($LVAd_{cla}$ and $LVAd_{scl}$), three soil pH incubation levels (5.5, 6.5, and 7.5), and three Zn sources (ZnSO4, Zn–EDTA, Zn–EDDS) with five doses(0.0, 4.0, 8.0, 16.0, and 32 mg kg^{-1} of Zn), with tree replicates (n = 3), summing up 270 experimental units. $ZnSO_4$ and Zn–EDDS promoted the highest Zn accumulations. The values of Zn content, dry matter mass and content were generally higher for the soil with sandier texture. Incubation pH significantly affected Zn uptake, especially for the sulfate source. Zn uptake was generally lower for Zn–EDTA, although this source promoted the least variations in Zn acquisition as a function of soil conditions and liming level.

4.1 INTRODUCTION

High doses of limestone and phosphate fertilizers are identified as causes of increasing Zn deficiencies, especially in crops with a higher sensitivity to low availability of this nutrient growing on intensely weathered tropical soils, that already counts very low Zn contents. In those cases, when signs or symptoms of deficiency become detectable, specially in annual crops, it is already too late to fix the fault and avoid productivity losses.

Arguably, nutrients mineral sources, like sulfates, nitrates, and chlorides, are practical solutions during the sowing operation. However, for Zn, as for the other cationic micro nutrients, the use of mineral sources in soil application may be inefficient because of factors related to the relation between these nutrients forms, the soil and the plant. The mobility of chemical species derived from the source dissolution and interactions between the Zn species, phosphates, carbonates, and iron oxides in the soil medium are some of the most relevant factors on the soil-nutrient side.

Chelates is a well-known strategy to mitigate these limitations, increasing the input Zn's availability to the plant uptake process. According to Mortvedt and Gilkes (1993), the chelate Zn source Zn–EDTA can be two to five times more efficient than $ZnSO_4$ in the zinc supply for cultures. Zn–EDTA showed higher mobility than $ZnSO_4$ and could provide enough Zn even at the initial stage of bean plants' development. In the same condition, Zn supplied by sulfate source appeared immobilized.

Using traditional chelating agents, such as EDTA, also has downsides related to environmental behavior. These substances may present elevated toxicity to living organisms and show resistance to biological and even physical-chemical degradation and removal processes. As an alternative, new generation chelating agents such as EDDHA, IDS, DS, EDDS, GLDA, and MGDA have been developed. These new products may be more efficient and present fewer environmental liabilities.

A variety of industrial purposes employ these ligands aiming for environmental applications, such as water and soil decontamination. However, few studies targeted these new chelating agents as potential substances for zinc composition and other micronutrient fertilizers for direct soil applications. Employing more efficient sources could be sensitive to restoring the Zn critical content levels, especially to crops under conditions where the soil Zn availability is already low. The conditions may include calcare-

ous soils or soils under excessive liming, high pH, and heavy phosphate fertilization. Worse and not coincidentally, in the last case, soils that require elevated amounts of P are also often Zn deficient, and the heavy phosphate applications contribute actively to reduce the available Zn to even lower levels.

López-Rayo, Nadal, and Lucena (2016) studied the supply of Mn, Zn, and Cu in nutrient solutions to soybean and fava bean plants, under high pH conditions (8.5) and $CaCO_3$ concentrations. They observed that Zn–EDDS incremented Zn leaf content up to three times than conventional chelate treatments such as EDTA or DTPA. Although this study considers high pH and high $CaCO_3$ concentrations in the nutrient solution, it requires other experiments adding soil medium effect.

To verify the efficiency of different chelating agents in the formulation of zinc sources via soil application and the residual Zn availability, we carried out greenhouse experiments to test the availability of Zn supplied as three different sources soils of contrasting textures and organic matter content. In this study, $ZnSO_4$, a conventional inorganic source, and two chelates, Zn–EDTA and Zn–EDDS, were investigated on the efficiency and residual effect potential for supplying Zn to maize plants under simulated over-liming conditions.

4.2 LITERATURE REVIEW

4.2.1 Zinc occurrence in minerals and soils

Under general conditions, Zn appears as the divalent cation Zn^{+2} in the earth's crust. Zinc-abundant mineral deposits are locally formed by natural geological processes and are found around the world. Mines with economic importance have rocks with Zn contents varying between 5-15% (MERTENS; SMOLDERS; KIEKENS, 2013), in the form of sulfides, such as sphalerite (αZnS) or wurtzite (βZnS), and, less importantly, other minerals of Zn, as carbonates: smithsonite ($ZnCO_3$); silicates: hemimorphite ($Zn_4Si_2O_7$ (OH) $2H_2O$) and willemite (Zn_2SiO_4) and oxides(zincite) (ZnO).

In the soils, the Zn content depends on the concentration of Zn in the source material, factors such as pH and organic matter content. According to Kabata-Pendias (2010), the average Zn content is 70 $mg\,kg^{-1}$, varying enormously according to the soil class, with levels as low as 31 $mg\,kg^{-1}$ in Podzols (sandy) 250 $mg\,kg^{-1}$ in Histosols (organic).

In the soil solution, this concentration is usually much lower, varying between 4 and 250 $\mu g\,kg^{-1}$, depending in significant part on the soil type. In contrast, in limestone soils, for example, Hodgson, Lindsay, and Trierweiler (1966) found Zn levels below 2.0 $\mu g\,L^{-1}$, indicating that deficiencies of this nutrient may be frequent in this type of soil. According to Mertens, Smolders, and Kiekens (2013), the concentration in solution is a function of precipitation-dissolution, sorption, and solution complexation reactions of this element.

4.2.2 Zinc interactions and availability in soils

According to Mertens, Smolders, and Kiekens (2013), the interactions of Zn in the soil depend on some characteristics such as the concentration of the element and other ions in the soil solution, species and amount of adsorption sites associated with the solid soil phase, the concentration of all the binders capable of forming organic complexes of Zn, pH and soil red-ox potential.

Based on the central chemical equilibria of the most common chemical species of Zn in solution, Graf (1980) proposed the following equation to estimate the concentration (4.1) and Zn^{+2} activity (4.2).

$$\left[Zn_{inorg}\right] = \frac{\left(Zn^{+2}\right)}{\gamma_{Zn^{+2}}} + \left(ZnSO_4^0\right) \tag{4.1}$$

$$\left(Zn^{+2}\right) = \frac{\left[Zn_{inorg}\right]}{\frac{1}{\gamma_{Zn^{+2}}} + 10^{2.33}\left(SO_4^{-2}\right) + \frac{10^{-7.69}}{\gamma_{ZnOH^+}}} \tag{4.2}$$

Where ( ) Indicate activities of the respective species, in $mol\,L^{-1}$, [ ] the concentrations, in $mol\,L^{-1}$, the coefficient of activity of the respective ion (dimensionless).

However, the distribution of these chemical species can be changed when an exogenous substance is added to the soil as a corrective or fertilizer, for example, increasing or reducing the concentration and Zn activity in solution.

The activity of Zn^{+2} in soils is directly proportional to the proton activity squared. Therefore, Zn's solubility will decrease with increasing pH (MERTENS; SMOLDERS; KIEKENS, 2013), due to the high soil adsorption capacity, resulting from increased pH-dependent charges, the formation of hydrolyzed forms of Zn, the chemisorption in

calcite and Fe oxides (ALLOWAY, 2009). According to TILLER and HODGSON (1962), silicate clay minerals can reversibly adsorb Zn, either by the cation exchange process or irreversibly, by the mineral's structural penetration. Besides these factors, phosphorus forms also contributes to Zn fixation.

4.3 MATERIAL AND METHODS

4.3.1 Physical-chemical properties of soils

In the current study, we employed two Oxisols ($LVAd_{cla}$ and $LVAd_{scl}$), of which chemical and physical characterizations were performed (Table 1). The soil samples were sieved through a 2 mm mesh sieve to remove larger clods and stones.

Chemical characterization included the determination of pH in water, organic carbon, available P and K, exchangeable Al, Ca, and Mg, and potential acidity (DONAGEMMA et al., 2011). The available levels of metallic micro-nutrients in soils were determined using the Mehlich-3 extractor, and the dosage was performed employing atomic absorption Spectrometry (EAA). P_{rem} was determined according to Alvarez et al. (2000). Available P was determined by extraction with Mehlich-1 and quantified by a molecular absorption spectrophotometer UV–VIS, as described by Braga and DeFelipo (1974). The organic carbon content was determined by the Walkley-Black method.

The physical characterization included the measurements of granulometry, apparent density, and real density analysis (CLAESSEN et al., 1997). The field capacity was determined according to the method recommended by BERNARDO, SOARES, and MANTOVANI (2006), using the tension of 0.033 MPa.

Table 4.1: Soils properties

Property	$LVAd_{cla}$	$LVAd_{scl}$
pH (H_2O)	4.90	5.30
Organic matter (dag kg^{-1})	5.40	1.80
P (mg dm^{-3})	0.60	2.10
P_{rem} (mg L^{-1})	23.00	28.60
K (mg dm^{-3})	13.00	29.00
Ca^{+2}($cmol_c$ dm^{-3})	0.00	0.39
Mg^{+2}($cmol_c$ dm^{-3})	0.05	0.12
Zn (mg dm^{-3})	0.81	0.62
Cu (mg dm^{-3})	1.93	0.39
Mn (mg dm^{-3})	13.10	6.00
Fe (mg dm^{-3})	60.60	32.20
Al^{+3} ($cmol_c$ dm^{-3})	0.85	0.36
H+Al ($cmol_c$ dm^{-3})	7.90	3.50
Bases sum ($cmol_c$ dm^{-3})	0.08	0.58
$CEC_{pH\ 7.0}$ ($cmol_c$ dm^{-3})	7.98	4.08
CEC ($cmol_c$ dm^{-3})	0.93	0.94
Bases saturation(%)	1.00	14.20
m(%)	91.00	38.00
Sand(%)	26.00	70.00
Silt(%)	1.00	6.00
Clay(%)	73.00	24.00
Density (kg dm^{-3})	1.04	1.39

4.3.2 Soil carbonate incubation curves

The liming demand was estimated based on the soils' chemical analysis, employing the H + Al neutralization method (RAIJ et al., 2001). From the estimated values we defined the hypothetical amount of the Ca and Mg carbonates mixture necessary to neutralize 100% of the potential acidity (H + Al), and then six derived level doses sufficient to neutralize 0, 40, 80, 120, 160, and 200 %.

The $CaCO_3$ + $MgCO_3$ mixture was prepared using the 3:1 (nCa:nMg) ratio with p.a. salts (Sigma-Aldrich, USA). The doses were applied in triplicate to 500 g aliquots of each soil, summing up 18 units. The soil aliquots were placed individually in transparent plastic pots with lids and added of the carbonate mixture doses. The pots were covered and thoroughly shaken and then the soil aliquots moistened with deionized water to 80% of the field capacity. Moisture in the soil pots was checked daily and corrected if necessary. The mixture was also periodically shaken to facilitate gas exchange and

speed up the neutralization reactions. After a reaction time of 15 d, the aliquots were air-dried and the pH determined using a 20 25 soil to water by mass ratio. Average pH values were plotted against the carbonate doses, obtaining the characteristic acidity neutralization curve for $LVAd_{cla}$(4.1a) and $LVAd_{scl}$ (4.1b).

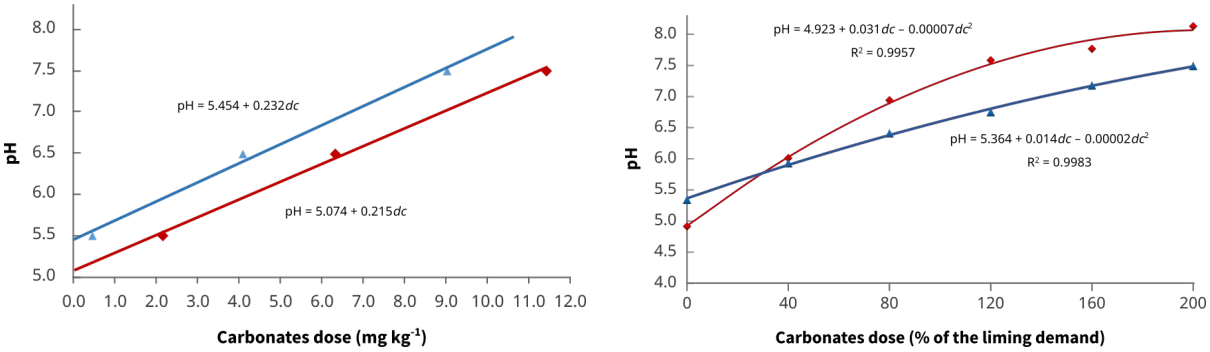

(a) pH as function of carbonate doses (b) pH as function of relative carbonate doses

Figure 4.1: Liming incubation curves for $LVAd_{cla}$ and $LVAd_{scl}$

4.3.3 Experimental Design

The experiment was organized in a completely randomized block design, comprising two soils ($LVAd_{cla}$ and $LVAd_{scl}$), three pH incubation values (5.5, 6.5, and 7.5), and three Zn sources ($ZnSO_4$, Zn–EDTA, Zn–EDDS) with five doses (0.0, 2.0, 4.0, 8.0, 16.0, and 32.0 mg kg^{-1} of Zn) and three blocks (n = 3). The total number of experimental units was 270.

From the characteristic incubation curve for each soil, we estimated three doses of the mixture 3:1 (m:m) $CaCO_3$ + $MgCO_3$ p.a. to reach pH_S values of 5.5, 6.5, and 7.5. The doses were added to dry soil aliquots of 6.00 kg and placed in plastic bags. The mixture was homogenized and moistened to 80% of the field capacity and incubated for 15 d. After this period, the plastic bags containing the soil aliquots were transferred to polyethylene pots, the soil was fertilized and sown.

4.3.4 Plant cultivation

We ran a pot experiment under greenhouse conditions to assess the effects of sources and pH level on plant development and Zn accumulation. Maize plants of the single cross hybrid BM-812 (Biomatrix, Brazil) raised in 7 dm3 plastic containers filled with 6.00 kg of soil incubated for each pH level.

Plants received macronutrients fertilization by applying solutions to the soil pots. Before sowing, we applied micronutrients in a single part and the first dose of macronutrients and fifteen days after, the second dose. The doses of nutrients, in mg kg^{-1} of soil, were: 100 of N, 500 of P, 150 of K, 100 of S, 0.40 of B, 0.66 Cu, 0.77 Fe, 1.83 Mn, and 0.07 Mo, adapted from Novaes, Neves, and Barros (1991)

Five days after germination, we thinned the seedlings, leaving the two most vigorous plants in each pot from the five that were sown. After seedlings thinning, we administered the Zn doses by spattering 100.00 mL of the respective source dose for each treatment level. During cultivation, soil moisture settled at around 80% of field capacity, irrigated with deionized water (0.05 ± 0.02 µS m^{-1}) distribute through a drip irrigation apparatus, equipped with 4.0 L h^{-1} pressure compensating droppers (Netafim, USA). Plants advanced until the V6 stage, which came 30 d after the seedlings' emergency.

4.3.5 Determination of nutrient contents in plant tissues

Thirty days after the emergency (V_6 stage), the plants had the aerial part collected, rinsed in deionized water and dried in a forced circulation oven at 65±5 °C until constant weight. After cooling, samples were ground in a Willey-type mill equipped with a 2.0 mm sieve.

An aliquot of approximately 0.500 g of the dry ground matter was mineralized by nitric-perchloric acid digestion (ZASOSKI; BURAU, 1977) to determine the Zn elemental concentrations. The concentrations were obtained by Inductively Coupled Plasma Optical Emission Spectrometry (ICP-OES).

4.3.6 Statistical analysis

Statistical analyzes were performed using the software R(R DEVELOPMENT CORE TEAM, 2019), employing the library *ExpDes* (FERREIRA; CAVALCANTI; NOGUEIRA, 2014). The confidence intervals for beta coefficients (beta weights) were estimated using the Bootstrap method implemented in the package *boot*(CANTY; RIPLEY, 2015) with $n \geq 1000$.

$$Q_{exp} = \frac{x_n - x_{n-1}}{x_n - x_1} \tag{4.3}$$

$$Q_{\alpha,n} = 0.05 \quad (4.4)$$

Q_{exp} is the Q statistic value, x_1 is the smallest (suspect) value, x_2 is the second smallest value, and x_n is the largest value.

Data obtained after outliers removal were submitted to analysis of variance (ANOVA), normality by the Shapiro–Wilk test, and regression analysis. Significant treatment levels interactions obtained from the F–test were compared by the Student-Newman-Keuls test at the 5% probability level.

4.4 RESULTS

4.4.1 Plant's visual aspects

On the $LVAd_{cla}$ plants, in general, delayed growth and development, compared with those growing on $LVAd_{scl}$. This pattern was noticiable regardeless of source or liming level. Under the pH 5.5 plants growing supplied by the chelates as Zn source visually appered shorter and thinner when compared with those supplied with $ZnSO_4$ (4.2).

Under pH 7.5 on $LVAd_{cla}$, plants present independently of the source or dose, diminished development and visual symptoms of micronutrients. Remarkably, when the suplied source was $ZnSO_4$ plants were very short, thin and presented intense chlorosis. This aspect was common for all sources at the 0dose, however for chelates from the *d*Zn 8.0 and subsequent these symptoms were practically reverted and plants appeared as the ones growing on pH 5.5 . On pH 7.5 and $LVAd_{cla}$ plants supplied with Zn–EDDS from *d*Zn 8.0 were vigorous, yet presented thinner stems than those growing on pH 5.5 .

Plants growing on $LVAd_{scl}$ had greater development compared with plants growing on $LVAd_{cla}$. At pH 5.5 experimental units that had $ZnSO_4$ as source had a quicker development and were more vigorous and greener than those supplied with chelates. At *d*Zn 32.0, however, for $ZnSO_4$, plants presented some shortening and a slight chlorosis, in comparison with the plants supplied with the preceding doses, *d*Zn 16.0 and *d*Zn 8.0.

On pH 7.5, plants supplied with the any of the sources with *d*Zn 0.0 had the development severely affected. From *d*Zn 8.0 and forward the development was similar to

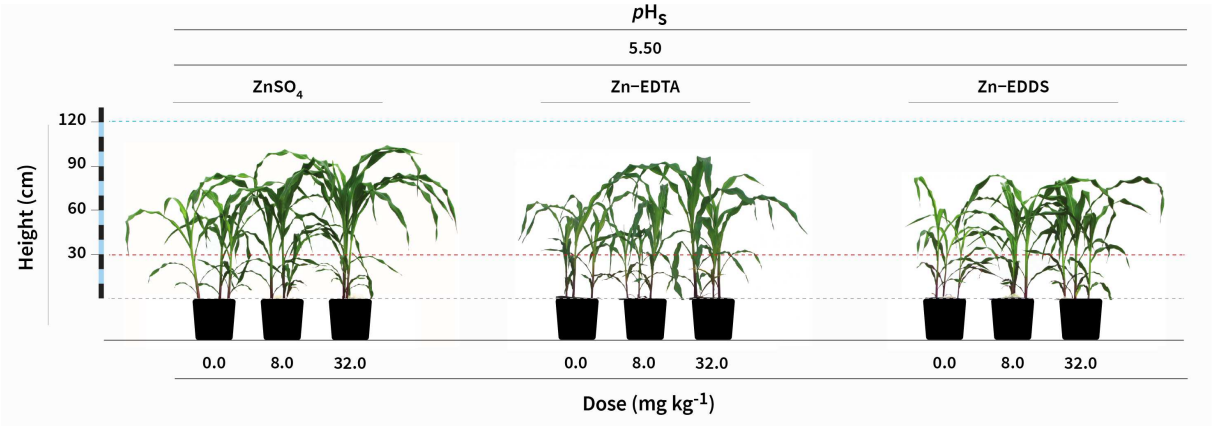

Figure 4.2: Plants' development on $LVAd_{cla}$ under pH_S = 5.5

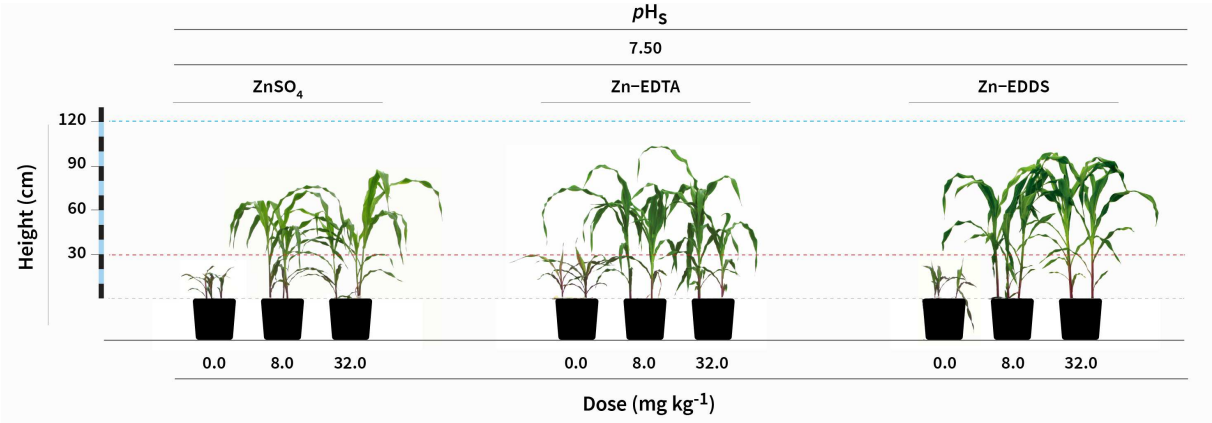

Figure 4.3: Plants' development on $LVAd_{cla}$ under pH_S = 7.5

plants on pH 5.5 , except for moderate stem thinning, and slight generalized chlorosis, which were more pronounced when $ZnSO_4$ was the Zn source.

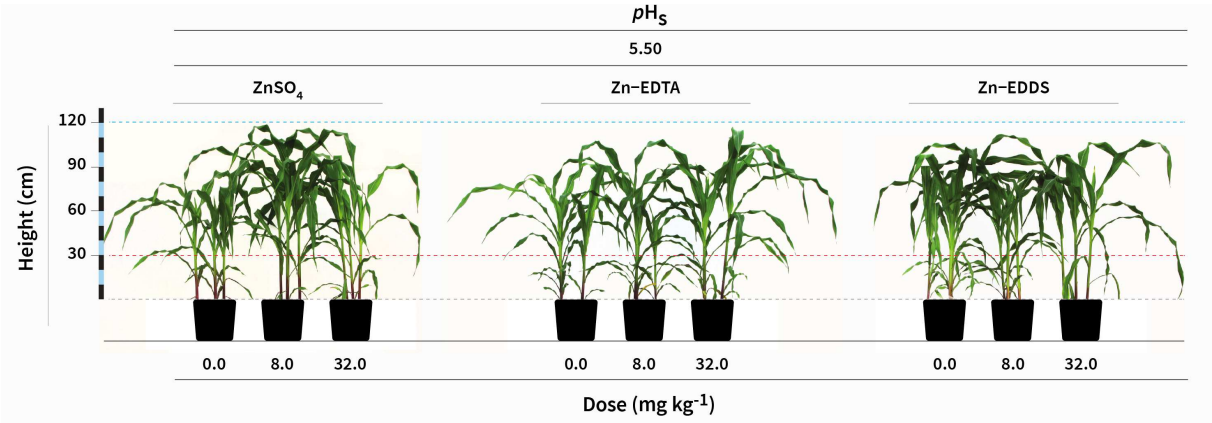

Figure 4.4: Plants' development on $LVAd_{scl}$ under pH_S = 5.5

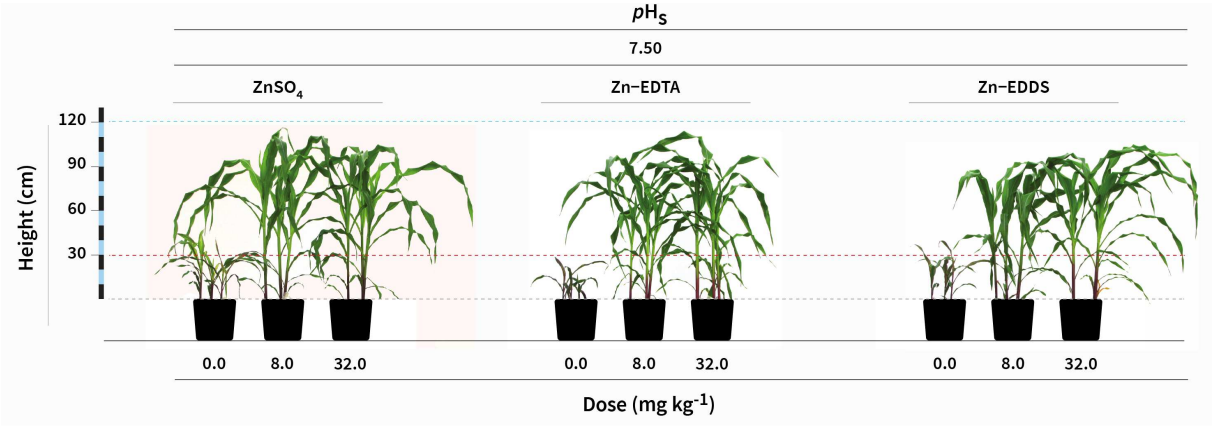

Figure 4.5: Plants' development on $LVAd_{scl}$ under pH_S = 7.5

4.4.2 Analysis of response variables

General variance

On table 4.2 are given the results for significance of the treatment factors on the response variables wDM_{APPt} , cZn_{AP} , and qZn_{APPt} .

For soil $LVAd_{cla}$, significant effects were found in the response wDM_{APPt} for pH ($p < 0.001$) , Zn doses ($p < 0.001$) , for the interaction Source × pH ($p < 0.01$) , and for the interaction source × dose ($p < 0.001$) . When evaluating the effects of treatments on $LVAd_{scl}$ on the response wDM_{APPt} , source ($p < 0.01$) , pH ($p < 0.001$) , dose ($p < 0.001$) and the interaction pH × doses ($p < 0.001$) were significant.

For cZn_{AP} , on $LVAd_{cla}$, all factors and interactions were found significant (source ($p < 0.001$) , pH ($p < 0.001$) , dose ($p < 0.001$) , interaction source × pH ($p < 0.001$) , interaction source × dose ($p < 0.01$) , pH × doses ($p < 0.01$) , source × pH × doses ($p < 0.05$) . For cZn_{AP} on $LVAd_{scl}$, the effects of source ($p < 0.05$) , pH ($p < 0.001$) , dose ($p < 0.001$) , interaction source × dose ($p < 0.01$) , and pH × doses ($p < 0.001$) presented significance.

The effects of all sources of variation were consistently significant, when the analyzed response was qZn_{APPt} , for both $LVAd_{cla}$ and $LVAd_{scl}$: pH ($p < 0.001$) , dose ($p < 0.001$) , interaction source × pH ($p < 0.001$) , interaction source × dose ($p < 0.001$) , pH × doses ($p < 0.001$) , source × pH × dose ($p < 0.001$) .

Table 4.2: Effects of Zn source, soil, pH_S (pH_S) and Zn doses on plant dry weight, plant Zn tissues concentration, and Zn content

Source of variation	df	wDM_{APPt}		cZn_{AP}		qZn_{APPt}	
		$LVAd_{cla}$	$LVAd_{scl}$	$LVAd_{cla}$	$LVAd_{scl}$	$LVAd_{cla}$	$LVAd_{scl}$
		— mg/pot —		— mg kg^{-1} —		— mg/pot —	
Source (S)	2	ns	**	***	*	***	***
Soil pH (P)	2	***	***	***	***	***	***
Zn dose (D)	4	***	***	***	***	***	***
S × P	4	**	ns	***	ns	***	***
S × D	8	***	ns	**	**	***	***
P × D	8	ns	***	**	***	***	***
S × P × D	16	ns	ns	*	ns	***	***

Significance probability level codes: * (0.05), ** (0.01), *** (0.001), and, ns (non-significant at 0.05 probability level)

Table 4.3 give the values of the beta standard beta coefficients for wDM_{APPt} as function of soil ($LVAd_{cla}$ and $LVAd_{scl}$) and Zn sources ($ZnSO_4$, Zn–EDTA, and Zn–EDDS) for the , followed by the significance notation from the regression analysis.

4.4.3 Plant dry weight (wDM_{APPt})

Figure 4.7e shows the surface and its contour plots for the response wDM_{APPt} , where in the x-axis are dZn , y-axis the pH and z-axis wDM_{APPt} for the Zn sources $ZnSO_4$, Zn–EDTA, Zn–EDDS applied to the soil $LVAd_{cla}$.

(a) **$ZnSO_4$** - Surface Plot

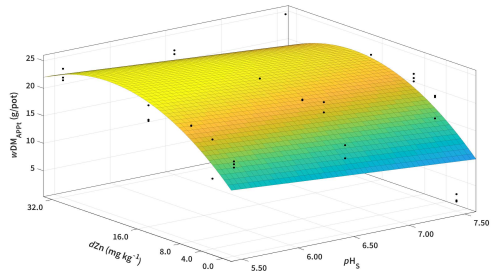

(b) **$ZnSO_4$** - Contour

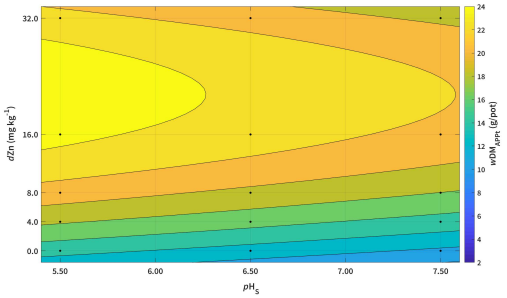

$$wDM_{APPt} = 23.056 + 0.976\ dZn - 1.523\ pH_S - 0.023\ dZn^2$$

$$R^2_{adj.} = 0.459$$

(c) **Zn–EDTA** - Surface Plot

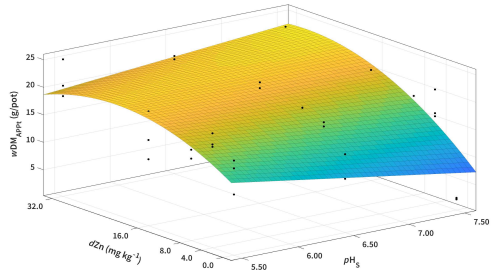

(d) **Zn–EDTA** - Contour

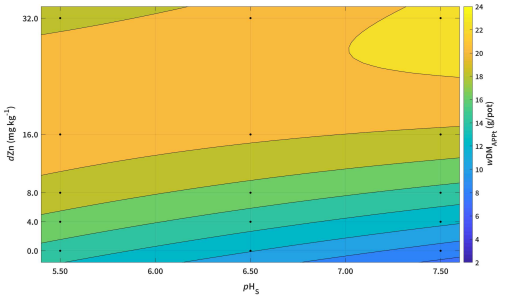

$$wDM_{APPt} = 23.088 - 0.161\ dZn - 1.691\ pH_S - 0.015\ dZn^2 + 0.141\ dZn \times pH_S$$

$$R^2_{adj.} = 0.455$$

(e) **Zn–EDDS** - Surface Plot

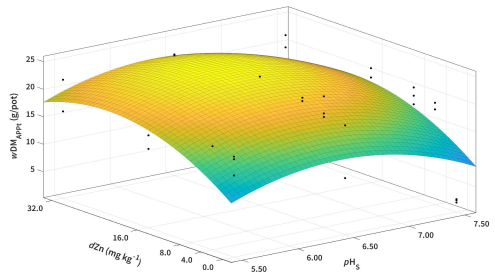

(f) **Zn–EDDS** - Contour)

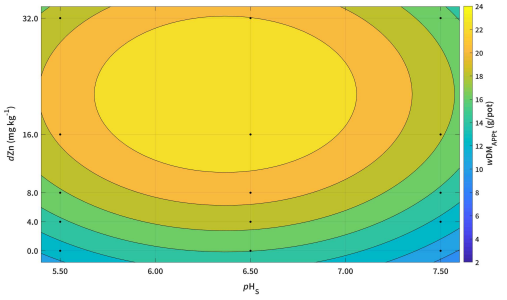

$$wDM_{APPt} = -157.364 + 0.728\ dZn + 53.356\ pH_S + 0.017\ dZn^2 - 4.104\ pH_S^2$$

$$R^2_{adj.} = 0.370$$

Figure 4.7: Effects of Zn doses and pH_S levels on plant dry weight per pot for $LVAd_{scl}$

(a) **$ZnSO_4$** - Surface Plot

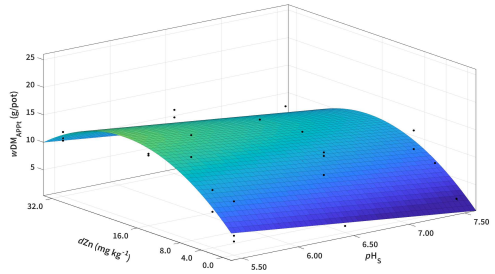

(b) **$ZnSO_4$** - Contour

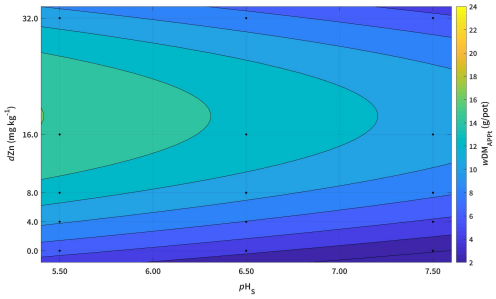

$$wDM_{APPt} = 18.946 + 0.989\ dZn - 2.235\ pH_S - 0.027\ dZn^2$$
$$R^2_{adj.} = 0.611$$

(c) **Zn–EDTA** - Surface Plot

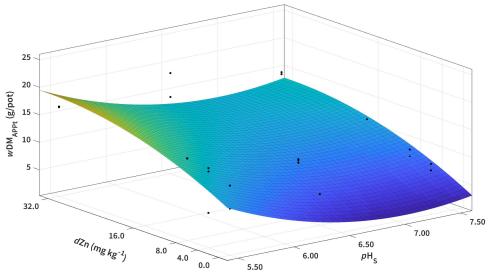

(d) **Zn–EDTA** - Contour)

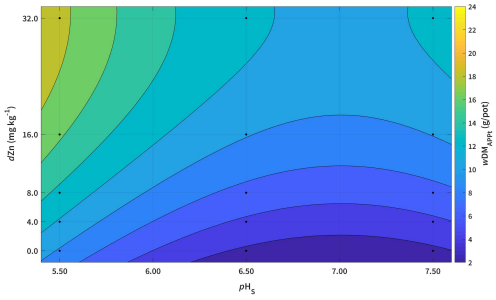

$$wDM_{APPt} = 152.185 + 0.533\ dZn - 42.610\ pH_S - 0.008\ dZn^2 + 3.040\ pH_S{}^2$$
$$R^2_{adj.} = 0.758$$

(e) **Zn–EDDS** - Surface Plot

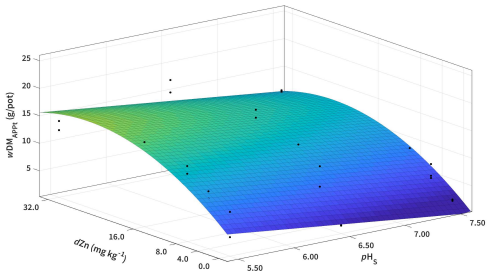

(f) **Zn–EDDS** - Contour

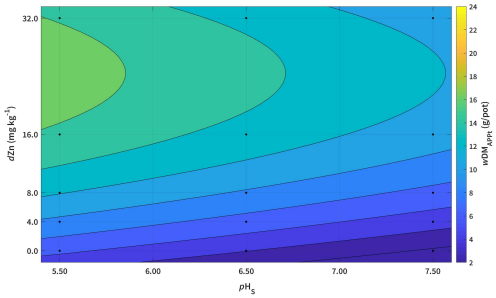

$$wDM_{APPt} = 19.222 + 0.854\ dZn - 2.333\ pH_S - 0.017\ dZn^2$$
$$R^2_{adj.} = 0.795$$

Figure 4.6: Effects of Zn doses and pH_S levels on plant dry weight per pot for $LVAd_{cla}$

Table 4.3: Standard beta coefficients for plant dry weight fitted models (wDM_{APPt})

Soil	Source of variation	$ZnSO_4$		Zn-EDTA		Zn-EDDS	
		β coefficient	95% CI	β coefficient	95% CI	β coefficient	95% CI
$LVAd_{cla}$	pH_S	-0.420***	[-0.423; -0.417]	-0.529***	[-0.533; -0.524]	-0.424***	[-0.426; -0.422]
	pH_S^2	-0.135ns	[-0.145; -0.125]	0.311***	[0.308; 0.314]	-0.092ns	[-0.100; -0.084]
	dZn	0.878***	[0.871; 0.885]	0.791***	[0.788; 0.795]	1.070***	[1.066; 1.074]
	dZn^2	-0.865***	[-0.870; -0.861]	-0.242*	[-0.246; -0.239]	-0.543***	[-0.547; -0.539]
	pH_S × dZn	-0.020ns	[-0.027; -0.014]	0.124ns	[0.118; 0.130]	0.026ns	[0.020; 0.031]
$LVAd_{scl}$	pH_S	-0.229*	[-0.233; -0.226]	-0.191ns	[-0.194; -0.187]	-0.151ns	[-0.158; -0.145]
	pH_S^2	-0.167ns	[-0.176; -0.158]	-0.173ns	[-0.181; -0.165]	-0.408**	[-0.411; -0.404]
	dZn	0.935***	[0.930; 0.940]	0.873***	[0.869; 0.878]	0.721***	[0.716; 0.727]
	dZn^2	-0.626***	[-0.631; -0.622]	-0.421**	[-0.426; -0.416]	-0.478**	[-0.483; -0.472]
	pH_S × dZn	0.150ns	[0.139; 0.161]	0.256*	[0.253; 0.259]	0.225ns	[0.213; 0.237]

Significance probability level codes: * (0.05), ** (0.01), *** (0.001), and, ns (non-significant at 0.05 probability level)

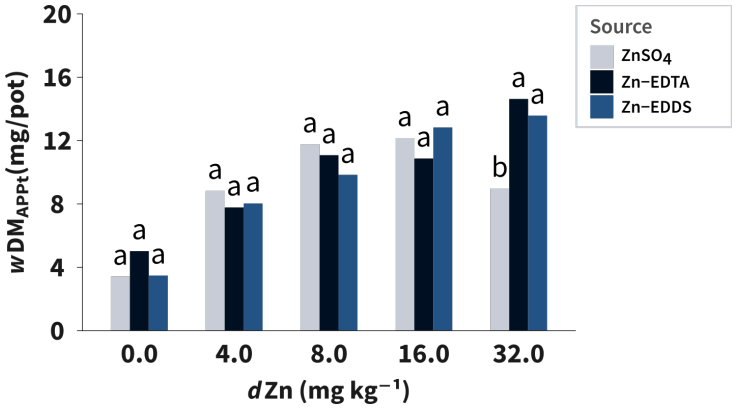

Figure 4.8: Source x Dose

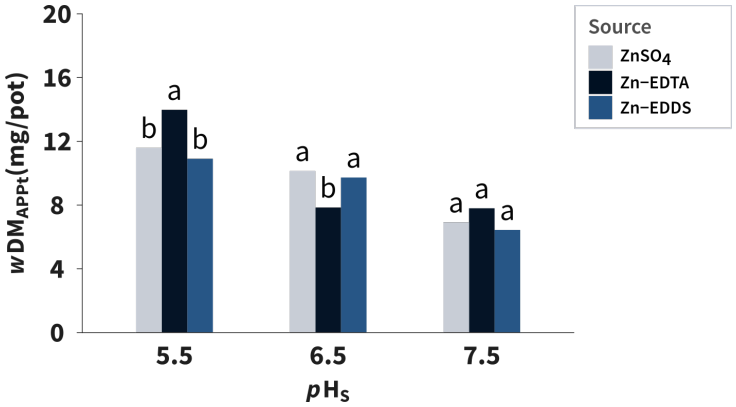

Figure 4.9: Source x pH_S

4.4.4 Zinc concentration in plant tissues (cZn_{AP})

(a) **$ZnSO_4$** - Surface Plot

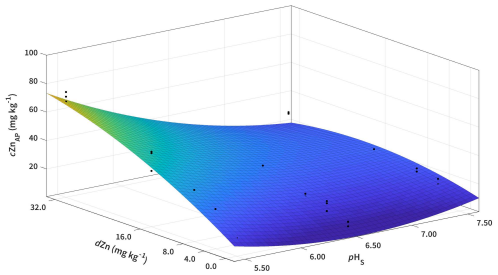

(b) **$ZnSO_4$** - Contour

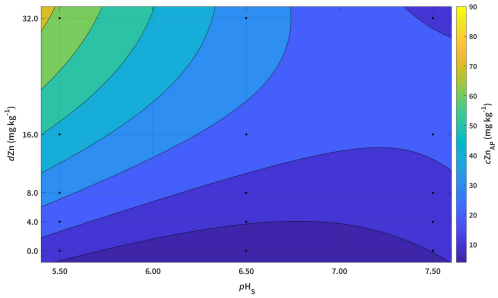

$$cZn_{AP} = 359.468 + 6.390\ dZn - 107.842\ pH_S - 0.025\ dZn^2 + 8.171\ pH_S{}^2 - 0.706\ dZn{\times}pH_S$$

$$R^2_{adj.} = 0.909$$

(c) **Zn–EDTA** - Surface Plot

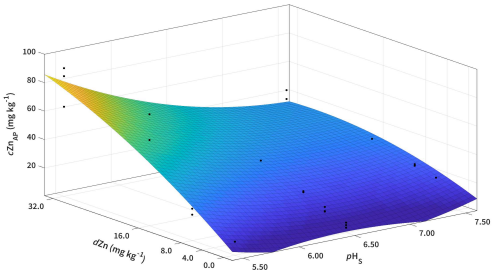

(d) **Zn–EDTA** - Contour

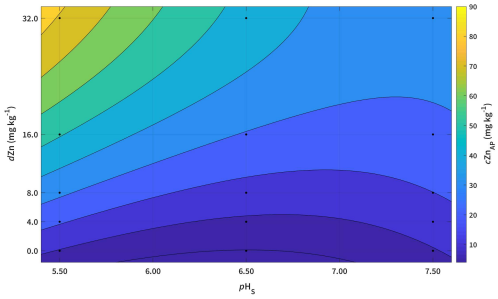

$$cZn_{AP} = 467.376 + 1.425\ dZn - 134.123\ pH_S + 9.640\ pH_S{}^2$$

$$R^2_{adj.} = 0.746$$

(e) **Zn–EDDS** - Surface Plot

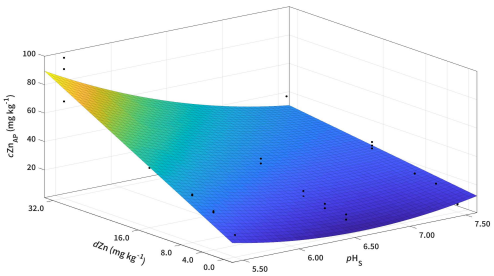

(f) **Zn–EDDS** - Contour

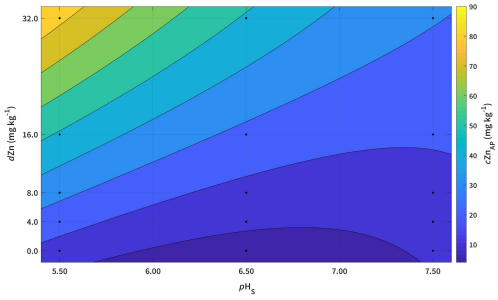

$$cZn_{AP} = 334.261 + 6.128\ dZn - 98.840\ pH_S + 7.466\ pH_S{}^2 - 0.738\ dZn{\times}\ pH_S$$

$$R^2_{adj.} = 0.913$$

Figure 4.11: Effects of Zn doses and pH_S levels on Zn concentration in plant tissues for $LVAd_{scl}$

(a) **$ZnSO_4$** - Surface Plot

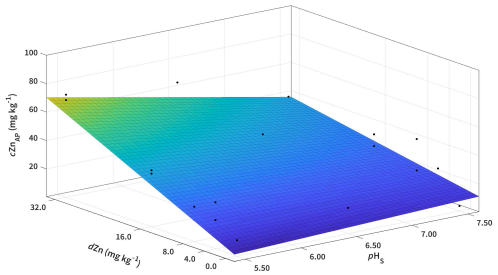

(b) **$ZnSO_4$** - Contour

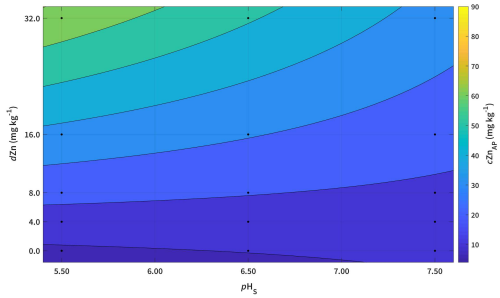

$$cZn_{AP} = -\ 1.270 + 4.660\ dZn + 1.790\ pH_S -\ 0.522\ dZn \times pH_S$$
$$R^2_{adj.} = 0.780$$

(c) **Zn–EDDS** - Surface Plot

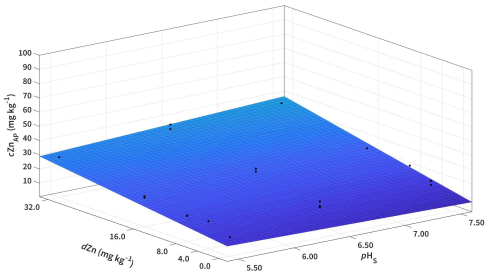

(d) **Zn–EDTA** - Contour

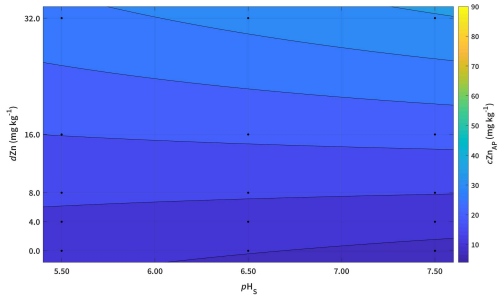

$$cZn_{AP} =\ 21.479 -\ 0.272\ dZn -\ 1.724\ pH_S + 0.144\ dZn \times pH_S$$
$$R^2_{adj.} = 0.866$$

(e) **Zn–EDDS** - Surface Plot

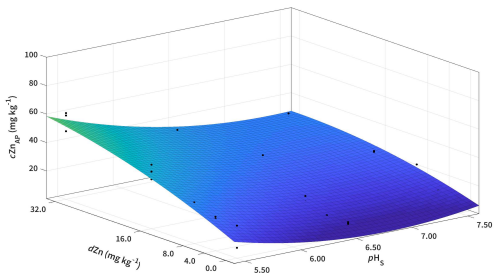

(f) **Zn–EDDS** - Contour

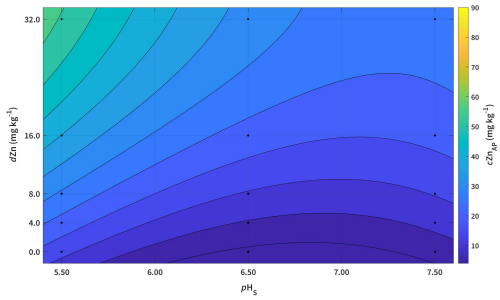

$$cZn_{AP} = 361.569 + 3.281\ dZn -\ 105.252\ pH_S -\ 0.017\ dZn^2 + 7.730\ pH_S{}^2 -\ 0.280\ dZn \times pH_S$$
$$R^2_{adj.} = 0.870$$

Figure 4.10: Effects of Zn doses and pH_S levels on Zn concentration in plant tissues for $LVAd_{cla}$

Table 4.4: Standard beta coefficients for plant tissue Zn concentration fitted models (cZn_{AP})

Soil	Source of variation	$ZnSO_4$		Zn-EDTA		Zn-EDDS	
		β coefficient	95% CI	β coefficient	95% CI	β coefficient	95% CI
$LVAd_{cla}$	pH	-0.207^{**}	[-0.212; -0.203]	0.018^{ns}	[0.014; 0.021]	-0.487^{***}	[-0.494; -0.480]
	pH^2	0.090^{ns}	[0.082; 0.098]	0.028^{ns}	[0.023; 0.034]	0.276^{***}	[0.271; 0.280]
	*d*Zn	0.820^{***}	[0.816; 0.825]	0.922^{***}	[0.920; 0.924]	0.859^{***}	[0.851; 0.866]
	dZn^2	-0.039^{ns}	[-0.050; -0.029]	-0.050^{ns}	[-0.057; -0.043]	-0.188^{*}	[-0.195; -0.182]
	$pH_S \times dZn$	-0.266^{***}	[-0.270; -0.262]	0.159^{**}	[0.156; 0.161]	-0.181^{**}	[-0.184; -0.178]
$LVAd_{scl}$	pH	-0.505^{***}	[-0.511; -0.499]	-0.346^{***}	[-0.352; -0.340]	-0.458^{***}	[-0.463; -0.453]
	pH^2	0.244^{***}	[0.240; 0.248]	0.232^{***}	[0.228; 0.235]	0.189^{***}	[0.186; 0.192]
	*d*Zn	0.837^{***}	[0.828; 0.845]	0.794^{***}	[0.788; 0.800]	0.781^{***}	[0.775; 0.787]
	dZn^2	-0.237^{**}	[-0.244; -0.231]	-0.051^{ns}	[-0.058; -0.044]	-0.051^{ns}	[-0.058; -0.044]
	$pH_S \times dZn$	-0.390^{***}	[-0.393; -0.386]	-0.322^{***}	[-0.326; -0.318]	-0.333^{***}	[-0.338; -0.329]

Significance probability level codes: ***** (0.05), ****** (0.01), ******* (0.001), and, ns (non-significant at 0.05 probability level)

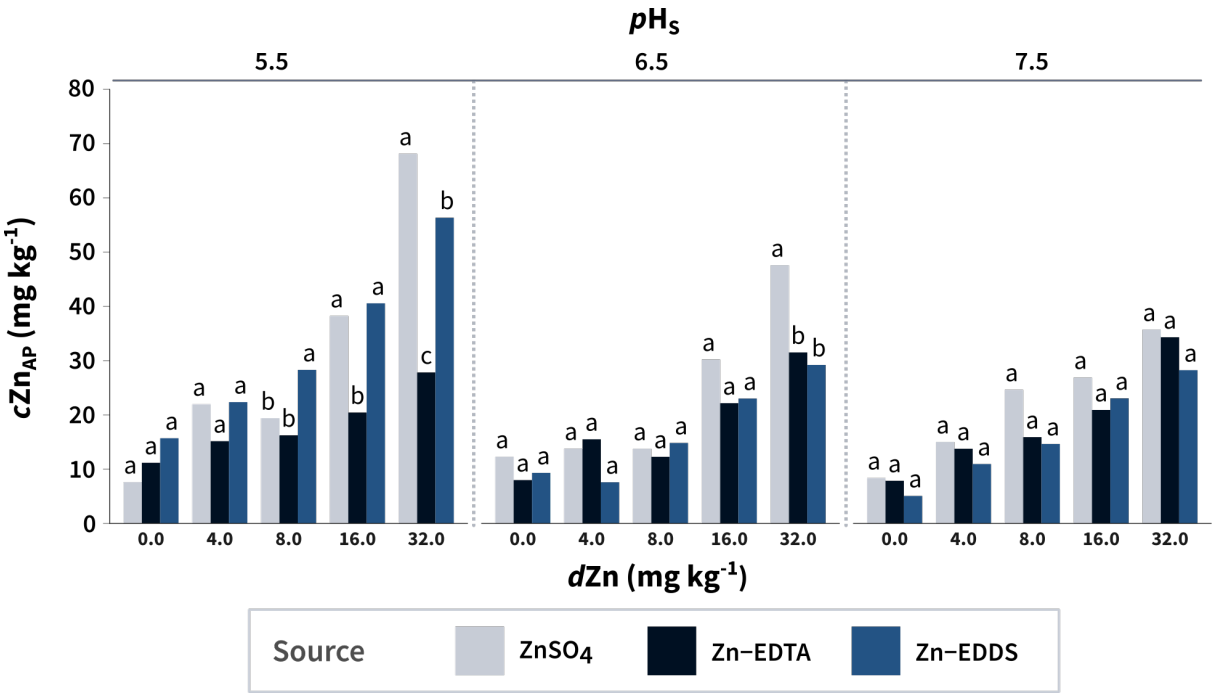

Figure 4.12: Source x pH_S x Dose

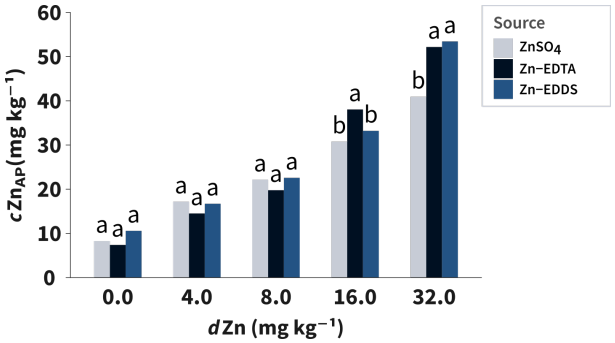

Figure 4.13: Source x Dose

4.4.5 Zinc content in plants (qZn_{APPt})

(a) **$ZnSO_4$** - Surface Plot

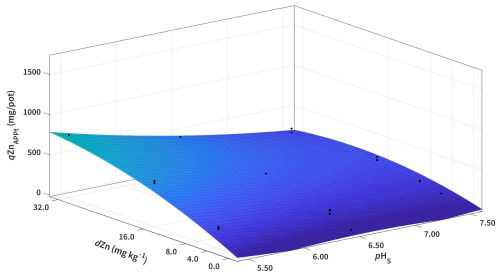

(b) **$ZnSO_4$** - Contour

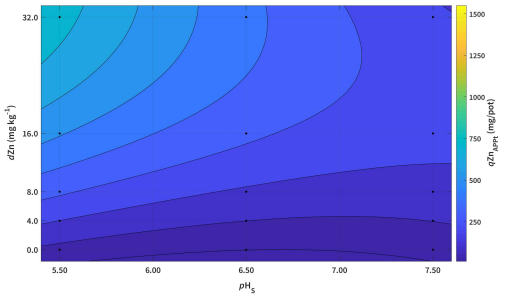

$$qZn_{APPt} = 233.124 + 74.894\ dZn + 667.804\ pH_S + 0.411\ dZn^2 + 49.910\ pH_S^2 + 7.466\ dZn \times pH_S$$

$$R^2_{adj.} = 0.955$$

(c) **Zn–EDTA** - Surface Plot

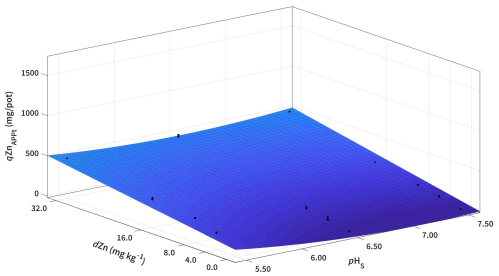

(d) **Zn–EDTA** - Contour

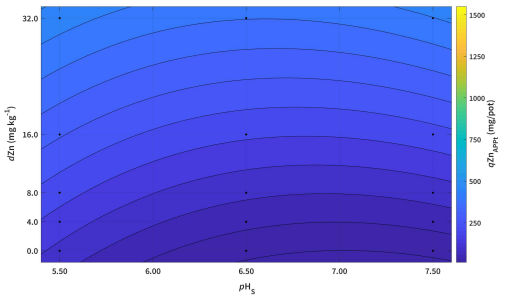

$$qZn_{APPt} = 2913.026 + 2.090\ dZn + 829.785\ pH_S + 59.078\ pH_S^2 + 1.537\ dZn \times pH_S$$

$$R^2_{adj.} = 0.927$$

(e) **Zn–EDDS** - Surface Plot

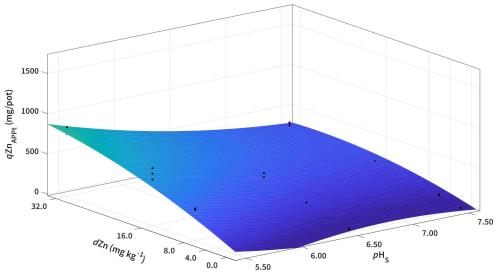

(f) **Zn–EDDS** - Contour

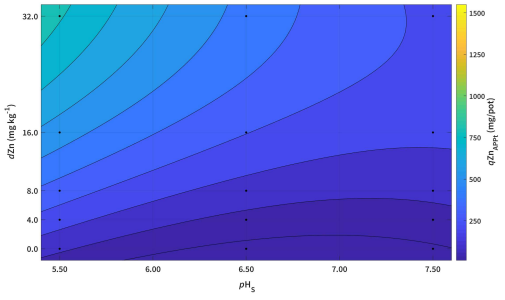

$$qZn_{APPt} = 846.377 + 66.273\ dZn + 1127.464\ pH_S + 0.334\ dZn2 + 81.711\ pH_S^2 + 6.173\ dZn \times pH_S$$

$$R^2_{adj.} = 0.962$$

Figure 4.14: Effects of Zn doses and pH_S levels on Zn contents in plant tissues per pot $LVAd_{cla}$

(a) **$ZnSO_4$** - Surface Plot

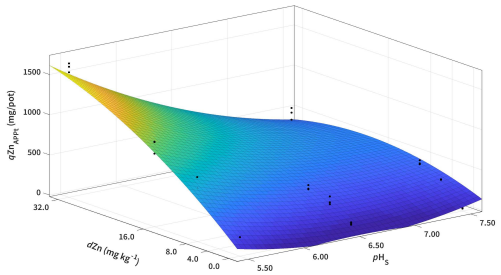

(b) **$ZnSO_4$** - Contour

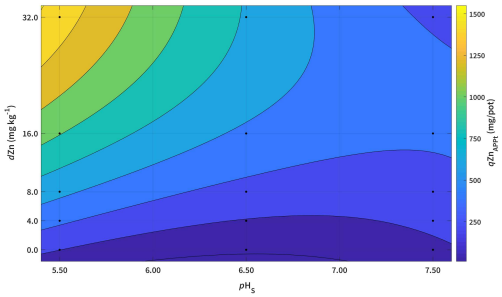

$$qZn_{APPt} = 6553.529 + 152.263\ dZn + 1982.471\ pH_S + 0.630\ dZn^2 + 150.490\ pH_S^2 + 16.688\ dZn \times pH_S$$

$$R^2_{adj.} = 0.934$$

(c) **Zn–EDTA** - Surface Plot

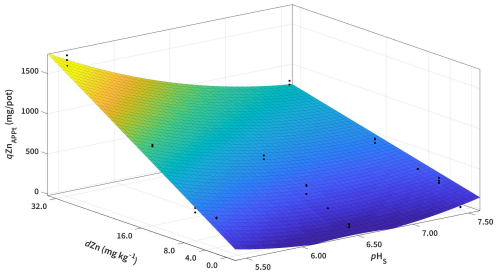

(d) **Zn–EDTA** - Contour)

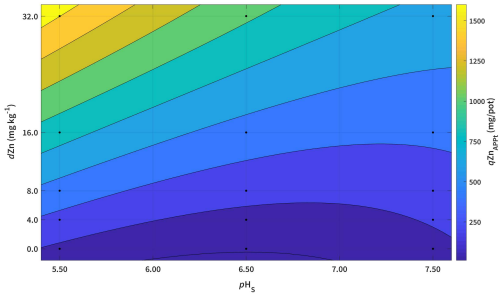

$$qZn_{APPt} = 4895.663 + 119.299\ dZn + 1490.288\ pH_S + 113.966\ pH_S^2 + 13.273\ dZn \times pH_S$$

$$R^2_{adj.} = 0.945$$

(e) **Zn–EDDS** - Surface Plot

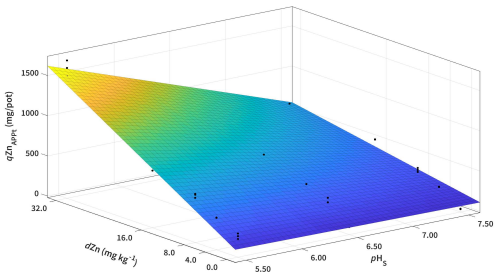

(f) **Zn–EDDS** - Contour

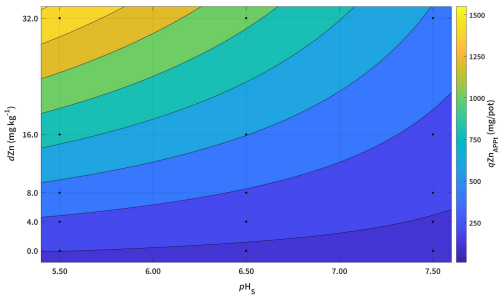

$$qZn_{APPt} = 397.347 + 114.606\ dZn + 35.343\ pH_S + 13.462\ dZn \times pH_S$$

$$R^2_{adj.} = 0.948$$

Figure 4.15: Effects of Zn doses and pH_S levels on Zn concentration in plant tissues for $LVAd_{scl}$

Table 4.5: Standard beta coefficients for plant Zn accumulated quantities (qZn_{APPt})

Soil	Source of variation	$ZnSO_4$		Zn-EDTA		Zn-EDDS	
		β coefficient	95% CI	β coefficient	95% CI	β coefficient	95% CI
$LVAd_{cla}$	pH_S	-0.461^{***}	[-0.465; -0.457]	-0.246^{***}	[-0.253; -0.240]	-0.519^{***}	[-0.524; -0.514]
	pH_S^2	0.125^{***}	[0.122; 0.127]	0.197^{***}	[0.194; 0.201]	0.182^{***}	[0.180; 0.185]
	dZn	0.970^{***}	[0.962; 0.978]	0.911^{***}	[0.908; 0.914]	0.92^{***}	[0.912; 0.927]
	dZn^2	-0.307^{***}	[-0.312; -0.302]	0.041^{ns}	[0.034; 0.047]	-0.214^{***}	[-0.217; -0.211]
	$pH_S \times dZn$	-0.344^{***}	[-0.347; -0.342]	0.087^{ns}	[0.084; 0.089]	-0.256^{***}	[-0.258; -0.253]
$LVAd_{scl}$	pH_S	-0.495^{***}	[-0.500; -0.490]	-0.328^{***}	[-0.333; -0.324]	-0.431^{***}	[-0.434; -0.427]
	pH_S^2	0.194^{***}	[0.191; 0.197]	0.161^{***}	[0.158; 0.164]	0.064^{ns}	[0.062; 0.067]
	dZn	0.884^{***}	[0.875; 0.894]	0.872^{***}	[0.867; 0.877]	0.834^{***}	[0.829; 0.839]
	dZn^2	-0.262^{***}	[-0.270; -0.255]	-0.087^{ns}	[-0.093; -0.081]	-0.086^{ns}	[-0.093; -0.079]
	$pH_S \times dZn$	-0.400^{***}	[-0.403; -0.396]	-0.284^{***}	[-0.287; -0.282]	-0.314^{***}	[-0.318; -0.311]

Significance probability level codes: * (0.05), ** (0.01), *** (0.001), and, ns (non-significant at 0.05 probability level)

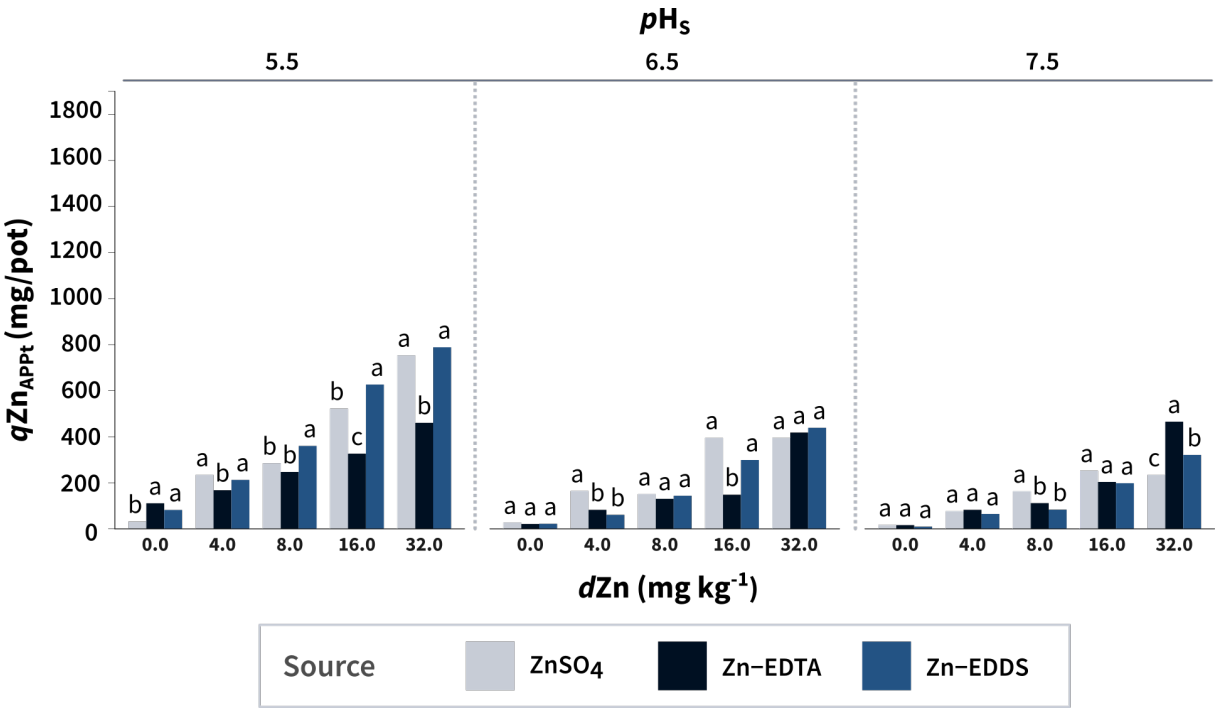

Figure 4.16: Source x pH_S x Dose

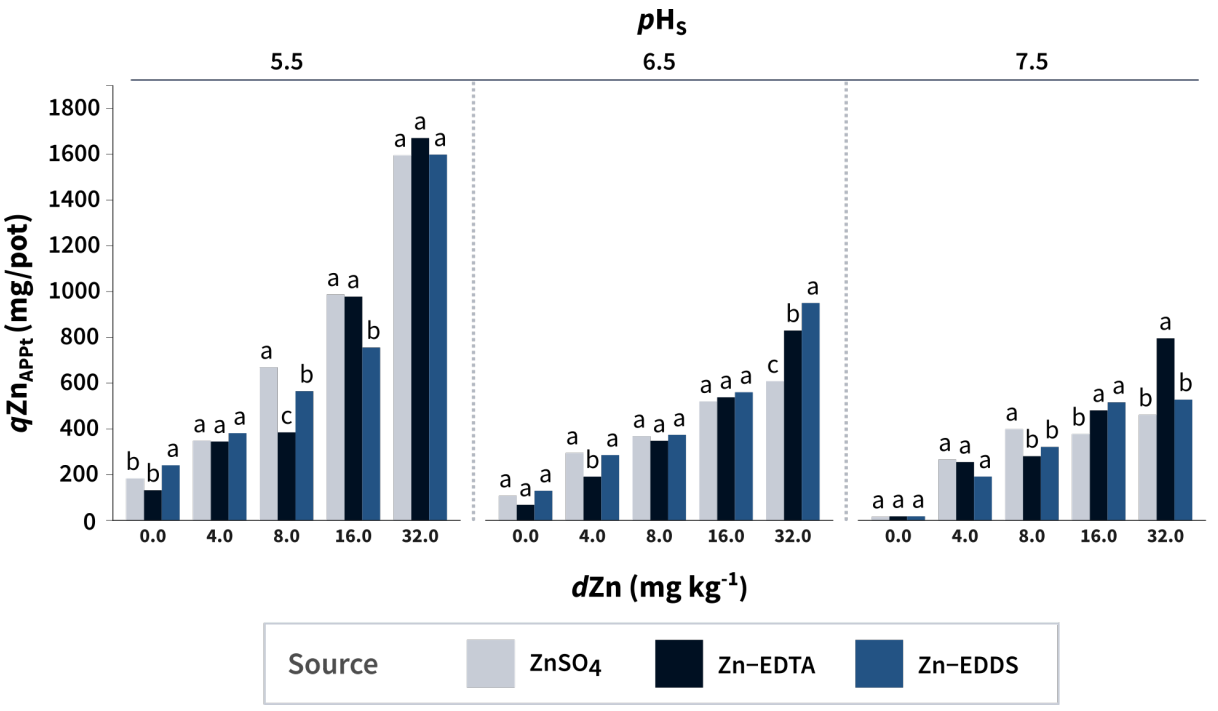

Figure 4.17: Source x pH_S x Dose

4.5 CHAPTER REMARKS

- $ZnSO_4$ and Zn–EDDS promoted the largest accumulations of Zn;
- The values of content, dry matter and Zn content were generally higher for $LVAd_{cla}$

;

- The incubation pH significantly affected Zn absorption, especially for the sulfated source;
- Zn absorption was generally lower for Zn–EDTA;
- Zn absorption was less affected when the source was Zn–EDTA;
- For $LVAd_{cla}$, when the source was $ZnSO_4$, the variation of Zn contents was extremely affected by pH;
- Zn–EDDS is a potential source for soil conditions with high pH values and concentrations of Ca and Mg.

CHAPTER 5

GENERAL WORK REMARKS AND PERSPECTIVES

As described in Chapter 2, Kinetica Web-App has some relevant features as the compatibility with any operating system, it does not require installation on the user device, broadly accessible through the internet, and rich statistical analysis and graphical visualization of the results. Moreover, new resources implementation, improvements and corrections are available at the time of update for all users.

The development of a modeling platform for estimating and interpreting ion kinetic uptake parameter values in plants may contribute for developing more efficient and higher quality plant products, among other applications as in the environmental studies field.

Considering the uptake of Zn by maize plants under overliming conditions we highlight that Zn uptake was less intense and also less affected by soil conditions and liming when the source employed was Zn–EDTA, while for $ZnSO_4$ this finding is inverted. Zn–EDDS showed an intermediate behavior, favoring Zn uptake in a balanced manner regardless of soil condition and pH and Ca and Mg activities.

$ZnSO_4$ and Zn–EDDS promoted the highest Zn accumulation. The values of Zn content, dry matter mass and content were generally higher for the soil with sandier texture. Incubation pH significantly affected Zn uptake, especially for the sulfate source. Zn uptake was generally lower for Zn-EDTA, although this source promoted the least variations in Zn acquisition as a function of soil conditions and liming level, even considering that Zn contents in plant tissues growing on the clayey soil were extremely affected by the higher liming levels.

Zn–EDDS was confirmed as a potential source for soil conditions with high pH values and Ca and Mg concentrations.

REFERENCES

ABBÈS, C. et al. Effect of NH4+:NO3- ratios on growth and nitrogen uptake by onions. *Plant and Soil*, v. 171, n. 2, p. 289–296, 1995.

ABEDIN, Mohammed Joinal; FELDMANN, Jörg; MEHARG, Andy A. Uptake kinetics of arsenic species in rice plants. *Plant Physiology*, v. 128, n. 3, p. 1120–1128, 2002.

ALLOWAY, B. J. Soil factors associated with zinc deficiency in crops and humans. *Environmental Geochemistry and Health*, v. 31, n. 5, p. 537–548, 2009.

ALVAREZ, Victor Hugo et al. Determinação e uso do fósforo remanescente. *Boletim Informativo SBCS*, v. 25, p. 21–32, 2000.

ARAÚJO, Osmário J L et al. OsNRT 2 . 2 , and Kinetics of Nitrate Uptake in Genetically Contrasting Rice Varieties. *American Journal of Plant Science*, v. 6, February, p. 306–313, 2015.

BARBER, S A. *Soil Nutrient Bioavailability: A Mechanistic Approach*. [S.l.]: Wiley, 1995. (Wiley Interscience publication).

_____. Growth Requirements for Nutrients in Relation To Demand At the Root Surface. In: HARLEY, J. L.; RUSSELL, R. SCOTT (Eds.). *The Soil–Root Interface*. New York&London: ACADEMIC PRESS, 1979. p. 5–20.

BASSIRIRAD, Hormoz. Kinetics of nutrient uptake by roots: Responses to global change. *New Phytologist*, v. 147, n. 1, p. 155–169, 2000.

BASSIRIRAD, Hormoz et al. A field method of determining NH 4 + and NO 3 - uptake kinetics in intact roots: Effects of CO2 enrichment on trees and crop species. *The Supporting Roots of Trees and Woody Plants: Form, Function and Physiology*, v. 217, p. 325–334, 2000.

BERNARDO, SALASSIER; SOARES, ANTÔNIO ALVES; MANTOVANI, EVERARDO CHARTUNI. Manual de irrigação. *UFV*, 625 p. 2006.

BHAT, K. K.S. Nutrient inflows into apple roots. *Plant and Soil*, v. 71, n. 1-3, p. 371–380, 1983.

BOAWN, Louis C. Comparison of Zinc Sulfate and Zinc EDTA as Zinc Fertilizer. *Soil Sci. Soc. Amer. Proc.*, v. 37, n. 15, p. 112–115, 1973.

BOWEN, John E. Kinetics of Active Uptake of Boron, Zinc, Copper And Manganese in Barley and Sugarcane. *Journal of Plant Nutrition*, v. 3, n. 1-4, p. 215–223, 1981.

BRAGA, J M; DEFELIPO, B. Determinação espectrofotométrica de fósforo em extratos de solos e plantas. *Rev. Ceres*, v. 21, n. 113, p. 73–84, 1974.

BRIX, Hans et al. Can differences in phosphorus uptake kinetics explain the distribution of cattail and sawgrass in the Florida Everglades? *BMC Plant Biology*, v. 10, 2010.

BROADLEY, Martin et al. Function of Nutrients: Micronutrients. In: MARSCHNER, Petra (Ed.). *Marschner's Mineral Nutrition of Higher Plants: Third Edition*. 3. ed. [S.l.]: Academic Press, 2011. chap. 7, p. 191–248.

CANTY, Angelo; RIPLEY, Brian. *boot: Bootstrap R*. [S.l.: s.n.], 2015.

CHAUHAN, Garima et al. The thermodynamics and biodegradability of chelating agents upon metal extraction. *Chemical Engineering Science*, Elsevier, v. 137, p. 768–785, 2015.

CHO, Yong-soon; LIM, Hyeong-seok. *Comparison of various estimation methods for the parameters of Michaelis – Menten equation*. v. 26. [S.l.: s.n.], 2018. p. 39–47.

CHRISTIANSEN, Nina H.; ANDERSEN, Frede O.; JENSEN, Henning S. Phosphate uptake kinetics for four species of submerged freshwater macrophytes measured by a 33P phosphate radioisotope technique. *Aquatic Botany*, Elsevier B.V., v. 128, p. 58–67, 2016.

CHUNG, Ik-Kyo et al. Application of Seaweed Cultivation to the Bioremediation of Nutrient-Rich Effluent. *Algae*, v. 17, n. 3, p. 187–194, 2002.

CLAASSEN, N; BARBER, S A. A Method for Characterizing the Relation between Nutrient Concentration and Flux into Roots of Intact Plants. *Plant physiology*, v. 54, n. 4, p. 564–568, 1974.

CLAESSEN, Christine Elisabeth Marie et al. *Manual de Métodos de Análise de Solo*. 2. ed. Rio de Janeiro: EMBRAPA-CNPS, 1997.

COTT, Grace M.; CAPLAN, Joshua S.; MOZDZER, Thomas J. Nitrogen uptake kinetics and saltmarsh plant responses to global change. *Scientific Reports*, Springer US, v. 8, n. 1, p. 1–10, 2018.

DIXON, M. The determination of enzyme inhibitor constants. *The Biochemical journal*, v. 55, n. 1, p. 170–171, 1953.

DONAGEMMA, Guilherme Kangussu et al. *Manual de métodos de análise de solo*. 2. ed. Rio de Janeiro: Embrapa Solos, 2011. 230p.

EPSTEIN, Emanuel; HAGEN, C. E. a Kinetic Study of the Absorption of Alkali Cations By Barley Roots. *Plant Physiology*, v. 27, n. 3, p. 457–474, 1952.

FERREIRA, Eric B.; CAVALCANTI, Pórtya P.; NOGUEIRA, Denismar A. ExpDes: An R Package for ANOVA and Experimental Designs. *Applied Mathematics*, 2014.

FRIEDRICH, Sarah; KONIETSCHKE, Frank; PAULY, Markus. GFD: An R package for the analysis of general factorial designs. *Journal of Statistical Software*, v. 79, July, 2017.

GANGLOFF, W. J. et al. Mobility of organic and inorganic zinc fertilizers in soils. *Communications in Soil Science and Plant Analysis*, v. 37, n. 1-2, p. 199–209, 2006.

GRAF, Donald L. Chemical Equilibria in Soils. *Clays and Clay Minerals*, v. 28, n. 4, p. 319–319, 1980.

GRAS, Amy F.; KOCH, Marguerite S.; MADDEN, Christopher J. Phosphorus uptake kinetics of a dominant tropical seagrass Thalassia testudinum. *Aquatic Botany*, v. 76, n. 4, p. 299–315, 2003.

GRESPAN, SI; DIAS, L E; NOVAIS, Rf. Crescimento e parâmetros cinéticos de absorção de amônio e nitrato por mudas de Eucalyptus spp submetidas a diferentes relações amônio/nitrato na presença e ausência de fósforo. *R. Bras. Ci. Solo*, v. 22, n. 3, p. 667–674, 1998.

GRIFFITHS, Marcus; ROY, Sonali, et al. A multiple ion-uptake phenotyping platform reveals shared mechanisms that affect nutrient uptake by maize roots. *bioRxiv*, p. 1–10, 2020.

GRIFFITHS, Marcus; YORK, Larry M. Targeting root ion uptake kinetics to increase plant productivity and nutrient use efficiency. *Plant Physiology*, v. 182, n. 4, p. 1854–1868, 2020.

HANES, Charles Samuel. Studies on plant amylases. *Biochemical Journal*, v. 26, n. 5, p. 1406–1421, Jan. 1932.

HOAGLAND, Dennis Robert; ARNON, Daniel Israel, et al. The water-culture method for growing plants without soil. *Circular. California agricultural experiment station*, v. 347, 1950.

HODGSON, J. F.; LINDSAY, W. L.; TRIERWEILER, J. F. Micronutrient Cation Complexing in Soil Solution: II. Complexing of Zinc and Copper in Displaced Solution from Calcareous Soils. *Soil Science Society of America Journal*, v. 30, n. 6, p. 723–726, 1966.

HOFSTEE, B. H.J. On the evaluation of the constants Vm and KM in enzyme reactions. *Science*, v. 116, n. 3013, p. 329–331, 1952.

HORN, Delson et al. Nutrient uptake kinetics and morphological traits of roots of maize cultivars with contrasting genetic variability. *Revista Brasileira de Ciencia do Solo*, v. 30, n. 1, p. 77–85, 2006.

JEKEL, Charles F; VENTER, Gerhard. *PieceWise Linear Fitting : A Python Library for Fitting 1D Continuous Piecewise Linear Functions*. [S.l.: s.n.], 2019. p. 1–15.

KABATA-PENDIAS, Alina. *1Chapter 8 Elements of Group 13 (Previously Group IIIa)*. [S.l.: s.n.], 2010. p. 343–360.

KELLER, Frieder; ZELLNER, Dietmar. The 1-Exp Function as an Alternative Model of Nonlinear Saturable Kinetics. *Clinical Chemistry and Laboratory Medicine*, v. 34, n. 3, p. 265–272, 1996.

KOCHIAN, Leon V. Zinc Absorption from Hydroponic Solutions by Plant Roots. In: ROBSON (Ed.). *Zinc in Soils and Plants*. 1. ed. Perth: Kluwer Academic Publishers, 1993. chap. 4, p. 45–57.

KOLODYNSKA, Dorota. Expanding Issues in Desalination. In: EXPANDING Issues in Desalination. [S.l.: s.n.], 2012. p. 339–370.

LANIGAN, Katherine C.; PIDSOSNY, Katie. Reflectance FTIR spectroscopic analysis of metal complexation to EDTA and EDDS. *Vibrational Spectroscopy*, v. 45, n. 1, p. 2–9, 2007.

LI, Jihua et al. Comparison of four aquatic plant treatment systems for nutrient removal from eutrophied water. *Bioresource Technology*, Elsevier Ltd, v. 179, p. 1–7, 2015.

LI, Qiang et al. Cultivar differences in root nitrogen uptake ability of maize hybrids. *Frontiers in Plant Science*, v. 8, June, p. 1–12, 2017.

LIMA, Augusto Miguel Nascimento et al. Cinética de absorção e eficiência nutricional de K+, Ca2+ e Mg2+ em plantas jovens de quatro clones de eucalipto. *Revista Brasileira de Ciência do Solo*, v. 29, n. 6, p. 903–909, 2005.

LIN, Wen; KELLY, J. Michael. Nutrient uptake estimates for woody species as described by the NST 3.0, SSAND, and PCATS mechanistic nutrient uptake models. *Plant and Soil*, v. 335, n. 1, p. 199–212, 2010.

LÓPEZ-RAYO, Sandra; CORREAS, Covadonga; LUCENA, Juan J. Novel chelating agents as manganese and zinc fertilisers: Characterisation, theoretical speciation and stability in solution. *Chemical Speciation and Bioavailability*, v. 24, n. 3, p. 147–158, 2012.

LÓPEZ-RAYO, Sandra; NADAL, Paloma; LUCENA, Juan J. Novel chelating agents for iron, manganese, zinc, and copper mixed fertilisation in high pH soil-less cultures. *Journal of the Science of Food and Agriculture*, v. 96, n. 4, p. 1111–1120, 2016.

LUBSCH, Alexander; TIMMERMANS, Klaas. Uptake kinetics and storage capacity of dissolved inorganic phosphorus and corresponding N:P dynamics in Ulva lactuca (Chlorophyta). *Journal of Phycology*, v. 54, n. 2, p. 215–223, 2018.

LUO, Min Bo; LIU, Feng; XU, Zhao Li. Growth and nutrient uptake capacity of two co-occurring species, Ulva prolifera and Ulva linza. *Aquatic Botany*, Elsevier B.V., v. 100, p. 18–24, 2012.

MACHADO, Cynthia Torres de Toledo; FURLANI, Angela Maria Cangiani. Cinética de absorção de fósforo e morfologia radicular de variedades locais e melhoradas de milho. *Scientia Agricola*, v. 61, n. 1, p. 69–76, 2004.

MALAGOLI, Philippe; LE DEUNFF, Erwan. An updated model for nitrate uptake modelling in plants. II. Assessment of active root involvement in nitrate uptake based on integrated root system age: measured versus modelled outputs. *Annals of Botany*, v. 113, n. 6, p. 1007–1019, 2014.

MARSCHNER, P (Ed.). *Marschner's Mineral Nutrition of Higher Plants*. 3. ed. London: Elsevier, 2012. v. 91, p. 668. (Academic Press, 5).

MARTINEZ, Herminia E.P. et al. Short-term water stress affecting NO3- absorption by almond plants. *Scientia Horticulturae*, Elsevier B.V., v. 197, n. 3, p. 50–56, 2015.

MARTÍNEZ, Brezo; RICO, Jose M. Inorganic nitrogen and phosphorus uptake kinetics in Palmaria palmata (Rhodophyta). *Journal of Phycology*, v. 40, n. 4, p. 642–650, 2004.

MENG, Sen et al. Nitrogen uptake and metabolism of *Populus simonii* in response to PEG-induced drought stress. *Environmental and Experimental Botany*, v. 123, p. 78–87, 2016.

MERTENS, Jelle; SMOLDERS, Erik; KIEKENS, L. Zinc. In: ALLOWAY, B. J. (Ed.). *Heavy Metals in Soils*. 3. ed. LONDON/NEW YORK: Springer Dordrecht Heidelberg, 2013. v. 22. chap. 17, p. 465–493.

MORTVEDT, J. J.; GILKES, R. J. Zinc Fertilizers. In: ZINC in Soils and Plants. Perth: [s.n.], 1993. chap. 3, p. 33–44.

MOZDZER, Thomas J.; ZIEMAN, Joseph C.; MCGLATHERY, Karen J. Nitrogen uptake by native and invasive temperate coastal macrophytes: Importance of dissolved organic nitrogen. *Estuaries and Coasts*, v. 33, n. 3, p. 784–797, 2010.

MULLINS, G. L.; SOMMERS, L. E. Cadmium and zinc influx characteristics by intact corn (Zea mays L.) seedlings. *Plant and Soil*, v. 96, n. 2, p. 153–164, 1986.

NIELSEN, Niels Erik. A transport kinetic concept of ion uptake from soil by plants - II. The concept and some theoretic considerations. *Plant and Soil*, v. 37, n. 3, p. 561–576, Mar. 1972.

NOCITO, Fabio F. et al. Cadmium-induced sulfate uptake in maize roots. *Plant Physiology*, v. 129, n. 4, p. 1872–1879, 2002.

NORVELL, Wendell A. Reactions of metal chelates in soils. In: MICRONUTRIENTS in Agriculture. SSSA Book Ser. 4. [S.l.: s.n.], 1991. p. 187–227.

NOVAES, R.F. de; NEVES, J.C.L.; BARROS, N.F. de. Ensaio em ambiente controlado. *Métodos de pesquisa em fertilidade do solo*, p. 189–253, 1991.

OLESEN, Annica et al. Nutrient kinetics in submerged plant beds: A mesocosm study simulating constructed drainage wetlands. *Ecological Engineering*, Elsevier, v. 122, August, p. 263–270, 2018.

ORAMA, Marjatta et al. Complexation of [S,S] and mixed stereoisomers of N,N'-ethylenediaminedisuccinic acid (EDDS) with Fe(III), Cu(II), Zn(II) and Mn(II) ions in aqueous solution. *Journal of the Chemical Society. Dalton Transactions*, n. 24, p. 4644–4648, 2002.

PAULA, Betania Vahl de et al. Morphological and kinetic parameters of the uptake of nitrogen forms in clonal peach rootstocks. *Scientia Horticulturae*, Elsevier, v. 239, August 2017, p. 205–209, 2018.

R DEVELOPMENT CORE TEAM, R. *R: A Language and Environment for Statistical Computing*. Ed. by R Development Core Team. v. 1. [S.l.]: R Foundation for Statistical Computing, 2019. p. 409. (R Foundation for Statistical Computing, 2.11.1).

RACE, Marco et al. *Copper and zinc removal from contaminated soils through soil washing process using ethylenediaminedisuccinic acid as a chelating agent: A modeling investigation*. [S.l.]: Elsevier B.V., 2016. v. 4, p. 2878–2891.

RAIJ, B. van et al. *Análise química para avaliação da fertilidade de solos tropicais*. [S.l.: s.n.], 2001. p. 285.

REID, Robert; HAYES, Julie. Mechanisms and control of nutrient uptake in plants. *International Review of Cytology*, v. 229, n. 3, p. 73–114, 2003.

REID, Robert J.; BROOKES, Justin D., et al. The mechanism of zinc uptake in plants Characterisation of the low-affinity system. *Planta*, v. 198, n. 1, p. 39–45, 1996.

RENGEL, Zdenko; GRAHAM, Robin D. Uptake of zinc from chelate-buffered nutrient solutions by wheat genotypes differing in zinc efficiency. *Journal of Experimental Botany*, v. 47, n. 295, p. 217–226, 1996.

RITCHIE, Raymond J.; PRVAN, Tania. A simulation study on designing experiments to measure the Km of Michaelis-Menten kinetics curves. *Journal of Theoretical Biology*, v. 178, n. 3, p. 239–254, Feb. 1996.

ROFKAR, Jordan R.; DWYER, Daryl F. Effects of light regime, temperature, and plant age on uptake of arsenic by Spartina pectinata and Carex stricta. *International Journal of Phytoremediation*, v. 13, n. 6, p. 528–537, 2011.

ROLEDA, Michael Y.; HURD, Catriona L. Seaweed nutrient physiology: application of concepts to aquaculture and bioremediation. *Phycologia*, Taylor & Francis, v. 58, n. 5, p. 552–562, 2019.

RUANO, A.; POSCHENRIEDER, Ch; BARCELB, J. Growth And Biomass Partitioning In Zinc-Toxic Bush Beans. *Journal of Plant Nutrition*, v. 11, n. 5, p. 577–588, 1988.

RUIZ, Hugo Alberto; Estimativa dos Parâmetros Cinéticos Km e Vmáx por uma aproximação gráfico-matemática. *Rev. Ceres*, v. 32, n. 179, p. 79–84, 1985.

RUIZ, Hugo Alberto; FERNANDES FILHO, E. I. Cinética: Software para estimar as constante Vmax e Km da equação de Michaelis-Menten. In: REUNIÃO Brasileira de Fertilidade do Solo e Nutrição de Plantas. Piracicaba: [s.n.], 1992. p. 124–125.

SANES, Fernanda San Martins et al. Morfologia de raízes e cinética de absorção de potássio em genótipos de arroz irrigado. *Revista Brasileira de Ciencia do Solo*, v. 37, n. 3, p. 688–697, 2013.

SILBERBUSH, M.; BEN-ASHER, J.; EPHRATH, J. E. A model for water flow and nutrient uptake by horticultural crops grown in a soilless culture system. *Acta Horticulturae*, v. 674, p. 357–358, 2005.

STAPEL, Johan et al. Nutrient uptake by leaves and roots of the seagrass Thalassia hemprichii in the Spermonde Archipelago, Indonesia. *Marine Ecology Progress Series*, v. 134, n. 1-3, p. 195–206, 1996.

STONE, Nand K. Fageria; F., Luís. *Micronutrient Deficiency Problems in South America(original en inglés)*. [S.l.: s.n.], 2008. p. 252.

STORN, Rainer; PRICE, Kenneth. Differential Evolution – A Simple and Efficient Heuristic for global Optimization over Continuous Spaces. *Journal of Global Optimization*, v. 11, n. 4, p. 341–359, 1997.

TILLER, KEVIN G.; HODGSON, J.F. the Specific Sorption of Cobalt and Zinc By Layer Silicates. *Clays and Clay Minerals*, n. 1950, p. 393–403, 1962.

TINKER, P B; NYE, P H. *Solute Movement in the Rhizosphere*. London: Oxford University Press, 2002.

VAN REES, K C J. Michaelis-Menten kinetics: Calculation and use in nutrient uptake models. *New Zealand Journal of Forestry Science*, v. 24, n. 2-3, p. 226–233, 1994.

VIRTANEN, Pauli et al. SciPy 1.0: Fundamental Algorithms for Scientific Computing in Python. *Nature Methods*, v. 17, p. 261–272, 2020.

WESSELLS, K. Ryan; BROWN, Kenneth H. Estimating the Global Prevalence of Zinc Deficiency: Results Based on Zinc Availability in National Food Supplies and the Prevalence of Stunting. *PLOS ONE*, Public Library of Science, v. 7, n. 11, p. 1–11, Nov. 2012.

WICKHAM, Hadley. httr: Tools for Working with URLs and HTTP. Elsevier, 2019.

YORK, Larry M.; SILBERBUSH, Moshe; LYNCH, Jonathan P. Spatiotemporal variation of nitrate uptake kinetics within the maize (Zea mays L.) root system is associated with greater nitrate uptake and interactions with architectural phenes. *Journal of experimental botany*, v. 67, n. 12, p. 3763–3775, 2016.

ZASOSKI, R. J.; BURAU, R. G. A rapid nitric-perchloric acid digestion method for multi-element tissue analysis. *Communications in Soil Science and Plant Analysis*, v. 8, n. 5, p. 425–436, 1977.

ZHANG, Q. et al. Effects of nitrogen fertilization on removal kinetics of thiocyanate (SCN–) in rice seedlings. *International Journal of Environmental Science and Technology*, n. 3, 2020.

ZHU, Q.; ZHUANG, Q. Modeling the effects of organic nitrogen uptake by plants on the carbon cycling of boreal forest and tundra ecosystems. *Biogeosciences*, v. 10, n. 12, p. 7943–7955, 2013.

ZHU, Qing; IVERSEN, Colleen M., et al. Root traits explain observed tundra vegetation nitrogen uptake patterns: Implications for trait-based land models. *Journal of Geophysical Research: Biogeosciences*, v. 121, n. 12, p. 3101–3112, 2016.

APPENDIX A - KINETICA API parameters specifications

Table S.1: Kinetica API input parameters

Table S.2: Kinetica API output variables

Table S.3: Equations implemented for fitting the models

Table S.4: Linearized transformations for the Michaelis-Menten equations

Table S.5: Statistical variables

Table S.1: Kinetica API input parameters

Input parameter	Variable type	Description	Input options
concentration_unit	String	Measure unit for the analytical ion concentration or activity	*µmol L^{-1}, µmol mL^{-1}, mmol L^{-1}, mmol mL^{-1}, nmol L^{-1}, nmol mL^{-1}*
time_unit	String	Time unit for sampling intervals	*h, min, s*
absorbing_tissue measure_unit	String	Mass, area or volume unit employed to measure the ion-absorbing plant tissue (e.g., roots, leaves)	*mg, g, cg, kg, cm^2, m^2, cm^3*
initial _volume	Float	Initial depletion solution volume	*mL, L* - Automatically set by the application based on the denominator of the "Concentration unit" previously selected by the user
final_volume	Float	Final depletion volume	*mL, L* - Automatically set by the application based on the denominator of the "Concentration unit" previously selected by the user
absorbing_tissue_measure	Float	Value for the ion-absorbing plant tissue measurement	To be filled by the user
sampling_times	Array	A vector containing numeric values for the sampling times of the ion-depletion experiment.	To be filled by the user
observed_concentrations	Array	A vector containing numeric values for analytical ion instant concentrations obtained from the depletion experiment	To be filled by the user
sampling_volumes	Array	A vector containing numeric values for the sampled volumes at each sampling event. In the case of the sampled volume was replenished, the field can be left blank or filled with zeros.	To be filled by the user

Table S.2: Kinetica API output variables

Variable alias	Variable type	Description
concentration_unit	String	Measure unit for the analytical ion concentration
time_unit	String	Time unit for sampling intervals
absorbing_tissue_measure_unit	String	Mass, area or volume unit employed to measure the ion-absorbing plant tissue (e.g., roots, leaves)
initial_volume	Float	Initial depletion solution volume
final_volume	Float	Final depletion volume
absorbing_tissue_measure	Float	Value for the ion-absorbing plant tissue measurement
sampling_times	Array	A vector containing numeric values for the ion depletion sampling times
observed_concentrations	Array	A vector containing numeric values for analytical ion concentration obtained from the depletion experiment
sampling_volumes	Array	A vector containing numeric values for the sampled volumes at each sampling event. In the case of the sampled volume was replenished, the field can be left blank or filled with zeros.
uptake_rate_unit	String	Uptake rate unit
observed_quantities	Array	Calculated ion quantities

Table S.2: Kinetica API output variables

Variable alias	Variable type	Description
Volumes	Array	Estimated solution volumes
observed_uptake_rates	Array	Calculated ion uptake rates
		Model-specific results
Model	String	Model
linear_points	Integer	Number of data points fitted to the linear segment for the Graphical-Mathematical Model
nonlinear_points	Integer	Number of data points fitted to the nonlinear segment for the Graphical-mathematical Model
a	Float	y-intercept for the linear segment fit on the Graphical-Mathematical method
b	Float	Slope (angular coefficient) for the linear segment fit on the Graphical-Mathematical method
s_lin	Float	S (linear points)
r_lin	Float	Adjusted R Squared (linear points)
c	Float	β_0 coefficient for the nonlinear segment fit for the Graphical-Mathematical method
d	Float	β_1 (nonlinear points)
r_nlin	Float	Adj. R Squared (linear points)

Table S.2: Kinetica API output variables

Variable alias	Variable type	Description
s_nlin	Float	*S* (nonlinear points)
estimated_quantities	Array	Estimated quantities
s_conj	Float	*S* (linear + nonlinear)
rmse_lin_nlin	Float	*RMSE* (linear + nonlinear)
r_conj	Float	Adj. R-squared (linear + nonlinear points)
f_stat_lin_nlin	Float	*F* (linear + nonlinear)
p_f_lin_nlin	Float	*p-value* (linear + nonlinear)
tm	Float	t_m
qm	Float	Q_m
vm	Float	v_m
km	Float	K_m
vmax	Float	v_{max}
cmin	Float	c_{min}

Table S.2: Kinetica API output variables

Variable alias	Variable type	Description
estimated_uptake_rates	Array	Estimated uptake rates
estimated_concentrations	Array	Estimated concentrations
rmse_mm	Float	*RMSE* (Michaelis-Menten)
r_2_mm	Float	Adjusted R-squared (Michaelis Menten)
f_stat_mm	Float	*F* (Michaelis-Menten)
p_f_mm	Float	*p-value* (Michaelis-Menten)
aicc_mm	Float	AIC_c (Michselis-Menten)
bic_mm	Float	*BIC* (Michaelis-Menten)
t_vmax	Float	*t* (v_{max})
t_km	Float	*t* (K_m)
t_cmin	Float	*t* (c_{min})
p_t_vmax	Float	p-value t-test (v_{max})
p_t_km	Float	p-value t-test (K_m)

Table S.2: Kinetica API output variables

Variable alias	Variable type	Description
p_t_cmin	Float	p-value t-test (c_{min})
ci_inf_vmax	Float	Confidence interval – inferior limit (v_{max})
ci_inf_km	Float	Confidence interval – inferior limit (K_m)
ci_inf_cmin	Float	Confidence interval – inferior limit (c_{min})
ci_sup_vmax	Float	Confidence interval – superior limit (v_{max})
ci_sup_km	Float	Confidence interval – superior limit (K_m)
ci_sup_cmin	Float	Confidence interval – superior limit (c_{min})
transf_lineweaver_burk_x_val	Array	Lineweaver-Burk plot x-axis values
transf_lineweaver_burk_y_val	Array	Lineweaver-Burk plot y-axis values
transf_eadie_hofstee_x_val	Array	Eadie-Hofstee plot x-axis values
transf_eadie_hofstee_y_val	Array	Eadie-Hofstee plot y-axis values
transf_hanes_woolf_x_val	Array	Hanes-Woolf plot x-axis values
transf_hanes_woolf_y_val	Array	Hanes-Woolf y-axis values

Table S.3: Equations implemented for fitting the models

Equation	Description
$v = \frac{v_{max}\, c}{K_m + c}$	Michaelis-Menten equation
$v = \frac{v_{max}(c - c_{min})}{K_m + (c - c_{min})}$	Michaelis-Menten equation (modified)
$Q = c\, V$	Quantities (general depletion model)
$Q(t) = a + b\, t$	Quantities (linear)
$Q(t) = c\, t^d$	Quantities (power)
$Q(t) = c\, e^{d\, t}$	Quantities (exponential)
$Q(t) = c\, e^{\frac{d}{t}}$	Quantities (exp-reciprocal)
$\frac{1}{2}\, b = c\, d\, t_m{}^{(d-1)}$	$\delta Q/\delta t$ linear-power
$\frac{1}{2}\, b = c\, d\, e^{(d\, t_m)}$	$\delta Q/\delta t$ linear-exponential

Table S.3: Equations implemented for fitting the models

Equation	Description
$\frac{1}{2}\, b = \; - \; \frac{c\; d\; e^{(d\; t_m)}}{{t_m}^2}$	$\delta Q/\delta t$ linear-exp-reciprocal
$v_{max} = \; - \frac{b}{r_m}$	v_{max}
$K_m = \frac{Q_m}{V_m}$	K_m
$V(t) = \; V_0 \; - \left(t\; \dot{V}_l \; + \; \sum_{0}^{n(t)} V_s \right)$	Volume (instantaneous)
$V_l = V_0 - V_{t_n} - \sum_{t=0}^{n(t)} V_s$	Volume loss (by evapotranspiration flow)
$\dot{V}_l \; = \; \frac{V_l}{\Delta t}$	Volume loss rate
$V_m \; = V_0 \; - \; \left(\dot{V}_l \; t_m \; + \; \sum_{t=0}^{n(t_m)} V_s \right)$	V_m
$v(t) \; = \; \frac{\Delta Q}{\Delta t \; r_m}$	Uptake rate (GM)

Table S.4: Linearized transformations for the Michaelis-Menten equations

Linearized plot	x-axis	y-axis	Slope	Intercept
Lineweaver-Burk $\frac{1}{v} = \frac{K_m + (c - c_{min})}{v_{max}(c - c_{min})} = \frac{K_m}{v_{max}} \frac{1}{(c - c_{min})} + \frac{1}{v_{max}}$	$\frac{1}{c - c_{min}}$	$\frac{1}{v}$	$\frac{K_m}{v_{max}}$	$\frac{1}{v_{max}}$
Eadie-Hofstee $v = - K_m \frac{v}{c - c_{min}} + v_{max}$	$\frac{v}{c - c_{min}}$	v	$- K_m$	v_{max}
Hanes-Wolf $\frac{c - c_{min}}{v} = \frac{1}{v_{max}}(c - c_{min}) + \frac{K_m}{v_{max}}$	$c - c_{min}$	$\frac{c - c_{min}}{v}$	$\frac{1}{v_{max}}$	$\frac{K_m}{v_{max}}$

Table S5. Statistical variables

Variable	Description	Equation
RSS	Residual sum of squares	$RSS = \sum_{i=1}^{n} (Y_i - \widehat{Y_i})^2$
TSS	Total sum of squares	$TSS = \sum_{i=0}^{N} (y_i - \overline{y})^2$

R^2	Coefficient of determination	$R^2 = 1 - \frac{RSS}{TSS}$
Adj. R^2	Adjusted R squared	$R^2_{adj.} = 1 - \frac{\frac{RSS}{n-d-1}}{\frac{TSS}{n-1}}$
SE	Standard error of regression	$SE = \sqrt{\frac{RSS}{n-p}}$
RMSE	Root mean square error	$RMSE = \sqrt{\frac{\sum_{i=1}^{n} (Y_i - \widehat{Y_i})^2}{n}}$
AIC	Akaike information criterion	$AIC = n\ log\left(\frac{RSS}{n}\right) + 2p$
AIC_C	Akaike information criterion with correction for small size samples	$AIC_c = AIC + 2p\left(\frac{p+1}{n-p-1}\right)$
BIC	Bayesian information criterion	$BIC = nlog\left(\frac{RSS}{n}\right) + p\log(n)$
MSM	Mean square model	$MSM = \frac{MSS}{p}$
MSE	Mean squared error	$MSE = \frac{RSS}{n-p-1}$

F-stat	Calculated F statistic	$F_{stat} = \frac{MSM}{MSE}$
F-prob (p-value)	p-value for the F test	$F_{prob} = 1 - (F_{stat}, p, n - p - 1)$
t-value	Value for the t-test statistic	$t = t_{(\alpha/2,\ n\ -\ p)}$
CI	Confidence interval	$CI = \overline{x} \pm z_{(1-(\alpha/2),n-p-1)}\ SE_x$

APPENDIX B - Example script using R Software environment for making requests to Kinetica API

R script for Kinetica API HTTP/GET Requests

R script for Kinetica API HTTP/POST Requests

B.1 R code for Kinetica API HTTP/GET Requests

a) Load the required packages

```
  library(httr)
  library(jsonlite)
  library(dplyr)
```

b) Store Kinetica API URL

```
api_url <- "https://api.kinetica.ufv.br"
```

c) Check the API version

```
response_get_version <- content(GET(url =  api_url, query = "version"),
  encoding = "UTF-8")
```

d) Obtain an input sample data

```
response_get_example <- content(GET(url =  api_url, query = "example"),
  encoding =  'UTF-8', 'parsed')


list_response_get_example <- list()
for (n in names(response_get_example)){
  name = names(response_get_example[n])
  value = unname(unlist(response_get_example[n]))
  list_response_get_example[n] <- vector_to_array_list(value, ', ' , n
ame)
}
```

B.2 R script for Kinetica API HTTP/POST Request

a) Load required packages

```
library(httr)
library(jsonlite)
library(dplyr)
```

b) Store Kinetica API URL

```
api_url <- "https://api.kinetica.ufv.br"
```

c) Input data

```
data_input = read.csv(
  'data_input_example.csv',
  header = T,
  sep = ",",
  dec = ".",
  stringsAsFactors = F,
  na.strings = c("", "-"))


data_input_list = list()
for (name in names(data_input)) {
  data_input_list[name] = na.omit(data_input[name])
}


data_input_list_names <- names(data_input_list)


data_input_count = c()
for (name in names(data_input_list)) {
  data_input_count[name] = nrow(data.frame(data_input_list[name], na.o
mit = T))
}
```

d) Create an application/json object with the data input

```
all_input_variables_json <-
  toJSON(data_input_list, auto_unbox = T)
```

e) Make a POST Request to Kinetica API

```
response_from_post <-
  content(
    POST(
      url = api_url,
      body = all_input_variables_json,
      content_type("application/json")
    ),
    encoding =  'UTF-8',
    'parsed'
  )
```

f) Handling, cleaning and parsing response data

```
response_from_post_common_results <-
  response_from_post[[c('all_results', 'system_common_results')]]
response_from_post_models_results <-
  response_from_post[[c('all_results', 'model_specific_results')]]


  vector_to_array_list <-
  function(vector, split_char_vector, array_name) {
    array0 = gsub("([.,/-])|[[:punct:]]", "\\1", as.matrix(vector))
    array = array(unlist(strsplit(array0, split_char_vector)))
    array_list = list (array)
    return(array_list)
  }


list_common_results = list()

for (n in names(response_from_post_common_results)) {
  name = names(response_from_post_common_results[n])
  value = unname(unlist(response_from_post_common_results[n]))
  list_common_results[n] <-    vector_to_array_list(value, ', ' , name)
}


list_models_results_count = list()
for (name in names(data_input)) {
  data_input_list[name] = na.omit(data_input[name])
}


list_models_results_direct_adjust <- list()
list_models_results_linear_power <- list()
list_models_results_linear_exponential <- list()
list_models_results_linear_reciprocal_exponential <- list()

for (var_name in names(response_from_post_models_results)) {
  value_direct_adjust = response_from_post_models_results[[var_name]]
['direct_adjust']
  value_linear_power = response_from_post_models_results[[var_name]]['
```

```
linear_power']
  value_linear_exponential =
  response_from_post_models_results[[var_name]]['linear_exponential']
  value_linear_reciprocal_exponential =
  response_from_post_models_results[[var_name]]['linear_reciprocal_expo
nential']


  list_models_results_direct_adjust[var_name] <-
    vector_to_array_list(value_direct_adjust, ', ', var_name)
  list_models_results_linear_power[var_name] <-
    vector_to_array_list(value_linear_power, ', ', var_name)
  list_models_results_linear_exponential[var_name] <-
    vector_to_array_list(value_linear_exponential, ', ', var_name)
  list_models_results_linear_reciprocal_exponential[var_name] <-
    vector_to_array_list(value_linear_reciprocal_exponential, ', ', var
_name)
  list_models_results_count = list()
  for (name in names(list_models_results_direct_adjust)) {
    list_models_results_count[name] =
    nrow(data.frame(list_models_results_direct_adjust[name], na.omit =
T))
  }}
```

g) Save response as tabulated data

```
write.table(list_common_results, "kinetica_common_var.txt")
write.csv2(list_common_results[10:14], "kinetica_common_arrays.csv")
write.csv2(list_models_results_da[1:50], "kinetica_models_var.csv")
```